Electrical resistivity structure of the southeast Australian lithosphere

A dissertation presented
by
Kate Robertson

In fulfilment of the requirements
for the degree of
Doctor of Philosophy
in the subject of
Geophysics

THE UNIVERSITY
of ADELAIDE

Submitted to the
Department of Earth Sciences,
School of Physical Sciences, Faculty of Sciences

Adelaide, December 2016

CONTENTS

LIST OF TABLES

LIST OF FIGURES

ABSTRACT

Electrical Resistivity Structure of the Southeast Australian Lithosphere

by Kate Robertson

In its ability to retain signatures of tectonic events that enrich or deplete its fertilization state, the lithosphere holds the key to the tectonic evolution and history of Earth. Dewatering of the subducting slab leads to released fluids and induced melt which act to fertilize the overlying mantle in incompatible elements such as hydrogen. Conversely, rifting events lead to partial melting with fertile elements entering the melt, leaving behind a depleted lithosphere. Signatures such as these can remain in the lithosphere for hundreds of millions of years in the absence of further high temperature/melt events.

Magnetotellurics (MT) is a passive geophysical tool that images the physical property of electrical resistivity and is capable of penetrating the entire lithosphere. MT is highly sensitive to minor interconnected conducting mineralogy and fluids, and thus is ideal for distinguishing between lithosphere of different degrees of enrichment. Additionally, the sensitivity to these minor phases means that fossil fluid pathways associated with the ascent of mineralising fluids and metals are detectable with MT. This is the cornerstone on which one of the main directions of the UNCOVER (Australian Academy of Science, 2012) initiative is based on- increasing the detectable signature of ore deposits by imaging the underlying fluid pathways and lateral dispersion of deposits.

With these capabilities in mind, MT surveys were undertaken across western Victoria, Australia and the Ikara-Flinders Ranges and Curnamona Province in South Australia, Australia. The collection, processing and modelling of new MT sites were conducted for this thesis, with many other existing MT sites utilised to expand the dataset.

In Chapter 2, 74 broadband (period of 0.001-2000 s) MT sites along the 1.2-5 km spaced east-west Southern Delamerian transect were processed, modelled and interpreted across western Victoria. The crust beneath the Delamerian Orogen has a heterogeneous resistivity structure, with low-resistivity fossil-fluid pathways stemming from Moho depths, intersecting an otherwise resistive upper crust. Serpentinite with interconnected magnetite is known to occur within the vicinity of the survey region, and conductivity measurements of hand samples indicate substantially lower resistivities for the serpentinised rocks, leading to the interpretation that serpentinite contributed to the low resistivity zones.

Chapter 3 expands on the Southern Delamerian transect of Chapter 2 by modelling the transect using a 3D inversion code, along with four other pre-existing datasets which, when combined, create a 500 km continuous east-west transect. Importantly, this transect traverses the transitional zone between the Delamerian and Lachlan Orogens. The elusive boundary between these Orogens has most recently been interpreted as a gradual boundary within the Stawell Zone. Results from modelling show that the lower crust and shallow upper mantle of the Delamerian Orogen are at least an order of magnitude more resistive than the adjacent Lachlan Orogen. If the location of this sharp gradient in resistivity is chosen as the Delamerian-Lachlan transition, then the boundary occurs about 20 km to the east of the Moyston Fault in a NNW-SSE orientation, in reasonable agreeance with seismologically and geochemically determined boundaries.

Finally, Chapter 4 involved the collection of the first set of AusLAMP measurements across an array of 50 km spaced long-period (2-17,000 s) MT sites across the Ikara-Flinders Ranges and Curnamona Province in South Australia. This longer-period dataset was capable of imaging the entire lithosphere, and resulted in the imaging of a surprisingly low resistivity crust for the Palaeo-Mesoproterozoic Curnamona Province, indicating either a long-lived retainment of enrichment from the Olarian Orogeny (over 1.5 Ga), a more widespread reworking of the province from the Delamerian Orogeny (540 Ma), or another unrelated more recent enrichment event. The Broken Hill Domain remains largely resistive, indicating that enrichment events associated with the emplacement of the word-class Broken Hill deposit may have been erased during a high temperature or melt event. Further, two conductivity anomalies were identified in the Nackara Arc of the Ikara-Flinders Ranges, and when combined with the Curnamona Conductor, can explain the phenomenon of induction vectors across eastern South Australia all pointing toward an anomalous zone spanning the Ikara-Flinders Ranges north to south in an arcuate fashion, which had previously been interpreted as one single continuous conductivity anomaly, the Flinders Conductivity Anomaly. Coincidence of the Nackara Arc Conductors with locations of discovered kimberlites give evidence for zones of lithospheric weakness, with pathways where CO_2-rich kimberlitic melts may have deposited graphite on ascent.

Thesis Supervisors: Prof. Graham Heinson and Dr. Stephan Thiel

STATEMENT OF ORIGINALITY

I certify that this work contains no material which has been accepted for the award of any other degree or diploma in my name in any university or other tertiary institution and, to the best of my knowledge and belief, contains no material previously published or written by another person, except where due reference has been made in the text. In addition, I certify that no part of this work will, in the future, be used in a submission in my name for any other degree or diploma in any university or other tertiary institution without the prior approval of the University of Adelaide and where applicable, any partner institution responsible for the joint award of this degree.

I give consent to this copy of my thesis when deposited in the University Library, being made available for loan and photocopying, subject to the provisions of the Copyright Act 1968.

The author acknowledges that copyright of published works contained within this thesis resides with the copyright holder(s) of those works.

I also give permission for the digital version of my thesis to be made available on the web, via the University's digital research repository, the Library Search and also through web search engines, unless permission has been granted by the University to restrict access for a period of time.

Signed _____ Date _____

ACKNOWLEDGEMENTS

Thankyou to my supervisors Graham Heinson and Stephan Thiel for inspiring and supporting me through my research so far. Thankyou for providing me with endless opportunities to attend conferences, go on fieldwork and for creating a positive research group. I am very grateful to David Taylor of the Victorian Geological Survey, your passion for your work is contagious, and I feel privileged to share in your boundless knowledge of the geology of Victoria. The lambs also thank you for your comments that prompted my vegetarianism.

Thankyou to Goran for keeping the MT instruments in tip-top shape and always being so happy and friendly. To the PhD group, I have truly enjoyed the years spent with you all. Sebastian, Paul and Alison- thank you for your friendship, donut-eating competitions and ultra-marathon running company. Thanks to the many people who have helped to collect my field data on many field trips, it is on these trips that I have forged memories that will last a lifetime- from flying over the Ikara-Flinders Ranges in a helicopter to digging holes in 40-plus degree heat!

Thankyou to my partner Bill, for your constant love and support and your advice on creating a work-life balance- advice which played a large part in my ability to complete my PhD with such a positive mindset. Thankyou to my parents, who have always encouraged and believed in me throughout my entire education and for all the thoughtful things you have done for me when Uni became stressful at times. To my sisters- there are no better friends than both of you. I am truly grateful for how close we all are as a family. I thank my friends for their love and friendship, and their understanding for all of the times when I chose study over them.

It is not possible to thank everyone here who played a part in this journey, but I hope I have shown you my gratitude over the years and I look forward to continuing my geophysical journey with you all.

CHAPTER

ONE

INTRODUCTION

1.1 Contextual Statement

'A predictive understanding of the relationships between ore systems, mantle melting and lithosphere-scale tectonism requires a whole-system approach. It should encompass processes operating in the asthenosphere, lithosphere and crust, and special attention should be paid to the structure, composition, fertility and evolution of the subcontinental lithospheric mantle' (Griffin et al., 2013).

There are many processes that occur within the entire continental lithosphere that are vital to our understanding of the complex 4.6 Ga tectonic history of Earth and our ability to continually discover new resources.

Many of the known mineral deposits are located in regions of outcrop or shallow basement. Despite the ever-depleting historic mineral resources and the ever-increasing demand for minerals, the discovery rate of new mineral deposits within Australia does not meet these urgent demands. The primary reason for this is that approximately 80% of Australia is covered by sedimentary rocks and regolith. Most of the discovered mineral deposits within Australia exist within the minority regions of outcropping or shallow cover. This is because traditional discovery methods include geological mapping, geochemical sampling and relatively shallow geophysical methods and are based around understanding the temperature and pressure conditions within the first few kilometres of the crust.

Traditionally, it has been assumed that the lithospheric mantle has a passive role in the generation of ore deposits, acting merely as a pathway from the asthenosphere to the crust. However, new evidence suggests that the lithosphere plays a much larger role,

with its ability to focus asthenospheric sourced heat, melt and fluids as they transition through the lithosphere (Griffin et al., 2013). It is now thought that the ascending melt and fluids may interact with the lithosphere through which it travels, potentially picking up ore-forming minerals along the way and, potentially, leaving behind a geophysically detectable signature of their path (e.g. Heinson et al., 2006; Jones et al., 2009; Evans et al., 2011; Thiel and Heinson, 2013). These signatures may be retained, giving an insight into the tectonic history of Earth over hundreds of millions of years, but are just as easily erased with the onset of high-temperature tectonothermal or melting events (Demouchy, 2010). In the case of the latter, incompatible elements preferentially partition into partial melt leaving behind a depleted lithosphere, which can be imaged as both electrically resistive and fast seismic velocity regions. Structures that span the lithosphere vertically or sub-vertically may be important to the location of ore deposits and diamondiferous kimberlites. Zones of weakness such as cratonic boundaries or major lithospheric-spanning faults correlate with regions of concentrated base-metal and diamond deposits and often coincide with large gradients of seismic velocity and electrical resistivity (e.g. Jones et al., 2009; Griffin et al., 2013).

1.2 Lithospheric scale surveys

An abundance of geophysical and geochemical datasets cover selected regions or the whole of Australia, to varying depths and with varying resolutions to investigate the lithosphere. Sediment thickness and basement depth is relatively well-known across Australia from the OZ SEEBASE™ model (Frogtech, 2014).

Seismological body waves and surface waves have been utilised in numerous continent-wide studies within Australia, starting in 1993 with the Skippy project which involved a moving array of seismometers across Australia at 400 km spacing (van der Hilst et al., 1994). More recently, information on the seismic structure of Australia has been collated in the AusREM model of the lithosphere to a depth of 350 km which contains P-wavespeeds, S-wavespeeds and densities (Kennett and Salmon, 2012). The target resolution is on the order of half of a degree (approximately 55 km) with an emphasis on linking the more detailed complex crustal structure to longer wavelength mantle features. Together, the seismic projects have determined Moho-depth estimations (Kennett et al., 2011; Salmon et al., 2013; Aitken et al., 2013), anisotropy (e.g. Debayle and Kennett, 2000) and the locations of broad-scale velocity variations linked to major geological boundaries and tectonic histories (e.g. Graeber et al., 2002; Rawlinson et al., 2014b). The continuing collection of deep seismic reflection data across Australia also offers useful but sparse information about faults, folds and boundaries within the lithosphere down to the Moho, but rarely any deeper with results summarized by Kennett and Saygin (2015).

Geochemical data aids the analysis and interpretation of geophysical data by providing the capability to define ages, geotherms and the evolution of the lithosphere. Geoscience Australia's national geochemical dataset offers the ability to identify major

lithologies and mineralization under cover (de Caritat et al., 2011). Expansive work across Australia has provided an insight into: the fertilisation state of the lithosphere in many parts of Australia; the determination of geotherms; and the design of schematic models on lithospheric controls on deposit-formation (e.g. O'Reilly and Griffin, 1988; Griffin et al., 1988; O'Reilly and Griffin, 1985; Foden et al., 2006; Hand et al., 2007; Griffin et al., 2013; Aitken et al., 2015).

Australia-wide magnetic and gravity maps allow identification of faults and domains of differing magnetic and density characteristics but depth of structures is difficult to resolve and scant information regarding the mantle can be obtained from potential methods. Advances in gravity inversion using MoGGIE (Aitken, 2010) have enabled 3D inversions that encompass seismic-defined Moho estimates and laterally heterogeneous crust and mantle. The results image extensive magmatic underplating, crustal shear zones and tectonic boundaries, while showing that little of Australia is in isostatic equilibrium.

1.2.1 Previous EM Studies

Passive electromagnetic methods have the capacity to reveal a great deal about the lithosphere, including information on the fertilisation state, temperature, significant lithospheric pathway structures and tectonic evolution (Chave and Jones, 2012). In the early times of passive electromagnetic methods in Australia, focus was on very large scale surveys of dimension of hundreds of kilometres. Geomagnetic depth sounding (GDS) surveys from which induction arrows (for which the real component points in the direction of increasing conductivity for the Parkinson convention) can be derived have been conducted across the country. Induction arrows were obtained for a 275 km spaced array of GDS sites covering Australia by Chamalaun and Barton (1993) in the AWAGS experiment, who used these to find that the broad shallow conductivity structure of Australia is dominated by major sedimentary basins. These results were progressed by Wang et al. (1997) and Wang and Lilley (1999) who obtained a conductance (the electrical conductivity of a material multiplied by its vertical thickness) map of Australia for the top 10 km and were able to support the notion of large (hundreds of kilometres) conductive anomalies inferred from induction arrow data, such as the Flinders Conductivity Anomaly (Gough et al., 1972). For an early review, see Constable (1990).

In the early 2000's focus turned to the collection of thousands of kilometres of broadband magnetotelluric (MT) transects, usually coinciding with existing seismic reflection transects. Generally collected at a site spacing of about 5 km or less for regional surveys, these transects are ideal for imaging the crust and shallow upper mantle at high resolution. Elsewhere in the world, projects such as Lithoprobe (Jones et al., 2014) in Canada, SAMTEX (Muller et al., 2009) in South Africa and the USarray in the United States of America have demonstrated major contributions to the understanding of the tectonic evolution in these regions, enabling electrical maps of the continent to be derived and inferences of temperature and water content of the lithosphere to be made. From these MT transects in Australia and across the world, generalisations can

be made about the resistivity structure of the lithosphere including a thin conducting sedimentary layer overlaying a resistive upper crust. This brittle upper crust is conductive when intersected by fluid alteration zones (Robertson et al., 2015), partial melt (Aivazpourporgou et al., 2015) or sulphides (Jones et al., 2005). Commonly the lower crust is imaged as less resistive than the upper crust, with these low resistivity zones tending to occur between the brittle-ductile transition zone and the Moho (Thiel et al., 2016).

While MT transects have been shown to provide ample information about a region of interest in 2D, they are fundamentally lacking the ability to resolve the tectonic framework in 3D. Thus, the Australian Lithospheric Architecture Magnetotelluric Project (AusLAMP) commenced in 2013 to fill this knowledge gap, with the intent to collect long-period MT data at sites in a 0.5 degree spaced (~55 km) array across all of Australia, to ultimately obtain a 3D electrical resistivity model of the entire lithosphere. It is only in the last decade or so with advances in computational power and improved 3D modelling capabilities (Siripunvaraporn, 2012) and availability of new codes (Egbert and Kelbert, 2012; Kelbert et al., 2014) that projects such as these (e.g. the USArray; Bedrosian and Feucht, 2014) are possible.

1.3 MT Theory

The origins of the MT method are attributed to Tikhonov (1950) and Cagniard (1953). For a detailed description of the MT method see Chave and Jones (2012) and Simpson and Bahr (2005). MT is a passive EM technique capable of determining the electrical resistivity structure of the Earth down to hundreds of kilometres. Electromagnetic fields with periods shorter than 1 s (frequencies greater than 1 Hz) arise from signals discharged by lightning and fluctuations with periods longer than 1 s (frequencies lower than 1 Hz) originate from interactions between the solar wind Parker (1958) and the Earth's magnetosphere and ionosphere. The variations in the natural magnetic fields and induced electric fields are measured in orthogonal directions at the Earth's surface. These natural variations occur across a period range of 10^{-3} to 10^{5} s (or frequencies of 10^{3} to 10^{-5} Hz), with low amplitudes between frequencies of 0.5-5 Hz known as the dead-band. Dependent on the target depth of investigation, either broadband MT (period 0.001-2000 s; ideal for crustal studies), or long-period MT (1-20 000 s; suited to full lithosphere studies) can be collected. Penetration depths depend on the EM sounding period and the Earth's resistivity structure. The depth of signal penetration approximately equals one skin depth (the depth at which EM fields are attenuated to e^{-1} of their surface amplitude). The skin depth δ(T) in simplified form is given by;

$$\delta(T) \approx 500\sqrt{T\rho_a} \tag{1.1}$$

where ρ_a is the averaged resistivity over periods shorter than T. In the frequency domain, complex impedances describe the natural fluctuations of the electric (**E**) and

magnetic fields (**H**). The impedance tensor **Z** is defined as:

$$\begin{pmatrix} E_x \\ E_y \end{pmatrix} = \begin{pmatrix} Z_{xx} & Z_{xy} \\ Z_{yx} & Z_{yy} \end{pmatrix} \begin{pmatrix} H_x \\ H_y \end{pmatrix} \tag{1.2}$$

where x is the north-south direction and y is the east-west direction.

For a 1D resistivity structure where resistivity only varies with depth, the diagonal components can be summarised as $Z_{xy} = -Z_{yx} = Z$, $Z_{xx} = Z_{yy} = 0$. For a 2D structure resistivity varies with depth and in one direction laterally, remaining constant in the other horizontal direction. For 2D resistivity the impedance tensor can theoretically be rotated to an angle known as the geo-electric strike, to eliminate Z_{xx} and Z_{yy}. The Z_{xy} is then referred to as the transverse electric (TE) mode, and has the electric field parallel to the strike, and the Z_{yx} is the transverse magnetic (TM) mode which has the magnetic field parallel to the strike. However in practice, the off-diagonal components are only minimised rather than eliminated.

The apparent resistivity ($\rho_{a_{ij}}(\omega)$ where $\omega = 2\pi f$ is the angular frequency), is the average resistivity represented by a uniform half-space sounded by period, T, where $T = \frac{1}{f}$, and is given by the equation:

$$\rho_{a_{ij}}(\omega) = \frac{1}{\mu_0 \omega} |Z_{ij}(\omega)|^2. \tag{1.3}$$

The phase (component of **Z**, Φ_{ij}) represents the phase difference between the electric and magnetic fields that are used to calculate the MT impedance, and is equal to:

$$\Phi_{ij} = \tan^{-1} \frac{\Im\{Z_{ij}\}}{\Re\{Z_{ij}\}}. \tag{1.4}$$

For a uniform half-space, impedance phases are 45° . Phase angles exceeding 45° are indicative of resistivity decreasing with depth, and impedance phases less than 45° means the subsurface is becoming more resistive with depth.

1.3.1 Phase Tensor Theory

The analysis of the phase tensor is an important task to undertake prior to performing inversion of the data. The phase tensor is useful as it is unaffected by galvanic distortion or static shift (Caldwell et al., 2004; Bibby et al., 2005; Booker, 2014), and requires no assumption about the resistivity dimensionality. The phase tensor,Φ is represented by the equation

$$\mathbf{\Phi} = \mathbf{X^{-1}Y}, \tag{1.5}$$

where **X** and **Y** are the real and imaginary components of **Z**. The coordinate invariants of the phase tensor are the minimum and maximum phases and the skew angle. For 1D regional electrical resistivity structures, the phase tensor is represented by a single

coordinate invariant phase equal to the 1D impedance tensor phase. For 2D regional electrical resistivity, the phase tensor is symmetric with one of its principal axes aligned parallel to the regional strike. The geoelectric strike is the preferred direction of current flow and is given by α or $\alpha + 90$ (as there is ambiguity between the two principal axes Caldwell et al., 2004), where:

$$\alpha = \frac{1}{2}\tan^{-1}\frac{\Phi_{xy} + \Phi_{yx}}{\Phi_{xx} - \Phi_{yy}}. \tag{1.6}$$

In the 3D case the phase tensor is non-symmetric and a third coordinate invariant, the skew (β), is introduced. The skew is a measure of the asymmetry of the regional MT response, and is given by:

$$\beta = \frac{1}{2}\tan^{-1}\frac{\Phi_{xy} - \Phi_{yx}}{\Phi_{xx} + \Phi_{yy}}. \tag{1.7}$$

The phase tensor is commonly represented graphically by an ellipse (Caldwell et al., 2004), which gives an indication of data dimensionality and strike direction. The major and minor axes of the ellipse represent the principal axes of the tensor. The orientations of the phase tensor principal axes reflect lateral variations (gradients) in the regional resistivity structure.

1.3.2 Geomagnetic Depth Sounding

Geomagnetic depth sounding was developed when Schuster and Lamb (1889) showed the existence of induced magnetovariational fields. GDS involves the measurement of the horizontal and vertical components of the magnetic field (H_x, H_y, H_z). The magnetic field transfer function is defined as follows;

$$\begin{pmatrix} H_z \end{pmatrix} = \begin{pmatrix} T_{xz} \\ T_{yz} \end{pmatrix} \begin{pmatrix} H_x \\ H_y \end{pmatrix}. \tag{1.8}$$

The advantage of not measuring the electric fields in GDS is immunity from the effects of local distortions of the electric field, manifest as static shift (Jones, 1988) and galvanic distortion (Bibby et al., 2005). A reference station outside of the survey area is used to improve signal to noise ratios (Gamble et al., 1979). GDS can probe over scale-lengths both laterally and vertically of a few hundred kilometres, as it detects lateral variations in resistivity. However, absoulute resistivity values cannot be determined and vertical resolution is poor compared to MT.

The vertical magnetic field transfer function can be expressed by the induction vector, $\vec{K}$, defined by;

$$H_z = -\vec{K} \cdot \mathbf{H}. \tag{1.9}$$

For a 2D resistivity structure, the real part of $\vec{K}$ points in the direction of increasing resistivity (this is the Wiese convention; Wiese, 1962). The vertical magnetic fields

(H_z) are generated by lateral resistivity gradients, so induction arrows can be used to infer the presence or absence of lateral variation in resistivity (Gregori and Lanzerotti, 1980). The Parkinson convention involves reversal of the induction arrows and is most commonly used (Parkinson, 1959), with arrows pointing towards conductive bodies. The length of the arrow is determined by a combination of the magnitude of the anomaly and its distance from the MT site, with range increasing for longer periods.

1.4 Factors that affect resistivity

1.4.1 Basins and Regolith

The resistivity of the brittle upper crust is primarily governed by porosity and permeability, and the presence of saline fluids and clay minerals. Sedimentary basins and regolith are generally comprised of young, unconsolidated sediments imaged with low resistivities ranging from ~1-100 Ωm due to high porosities (up to 50%; Freeze and Cherry, 1979) and permeabilities. Their low resistivities attenuate signal, decreasing skin depth substantially in regions of thick cover and often distorting the signal (Jones, 1988). Clay lithology can significantly reduce resistivity by surface conduction mechanisms (Simpson and Bahr, 2005).

1.4.2 Upper Crust

Generally the upper crust is quite resistive with a bulk resistivity on the order of ~10^3-10^5 Ωm (Gough, 1986). Older sedimentary rocks have likely been buried and compacted, and porosities will reduce to less than 5% (Freeze and Cherry, 1979) giving a resistivity of 10-1000 Ωm (Chave and Jones, 2012).

Interconnected saline fluids in upper crustal shear zones can reduce resistivity via electrolytic conduction, to the order of 0.1-1 Ωm. Grain boundary graphite films are stable below temperatures of 600-900°C and are likely to explain many low resistivity regions (reducing resistivity by one to two orders of magnitude; Glover, 1996; Yoshino and Noritake, 2011). Within the upper crust, this graphite may occur within biogenic carbonaceous black shales (Duba et al., 1988), with its ability to form at low crustal temperatures (possibly less than 450°C) likely due to shear stress (Ross and Bustin, 1990).

1.4.3 Lower Crust

The depth of the brittle-ductile transiton is dependent on the geotherm, but generally occurs at around 15 km. Studies on the resistivity of the lower, ductile crust are well-summarised in Shankland and Ander (1983); Jones (1992) and Yang (2011). Resistivity varies greatly from region to region between ~1-500 Ωm (Haak and Hutton, 1986; Jones, 1992; Yang, 2011), but in many places is substantially lower than the upper crust and

the shallow upper mantle. Resistivity values at the lower end are not explained by laboratory measurements of electrical resistivity on common lower-crustal minerals such as orthopyroxene and plagioclase (Yang et al., 2012; Fuji-ta et al., 2004). Instead, the presence of minor conducting phases such as graphite (Glover, 1996; Frost et al., 1989) and water (Yoshino et al., 2009, 2010) are invoked to explain low resistivities. Free fluids are not expected to exist in the mid-lower crust of stable lithosphere due to closed pore-space (Connolly and Podladchikov, 2004), although fluids can be generated under low strain conditions from metamorphic breakdown reaction of hydrous phases (Thiel et al., 2016). In active tectonic regions, partial melt can enhance conductivity through electrolytic conduction by 1-2 orders of magnitude (e.g. Maumus et al., 2005; Unsworth, 2010), and supplementary knowledge of coincident conductors with high heat flow and low velocity zones can increase confidence in identifying partial melt zones (e.g. Wei, 2001; Unsworth et al., 2005). Graphite can decrease resistivity in the lower crust, with some possible sources including subduction-related fluids and melts, initiated by the release of water bound in the structure of hydrous minerals in the down-going slab (Peacock, 1990), and degassing of CO_2-rich kimberlitic melts (Pearson et al., 1994). Lastly, at lithospheric temperatures and pressures, the presence of hydrogen in nominally anhydrous minerals can significantly enhance conductivity and is stable throughout the lower crust and entire lithospheric mantle (Karato, 1990).

1.4.4 Sub-continental Lithospheric Mantle

Olivine makes up 60-70% of the upper mantle, however observed resistivities obtained from MT (on the order of 10^1 to 10^3) are one to two orders of magnitude lower than those of dry olivine laboratory studies (Constable et al., 1992; Constable, 2006; Wang et al., 2006; Yoshino et al., 2006, 2009). Reviews of both laboratory measurements and MT-derived values of upper mantle resistivity can be found in Yoshino (2010); Jones et al. (2012); Pommier (2014) and Selway (2014). Studies suggest hydrogen diffusion within olivine (Karato, 1990, 2006) and the other major mantle constituents- garnet (Dai et al., 2012; Mookherjee and Karato, 2010; Yoshino et al., 2008), orthopyroxene (Dai and Karato, 2009; Yang et al., 2012) and clinopyroxene (Yang et al., 2011) is the cause for decreased resistivities in the lithospheric mantle.

Tectonothermal and partial melting events can leave a depleted and resistive mantle behind, as high temperatures will result in graphite becoming unstable, and partial melting will result in hydrogen behaving as an incompatible element that will preferentially partition into partial melt. On the other hand, refertilisation, and resultant enhanced conductivity, can occur from metasomatism by fluids or melts enriched in incompatible elements, emphasising the importance of considering the state of enrichment of the lithosphere when interpreting conductive anomalies.

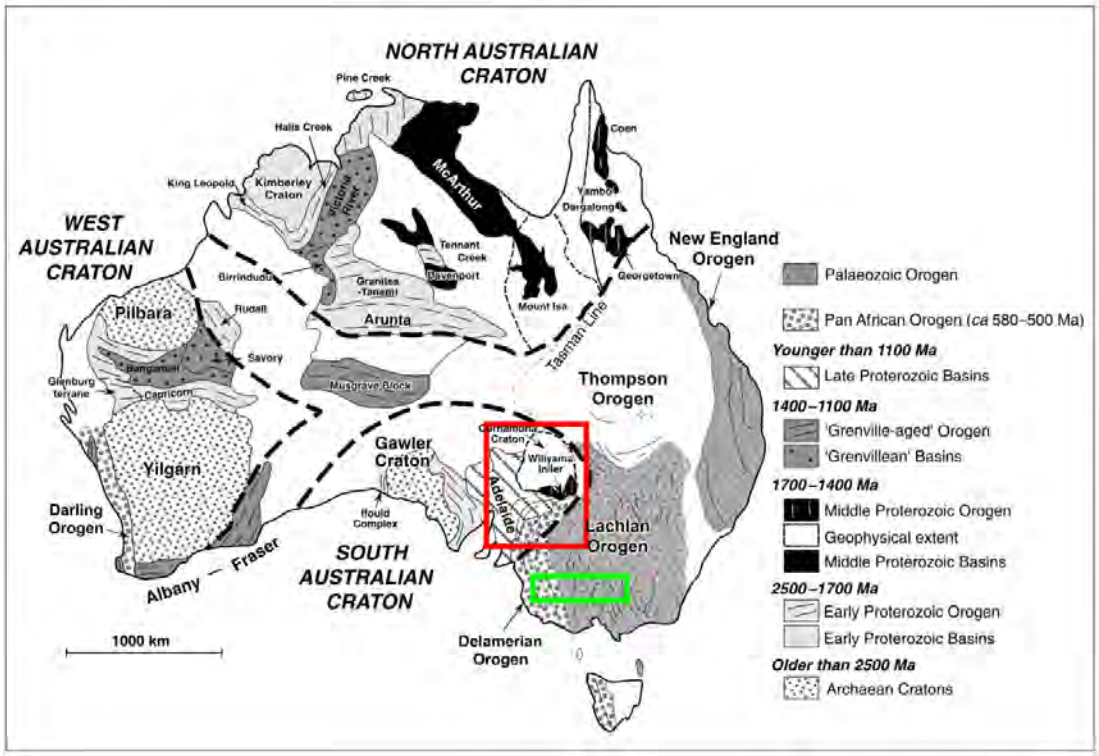

Figure 1.1: Terrane map of Australia showing the western Archaean to Proterozoic regions, and the eastern Palaeozoic Tasmanides. Green box outlines the survey area of Chapter 2 and 3. Red box outlines survey area of Chapter 4. Adapted from Betts et al. (2002).

1.5 Geological and Geophysical Background

Australia hosts some of the longest tectonic records on Earth, with zircons found in the Yilgarn Craton, Western Australia dating back to over 4.4 Ga (Wilde et al., 2000). The western two-thirds of Australia consists of the Archaean-Proterozoic, or Precambrian, Australia, at which Phanerozoic orogenic belts have accreted forming the eastern part of Australia, collectively termed the Tasmanides (Figure 1.1).

In southeast Australia the Tasmanides mostly consist of the Delamerian and Lachlan Orogens. The transition from Proterozoic to Phanerozoic Australia is mostly difficult to pinpoint due to widespread cover such as the Mesozoic to Cenozoic metasedimentary and metavolcanic rocks across western Victoria (Glen, 2005). The Tasman Line spans Australia from north to south and is delineated by the eastern-most outcrops of contiguous Proterozoic rocks (Direen and Crawford, 2003), although outlying Proterozoic blocks exist within the Tasmanides. Seismic wavespeed models show a transition in wavespeeds (from faster in the west to slower in the east) occurring beneath the Stawell Zone at depth, suggesting the Proterozoic basement may extend beneath parts of the Tasmanides in southeast Australia (Rawlinson et al., 2014b).

The location of the transition between the Delamerian and Lachlan Orogen is debated (Miller et al., 2005) but the east-dipping Moyston Fault appears to be of particular sig-

nificance from seismic reflection data (Korsch et al., 2002), seismic tomography (Graeber et al., 2002) and Sr isotope data (Price et al., 1997). The Mortlake Discontinuity roughly coincides with the Moyston Fault, and represents a boundary across which the Sr isotope ratio changes from a lower $^{87}Sr/^{86}Sr$ in the west to higher in the east. Graeber et al. (2002) image a 2% decrease in P-wave velocity from the Delamerian Orogen to the Lachlan Orogen at a latitude of 36-38 °S, to a depth of around 200 km, which they attribute partly to compositional variation. While the Moyston Fault continues further south than these latitudes, the velocity increase does not, which the authors attribute to reworking of the lithosphere from one of the more recent events to affect the region. These include the breakup of Australia and Antarctica at 90 Ma which involved the opening of the Tasman Sea and Bass Strait, and the hot-spot volcanics of the Pliocence-Pleistocene basalts known as the Newer Volcanic Province (Johnson, 1989), imaged in seismics as a low velocity anomaly (e.g. Graeber et al., 2002; Rawlinson et al., 2011) and in MT as a low resistivity region (Aivazpourporgou et al., 2015).

The Delamerian Orogeny commenced at 514 Ma from a postulated westward dipping subduction zone, indicated by the presence of boninites (a rare igneous rock found above subducting plates) found in the Grampians-Stavely Zone (Foden et al., 2006). Subduction ceased at 490 Ma with the onset of an extensional regime and possible slab rollback. In addition to the orogeny altering western Victoria, its effects reached as far west as the Adelaide Fold Belt and may extend south into Tasmania where it is known as the Tyennan Orogeny. The Adelaide Fold Belt includes the thick Neoproterozoic to Cambrian rift sediments of the Ikara-Flinders Ranges, covering Palaeo-Mesoproterozoic basement (Preiss, 2000). The Ikara-Flinders Ranges is an intraplate deformation region that was affected by several rift phases between 827-700 Ma, with cessation corresponding with basin formation. The rift-associated normal faults were reactivated during the Delamerian Orogeny as thrust faults, despite residing west of the Tasman Line.

The Ikara-Flinders Ranges have relatively high levels of seismicity for an intraplate region, with the cause unknown. Suggestions of a thermally weakened area (Holford et al., 2011) due to high surface heat flow of the South Australian Heat Flow Anomaly (average heat flow of 92 ± 10 mW/m^2; Neumann et al., 2000) can explain upper crustal seismic activity, but struggle to explain the lower crustal earthquakes that would occur in crust of ductile nature. Mechanically weakened lithosphere is suggested through a variety of different models (Célérier et al., 2005; Dyksterhuis and Müller, 2008; Pilia et al., 2013), and most recently hypothesised is that high pore fluid pressue in lower crustal rocks may account for fault slip and lower crustal earthquakes (Balfour et al., 2015).

To the north east of the ranges lies the Palaeo-Mesoproterozoic Curnamona Province, an almost-circular region easily identifiable from magnetic and gravity data (Robertson et al., 1998). The province was initially thought to be unaffected from the Delamerian Orogen and so was named the Curnamona Cratonic Nucleus, until it was realised that the Delamerian Orogeny indeed altered at least the edges of the Province. A high seismic velocity anomaly beneath the Curnamona Province extends to at least 200 km, indicating a deep Archaean root to the province, with results also suggesting

the province extends about 100 km further south than the upper crustal expression (Rawlinson et al., 2011). The Curnamona Province is believed to have once been connected to the Gawler Craton prior to rifting, with seismic results showing the lithosphere of the craton and the province may still be connected at depth (Pilia et al., 2013). The Benagerie Volcanics of the Curnamona Province have similar ages to the Gawler Range Volcanics of the Gawler Craton with both erupting within 10 Ma of each other at 1595 Ma (Wade et al., 2012).

Shortly after the Delamerian Orogeny ceased, the Lachlan Orogen was accreted outboard, with orogenesis spanning 485 Ma to 340 Ma (Kemp et al., 2009). The composition of the Lachlan Orogen lithosphere has been debated between wholly oceanic, or oceanic with some continental components. Recently, a low velocity region has been identified around the Bass Strait and southern Victoria, supporting predictions of Proterozoic continental material, the Selwyn Block, encompassed by oceanic lithosphere (Pilia et al., 2015; Cayley, 2011). The Selwyn Block may have caused the orogen parallel subduction to enter slab-rollback phase and the eventual formation of the large orocline that exists today in central Victoria (Moresi et al., 2015).

Griffin et al. (1988) infer from xenolith data that the thickness of the lithosphere beneath Phanerozoic Australia would not exceed 100 km, but may reach up to 140 km beneath the Proterozoic Delamerian Orogen. The AusMoho model predicts a crustal thickness of around 35-40 km in the Delamerian Orogen part of western Victoria and the Ikara-Flinders Ranges, thickening to around 40 km at the Lachlan Orogen and within the Curnamona Province (Salmon et al., 2013; Kennett et al., 2011).

1.6 Objectives

This project aims to address many questions about the lithosphere, employing case studies from two different regions of southeast Australia. Across western Victoria, extensive reprocessing, modelling and interpretation of existing broadband datasets has been undertaken, resulting in a model of the electrical resistivity to a depth of 100 km along a 500 km east-west profile traversing the eastern Delamerian Orogen and the western Lachlan Orogen (published as Robertson et al., 2015) and as submitted paper, 'The lithospheric structure of the transition between the Delamerian and Lachlan Orogens: New insights from 3D magnetotelluric imaging,' (Robertson et al., 2016a). The second case study involves the Ikara-Flinders Ranges and the Curnamona Province of South Australia, where 74 long-period MT sites were collected across a ~55 km spaced array as part of the Australian Lithospheric Architecture Magnetotelluric Project (AusLAMP). Processing and modelling of this data has led to a 3D model of the electrical resistivity structure down to ~200 kms (published as Robertson et al., 2016b).

The project aims to help unravel the complex tectonic history of Australia by using electrical resistivity to gain new knowledge on the entire lithospheric column beneath the survey regions and, more specifically, to answer the following questions:

- What can the electrical resistivity structure of the Australian lithosphere tell us about the tectonic evolution of Australia?
- Does electrical resistivity agree with seismologically and geochemically defined boundaries and help to resolve the locations of boundaries between Palaeozoic orogens in eastern Australia?
- Can electrical resistivity give insight into the cause of intraplate deformation and seismicity?
- What can we understand about the link between upper mantle and crustal resistivity heterogeneity?
- What is the cause of major conductivity anomalies inferred from GDS data, and over what length scale do they exist?

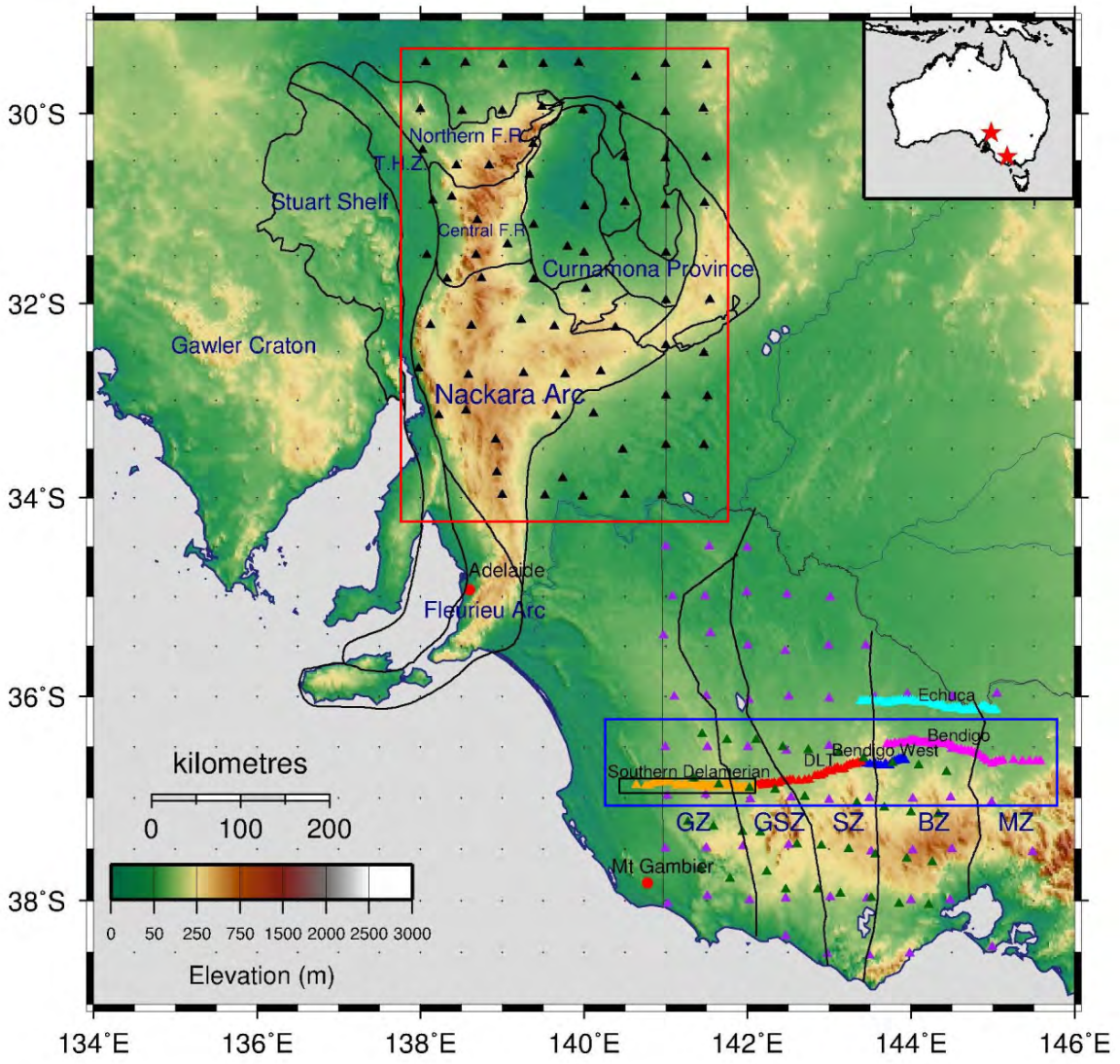

Figure 1.2: Overview map of MT sites locations used in each Chapter. Rectangles correspond to Chapter survey regions; Chapter 2: Black, Chapter 3: Blue, Chapter 4: Red.

CHAPTER

TWO

MAGNETOTELLURIC EVIDENCE FOR SERPENTINISATION IN A CAMBRIAN SUBDUCTION ZONE BENEATH THE DELAMERIAN OROGEN, SOUTHEAST AUSTRALIA

Robertson, K.[1], Taylor, D.[2], Heinson, G.[1], Thiel, S.[1,*]

[1]Electrical Earth Imaging Group, Department of Earth Sciences,
School of Physical Sciences, University of Adelaide, Adelaide SA 5005, Australia
[2] Geological Survey of Victoria, Department of Economic Development, Jobs, Transport and Resources, Melbourne, Victoria 3001, Australia
$*$ *now at* Geological Survey of South Australia, Department of State Development, Adelaide SA 5000, Australia

Published on 30th September, 2015 as:
Robertson, K., Taylor, D., Thiel, S. and Heinson, G. (2015) Magnetotelluric evidence for serpentinisation in a Cambrian subduction zone beneath the Delamerian Orogen, southeast Australia. *Gondwana Research*, 28(2):601-611. doi: 10.1016/j.gr.2014.07.013

Statement of Authorship

+Title of Paper	Magnetotelluric evidence for serpentinisation in a Cambrian subduction zone beneath the Delamerian Orogen, southeast Australia
Publication Status	☑ Published ☐ Accepted for Publication ☐ Submitted for Publication ☐ Unpublished and Unsubmitted work written in manuscript style
Publication Details	Robertson, K., Taylor, D., Thiel, S. and Heinson, G., 2015. Magnetotelluric evidence for serpentinisation in a Cambrian subduction zone beneath the Delamerian Orogen, southeast Australia. Gondwana Research, 28, 601–611.

Principal Author

Name of Principal Author (Candidate)	Kate Robertson
Contribution to the Paper	Performed data collection, processed, modelled and interpreted data. Wrote the manuscript and acted as corresponding author.
Overall percentage (%)	80 %
Certification:	This paper reports on original research I conducted during the period of my Higher Degree by Research candidature and is not subject to any obligations or contractual agreements with a third party that would constrain its inclusion in this thesis. I am the primary author of this paper.
Signature	Date 8/9/16

Co-Author Contributions

By signing the Statement of Authorship, each author certifies that:

i. the candidate's stated contribution to the publication is accurate (as detailed above);

ii. permission is granted for the candidate in include the publication in the thesis; and

iii. the sum of all co-author contributions is equal to 100% less the candidate's stated contribution.

Name of Co-Author	David Taylor
Contribution to the Paper	Assisted with field data collection, helped with geological interpretation of data and manuscript evaluation.
Signature	Date 12/9/16

Name of Co-Author	Stephan Thiel
Contribution to the Paper	Supervised development of work, helped in data interpretation and manuscript evaluation.
Signature	Date 12/09/16

Name of Co-Author	Graham Heinson
Contribution to the Paper	Supervised development of work, helped in data interpretation and manuscript evaluation.
Signature	Date 8 SEPT 2016

SUMMARY

The Delamerian Orogen in southeast Australia represents a Proterozoic continental rift margin, overprinted by convergent margin Andean-style subduction in the Cambrian. A detailed 150 km east-west magnetotelluric transect was collected across the orogen to investigate the electrical resistivity structure. The magnetotelluric transect follows an existing full crustal reflection seismic transect, of which interpretations support a westward-dipping Cambrian subduction model as derived from field mapping and geochemistry. A 2D inversion of the data from the 68 station broadband magnetotelluric transect imaged a heterogeneous crust with lateral changes as large as 10,000 Ωm occurring over ~15 km. The crust within the western Glenelg Zone is resistive, in contrast to the eastern Glenelg Zone and the Grampians-Stavely Zone (above the paleo-subduction zone), which host three conductive pathways. The main low resistivity regions (~1-10 Ωm) reside at mid-lower crustal depths (~10-30 km), extending up to the surface with a higher resistivity (~300 Ωm), but still much less than surrounding resistivity (mantle ~1000 Ωm, crust ~10,000 Ωm). Fluids released from the upper mantle during the Cambrian west-dipping subduction are interpreted to have moved up crustal faults to create the observed low resistivity pathways by serpentinisation and magnetite creation in mafic-ultramafic rocks. The electrical conductivity of hand samples of serpentinised mafic-ultramafic rocks in the region was found to be much greater than most other rock types present. In addition to adding insight into the crustal structure, the magnetotelluric data also supports geological surface mapping, as the major Lawloit and Yarramyljup faults that bound different geological domains also mark domains of different electrical structure.

2.1 Introduction

Magnetotellurics (MT) has proven an effective tool to image modern subduction zones, as the technique is particularly sensitive to the presence of interconnected conducting materials, such as the free fluids found in subduction regions (e.g. Jödicke et al., 2006; Wannamaker et al., 2009; Worzewski et al., 2011). The fluid systems are complex, but can be broadly categorised into two main types. At crustal depths, large amounts of pore waters and CH_4-H_2O rich fluids are released from diagenetic and low-grade metamorphic reactions of the subducting oceanic material. At sub-crustal depths (greater than ~40 km), metamorphic reactions in the subducting oceanic crust release H_2O and CO_2 up into the overlying mantle wedge. Hydration and carbonation reactions from these fluids in the wedge can induce partial melting and cause serpentinisation (Peacock, 1990). Such partial melts and serpentinisation have been interpreted as the cause for low resistivity (high conductivity) regions observed in active subduction zones from MT studies around the world (e.g. Kurtz. et al., 1986; Jödicke et al., 2006; Wannamaker et al., 2009; Reynard et al., 2011; Worzewski et al., 2011). This study provides evidence that these serpentinite signatures that contribute to low resistivity regions within active subduction zones may still be apparent within the electrical structure of an ancient subduction zone - in this case - the Cambrian Delamerian Orogen.

The latest tectonic model for the Delamerian Orogen (515-500 Ma) invokes initiation of a convergent Cambrian west dipping Andean-style subduction setting overprinting an earlier rifted continental margin (Kemp, 2004; Foden et al., 2006). The preliminary interpretation of a recent full crustal seismic reflection line (the 2009 L193 AuScope 09GA-SD1 Southern Delamerian seismic line; Cayley et al., 2011a,b) shows a crustal framework remarkably consistent with that predicted by the Andean subduction model (Fig. 2.1).

To investigate the electrical resistivity structure of the Delamerian Orogen, a 150 km east-west transect of 68 broadband MT stations was collected in two stages. In 2010, 29 stations were collected at 5 km spacing along the full seismic transect. In 2012, an additional 39 stations in-filled the eastern half of the transect to 1.5 km spacing, to better match the greater complexity of the geology in the east as seen in the seismic reflection interpretation.

The 2D MT inversion using Occam (Constable et al., 1987; de Groot-Hedlin and Constable, 1990) produced an image of the crustal resistivity that correlates well to the crustal framework interpreted from surface mapping and the seismic reflection studies. The MT images several regions of anomalously low resistivity within a highly reflective mid-crustal seismic package. These anomalies are within low resistivity pathways appearing to emanate up from the mantle. Their location is consistent with fluid movement upwards from an inferred west dipping subducting slab operating in the Cambrian, when the present day crustal architecture was assembled. Faults at the surface hosting variably serpentinised mafic-ultramafic rocks can be traced downwards

into the mid-crustal reflective package that hosts the anomalies.

Magnetite is a conductive mineral known to form during serpentinisation. It is documented in the exposed mafic-ultramafic packages and is thus a likely contributor to the anomalies. Where alteration is intense and interconnectivity of the magnetite is enhanced by shearing, very low resistivities, as observed in the anomalies, could be created (Kawano et al., 2012). Measuring of fresh rocks and drill core with a hand held electrical conductivity meter shows that the serpentinised mafic-ultramafics can be much less resistive than the other regional rock types (~10-50 Ωm versus ~100-1000 Ωm).

2.2 Geological Background

The Cambrian Delamerian Orogen (515-500 Ma) is the oldest part of the Phanerozoic Tasman Fold Belt system which now forms the continental crust of eastern Australia (Coney et al., 1990; Foster and Gray, 2000; Glen, 2005). The Tasmanides were oceanic terranes and microcontinental blocks accreted from the paleo-Pacific, back onto an older Proterozoic continental margin. The rocks in the Delamerian Orogen include the Adelaide Geosyncline, a thick passive margin sequence related to the break-up of the pre-existing Proterozoic continent (see Preiss (2000) and Foden et al. (2001) for description of the succession and its evolution).

The western (inboard) portion of the orogen is well exposed in the Adelaide Hills where the platformal to deep marine passive margin sequence has been thrust westward back onto the older craton as a foreland fold and thrust belt (Jenkins, 1990). Much of the central portion of the orogen is hidden under younger cover sequences (Cretaceous to Cenozoic Otway and Murray Basins) but continuity to the eastern (outboard) portion is provided by the magnetic marker beds of the basaltic Truro Volcanics which are traceable under the shallow central cover (Morand et al., 2003).

The MT and seismic data were collected over the exposed outboard portion (Figs. 2.2 and 2.3) where detailed geological mapping (Gray et al., 2002; Kemp et al., 2002; Morand et al., 2003) confirmed early reconnaissance and compilation work showing two very distinct geological zones (VandenBerg, 1978). The Glenelg Zone to the west comprises a Buchan-type metamorphic terrane of deep marine clastics, shale and rare basalt that have been strongly deformed and experienced voluminous granite intrusion with migmatite formation at amphibolite grade. The Grampians-Stavely Zone to the east is a complete contrast, with only weak deformation and low greenschist metamorphism. Its clastic marine sequences have distinctive in-faulted belts of Mt Stavely andesite volcanics erupted in a submarine setting. The Grampians are a younger Silurian redbed cover that have no bearing on the Cambrian deformation history.

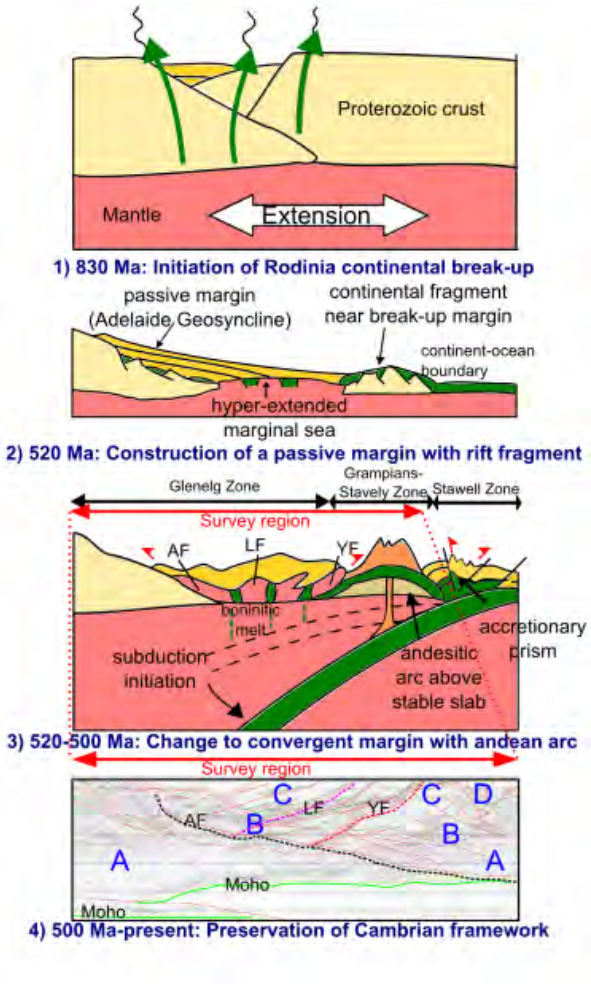

Figure 2.1: AF= Apsley Fault, LF = Lawloit Fault, YF = Yarramyljup Fault. 1) About 830 Ma the onset of continental rifting is marked by initial deposits of Adelaide Geosyncline sequence which include episodic eruption of rift basalts. 2) By 520 Ma post continental break-up has allowed a thick passive margin sequence to accumulate on the hyperextended marginal sea with an outboard continental fragment near the transition to the developing paleo-Pacific ocean. 3) By 515-500 Ma initiation of Andean subduction (into mantle depleted by previous rift volcanism) spawns early phase of boninitic melt intrusion. The slab stabilises against the continental fragment and leads to: the hot, newly formed back-arc region undergoing shortening (Glenelg Zone); a mature calcalkaline andesitic arc developing (Grampians-Stavely Zone) and an accretionary prism growing (Stawell Zone). 4) This Cambrian crustal architecture is still visible today in the seismic data. A) Transparent continental basement crust is interpreted to be the lower crust in the west and east. B) Regions of reflective mid-crust in the centre interpreted as packages of deformed maficultramafic rocks. C) Transparent upper crust of largely metamorphosed sedimentary rocks with rare fault slices of maficultramafics. D) The Andean Arc edifice is interpreted as the semi-reflective package high in the east.

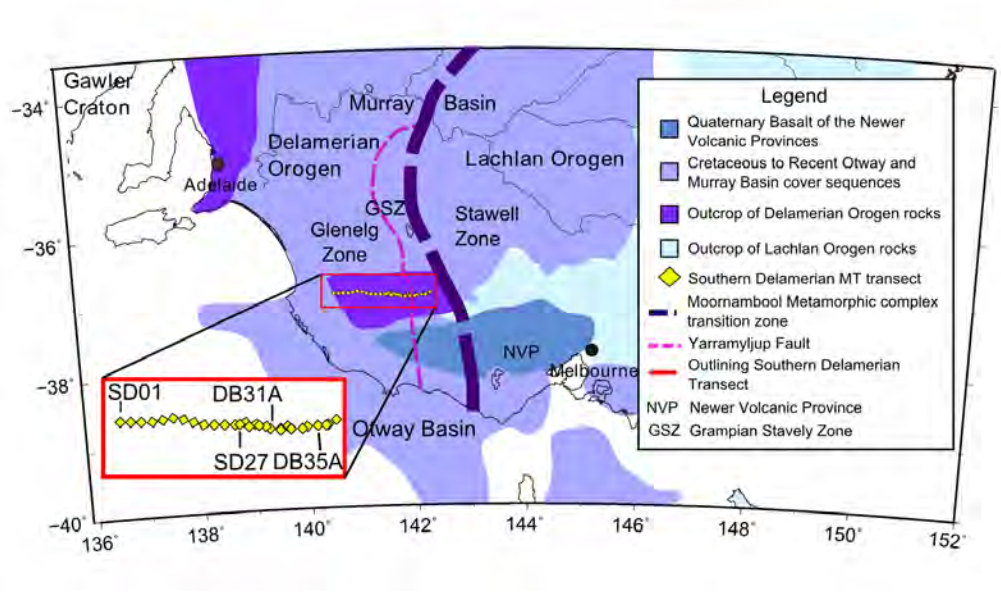

Figure 2.2: Simplified geological map showing basins and cover sequences. The location of the Southern Delamerian MT transect is indicated in yellow. Labelled stations SD01, SD27, DB31A and DB35A will be used in a later figure. The transect crosses the Glenelg and the Grampians-Stavely zones. Adapted from Rawlinson and Fishwick (2012).

Fault slivers of serpentinised mafic-ultramafic rocks occur across this outboard region. The Hummocks Serpentinite in the Glenelg Zone has geochemistry and texture indicative of depleted mantle but other slivers in the Grampians-Stavely Zone seem to be primitive boninitic lavas and cumulates. Their presence led to a tectonic model suggesting that the slivers are remnants of obducted ophiolite emplaced during an arc-continent collision that caused the Delamerian deformation (Turner et al., 1993; Crawford et al., 2003).

More recent geochemical work has developed a new tectonic model (Foden et al., 2006). The Hummocks Serpentinite in the Glenelg Zone is now interpreted as being mantle exhumed during passive margin hyper-extension, with later incorporation into the crust during convergent margin deformation above Andean-style subduction. This model of tectonic switching between episodes of extension then convergence driven by slab-rollback or advancements has already been suggested for the creation of much of the Tasmanides (Collins, 2002).

Mafic magmas intruded into the Glenelg Zone appear to have thermally weakened this region, causing it to undergo significant crustal shortening during the Delamerian Orogeny (Sandiford et al., 1992). Some of these mafic magmas have boninitic geochemistry diagnostic of subduction initiation, as the hydrated slab first plunges into hot depleted mantle (Kemp, 2003, 2004; Foden et al., 2006). As subduction progresses, mantle counter flow in the wedge replaces the depleted mantle with new material and

the mantle geotherm is suppressed by the cold subducting slab, generating more typical arc magma.

The calc-alkaline andesites of the Mount Stavely Volcanics in the Grampians-Stavely Zone mark this maturing development of the subduction zone into a true Andean arc. These andesites have geochemistry indicative of subduction, with low abundances of high field strength rare earth elements within an overall enrichment trend (Whelan et al., 2007). Mineralised copper porphyry prospects of Cambrian age in this region (Rajagopalan, 1999) are also typical of Andean margins.

In the new subduction model (Foden et al., 2006) and as imaged in the seismic profile (Cayley et al., 2011a,b), the more outboard Grampians-Stavely Zone is interpreted to be floored by a thin fragment of Proterozoic continental crust. This block likely rifted from the main continent during the passive margin formation prior to subduction. Such continental ribbons are a common outcome of hyper-extended rifted margins (Brun and Beslier, 1996; Reston, 2009). This continental basement buttress explains why the Cambrian rocks in this region have suffered less deformation and lower metamorphic grades than the adjacent Glenelg Zone.

The stabilisation of the subduction zone against the continental basement block beneath the Grampians-Stavely Zone transferred the compressive convergent force into the Glenelg Zone, recently thermally weakened by the boninitic magma injection. This region thus accommodated the bulk of the deformation and started to thicken and overthrust the continental margin to the west and continental block to the east, bringing some slivers of the mafic-ultramafics to the surface.

Outboard of the Grampians-Stavely Zone (and east of the MT transect) is the Moornambool Metamorphic Complex of the Stawell Zone (Fig. 2.3). Dating of the metamorphism at 500 Ma shows that it is part of the Delamerian Orogeny and not the younger Lachlan Orogeny as thought earlier. The dating allows the complex to be interpreted as the subduction-accretion prism forming contemporaneously to the subduction magmatism further west (Miller et al., 2005).

The subduction and deformation of the Cambrian Delamerian Orogeny effectively accreted this region back onto the continental margin so that the Tasmanide deformation front moved further east. Rapid uplift, erosion, and a late pulse of 490 Ma A-type granite magmatism mark the end of tectonism on the Delamerian margin (Foden et al., 2006).

Thus the MT and seismic data image a region of crust that has recorded remarkably little disturbance since the Cambrian. Three later geological events have potentially caused some disturbance but not enough to disrupt the crustal architecture assembled in the Cambrian. Deformation of the Silurian Grampians group included some

basement wrench faulting (Cayley and Taylor, 1997) and current Geological Survey of Victoria mapping shows that these faults are more widespread than initially mapped. The continental breakup of Australia and Antarctica occurred about 100 km to the south at about 90-50 Ma (Gaina et al., 1998), and this potentially caused some lithospheric thinning and mafic underplating (Rawlinson et al., 2011; Rawlinson and Fishwick, 2012). The Newer Volcanic Province has also developed to the south and east in the last 8 Ma as a continental basalt province of hot-spot volcanism (Price et al., 1997).

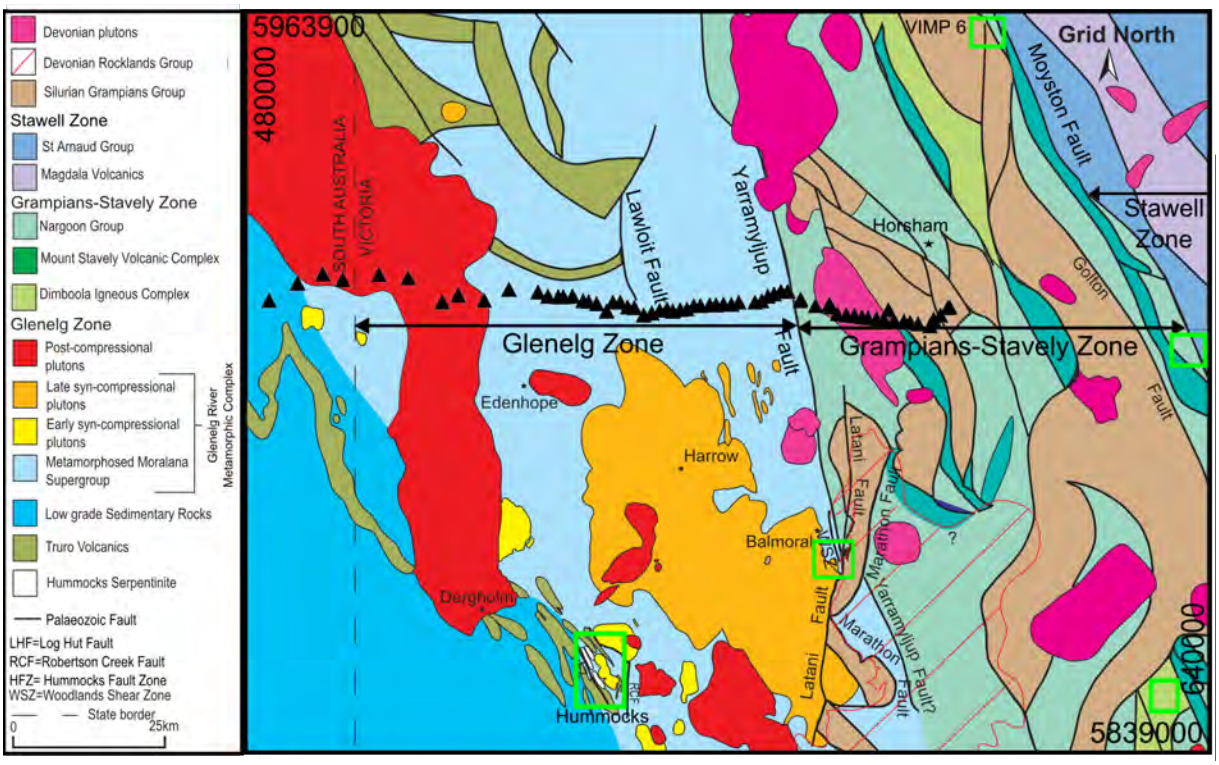

Figure 2.3: The regional geology of the survey region with post-Palaeozoic cover removed. Black triangles are station locations. The green boxes outline locations of serpentinite. Serpentinite is also interpreted to exist within the transect region because of fault bounded reflective packages seen in the seismic image. Modified from Morand et al. (2003).

2.3 Methods

2.3.1 MT Method

MT is a passive electromagnetic (EM) technique capable of determining the electrical resistivity response of the Earth down to the mantle transition zone. The technique involves recording magnetic and electric field variations in the Earth due to a naturally

occurring, time-varying magnetic field (Tikhonov, 1950; Cagniard, 1953). The distance over which EM fields diffuse is dependent on the frequency of the variations and the resistivity of the Earth, allowing MT to yield both lateral and vertical constraints. The periods of these magnetic variations are of the order of 10^{-3} to 10^{5} s (frequencies 10^{3} to 10^{-5} Hz), a result of lightning activity at equatorial latitudes and solar-driven ionospheric electric currents.

In the frequency domain, complex ratios known as impedances can be derived, describing the natural variations of the electric (E) and magnetic fields (H) at a particular frequency. The impedance tensor Z is defined as follows:

$$\begin{pmatrix} E_x \\ E_y \end{pmatrix} = \begin{pmatrix} Z_{xx} & Z_{xy} \\ Z_{yx} & Z_{yy} \end{pmatrix} \begin{pmatrix} H_x \\ H_y \end{pmatrix} . \tag{2.1}$$

In the 2D case, the impedance tensor can be separated into two components; the transverse electric (TE) mode has the electric field parallel to the strike and the transverse magnetic (TM) mode has the magnetic field parallel to the strike.

The components of $\mathbf{Z}$ have both magnitude and phase; the apparent resistivity ($\rho_{a_{ij}}(\omega)$ is related to the magnitude of $\mathbf{Z}$, where $\omega = 2\pi f$ is the angular frequency) is the depth-weighted average resistivity for the volume of Earth penetrated by signals of a particular period, T ($T = \frac{1}{f}$). The period can be related to the approximate penetration depth, δ, by the skin depth equation;

$$\delta(T) = 500\sqrt{T\rho_a} \tag{2.2}$$

where ρ_a is the averaged resistivity over periods shorter than T. The phase of $\mathbf{Z}$, Φ_{ij}, is the phase difference between the recorded electric and magnetic fields (Chave and Jones, 2012).

2.3.2 Data Acquisition

Magnetotelluric data were collected at 68 stations along an east-west transect following the L193 AuScope 09GA-SD1 Southern Delamerian seismic line. The survey was conducted in two parts: the first 29 stations at 5 km spacing were collected in 2010 over the entire seismic line, with preliminary inversions showing a complex electrical resistivity structure in the east. This resulted in the second phase of the data collection in 2012; the complex region was infilled with an additional 39 stations, reducing site spacing to about 1.5 km so that the sampling frequency of the MT data better matched both the geological and electrical resistivity complexity.

Data were recorded at a frequency of 1000 Hz for a duration of 20-40 h using AuScope equipment. Each station recorded two horizontal components of the electric field using 40-50 m dipoles (Ex, Ey with x geomagnetic north-south and y geomagnetic east-west) and two components of the magnetic field (Hx, Hy). At least 3 stations recorded

simultaneously allowing for remote referencing to reduce electromagnetic noise (Gamble et al., 1979).

2.3.3 Data processing and pre-inversion analysis

A section of the time-series data with the least amount of noise was selected by visual inspection. The robust remote referencing code, BIRRP (Chave and Thomson, 2004) was used to convert the time-series data for each site to the frequency-domain, incorporating a notch filter which removed noise from nearby power lines at frequencies of 50, 150 and 250 Hz. Apparent resistivity and phases were calculated across the processed frequency range of 0.0122-156 Hz. Coherence values comparing the electric response with the magnetic response provided a numerical indication of the data quality, with coherence values usually greater than 0.8 for most frequencies, with the exception of the deadband (a frequency band of low natural signal at about 0.1-1 Hz).

Phase tensor ellipses (Caldwell et al., 2004) were used to investigate strike, dimensionality and broad-scale resistivity trends. The survey region can be divided into three distinct electrical zones from changing ellipses (Fig. 2.4). For a period of 0.1 s (approximating upper crustal depths), ellipses are mostly non-coherent due to the influence of near-surface, small-scale features. The dimensionality of the resistivity responses are represented by the shape of the ellipse - circular for 1D and elliptical for 2- or 3-D. Thus it can be seen that all regions are either 2- or 3-D, with the exception of region 2 at a period of 1 s, where some ellipses are circular. A resistivity boundary exists between regions 1 and 2 for periods 1 and 10 s (upper-mid crustal depths), separated by the Lawloit Fault, a major fault interpreted as separating geological domains of different magnetic characters in the Glenelg Zone (Moore, 1996).

Region 1 is distinguished by low phase angles (minimum phase angles broadly indicate the vertical resistivity trends-minimum phase $<45^\circ$ indicates resistivity increasing with depth, and $>45^\circ$ is indicative of resistivity decreasing with depth) and northeast oriented ellipses that become narrower eastward (orientation of either minor or major ellipse axis aligns with maximum conductivity direction). At 50 s (mid-lower crustal depths), the ellipses are rotated slightly more northward.

Region 2 has higher phase angles, residing within the Glenelg Zone and is enclosed by the Lawloit Fault to the west and Yarramyljup Fault to the east. The Yarramyljup Fault is the boundary between the Glenelg and the Grampians-Stavely Zones. Within region 2, for periods greater than 1 s, the majority of ellipses are rotated northeast to north-northeast. There is a very distinct change in ellipses in region 3, corresponding to the Grampians-Stavely Zone, as ellipses become approximately north-northeast to north oriented and narrow, with lower minimum phase angles. This change is observed also at periods of 10 and 50 s, where phase tensors are oriented northeast in the Glenelg

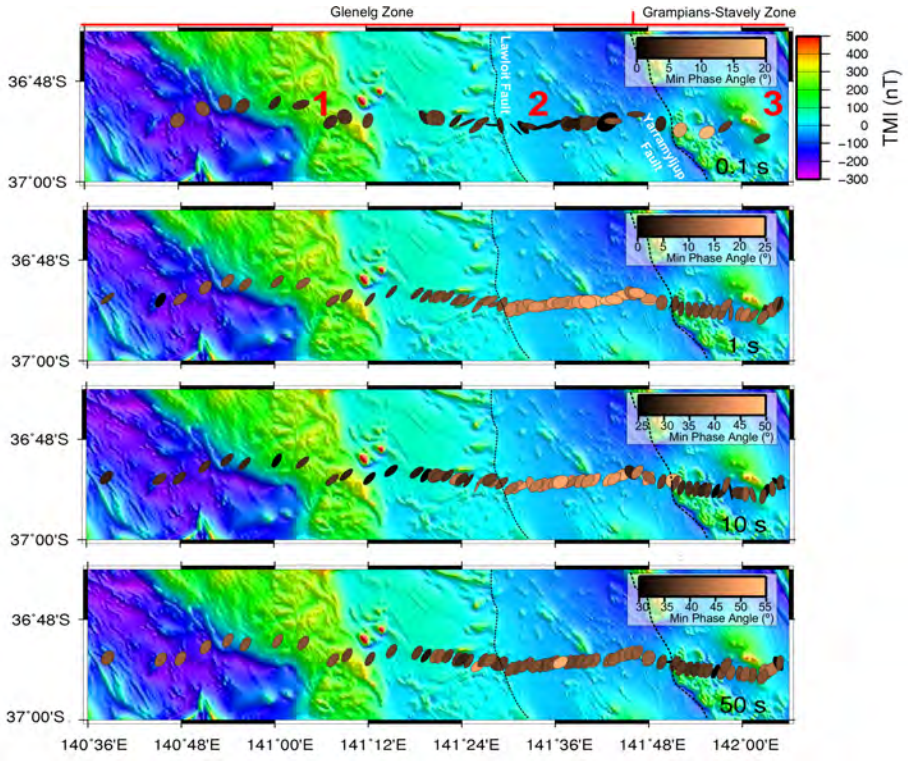

Figure 2.4: The total magnetic intensity (TMI) with phase tensor ellipses for each station at periods of 0.1 s, 1 s, 10 s and 50 s. Shading represents minimum phase angle, with values less than 45° representing resistivity increasing with depth and greater than 45° means decreasing resistivity with depth. Orientation of ellipses indicates direction of current flow. There are three distinct phase tensor gradients, numbered in red, separated by the Lawloit and the Yarramyljup Fault.

Zone and approximately north in the Grampians-Stavely Zone.

For best results, it is necessary to separate the modes of the impedance tensor into the TE and TM modes with the electric field aligned parallel and perpendicular to geoelectric strike prior to 2D inversion. The orientation of the phase tensors was used across all periods and stations to determine the dominant geoelectric strike direction. We recognise data of three-dimensional nature as skew (β) values larger than 5° (Caldwell et al., 2004; Bibby et al., 2005) and discard those from strike analysis and 2D inversion. While the azimuth of the phase tensor major axis is unique, there remains a 90° ambiguity in its relation to geoelectric strike. Taking this into account we average major or minor axes orientations in the 0-90° range to yield a strike of 49° west of geographic North (Fig. 2.5). We resolve the strike ambiguity through examination of regional TMI images and regional geology (Figs. 2.4 and 2.5), and conclude the geoelectric strike is indeed 49° west of north.

In the western half of the profile, strike direction is consistently between 40° and 50°, roughly matching the averaged angle of 49°. For stations SD22-SD28, strike is close to

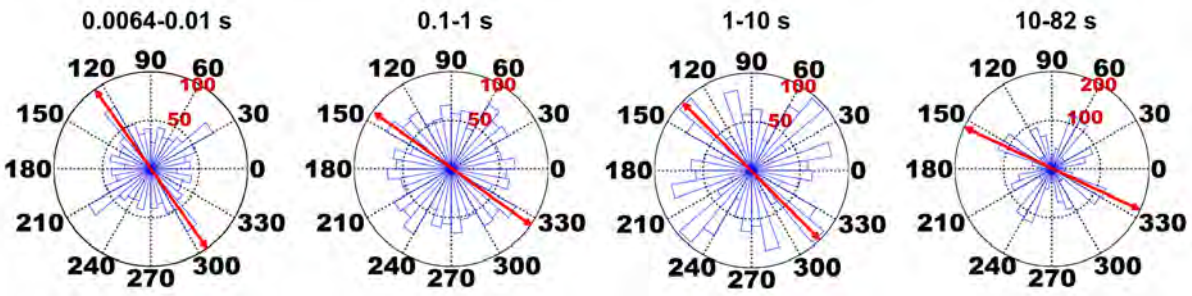

Figure 2.5: Rose plots for periods ranging from 0.0064 to 82 s. The geo-electric strike direction averaged for every station is indicated with a red arrow (geological strike discerned the 90 ˚ ambiguity in strike). Overall, using these rose plots, and phase tensor analysis in conjunction with geological strike from magnetic and gravity images, data were corrected to the geo-electric strike of 49 ˚ west of north.

49° for periods greater than 0.1 s. For stations SD28 to SD35, for periods greater than 1 s, strike direction is approximately 30-45°. East of SD35, the strike approximates to 50° for short periods (<~1 s). For greater periods, strike is variable between 10° and 60°. The more complex geology as seen in the eastern half of the profile in Fig. 2.3 can help to explain the inconsistent strike direction.

2.4 Results

A 2D inversion of the MT data produced results that highlighted several conductive regions in the eastern half of the profile in contrast to the otherwise resistive crust.

2.4.1 2D Inversion

The 2D smooth inversion code, Occam (Constable et al., 1987; de Groot-Hedlin and Constable, 1990), was used to invert the strike rotated TE and TM modes. Removed points with skew (β) values greater than |5°| constituting about 15% of the total data, more commonly from the eastern half of the profile, are usually within the range of ~0.06-0.6 s, or ~10-25 s. Skew values are low for most of the western and central profile (β <|5°|, with most β <|3°|). East of station SD36, β values are larger, so a slightly larger portion of data points were removed within this section. However, most β are still <|5°|, but some are as large as 12°. The data from all 68 stations of the MT transect (6668 points) were inverted using Occam with error floors set to 10% and 20% for the phase and apparent resistivity, respectively (Constable et al., 1987; de Groot-Hedlin and Constable, 1990). The relatively higher error in the apparent resistivity effectively deals with the effects of static shift in the data, which were minimal for the dataset. The resulting model from the inversion in Fig. 2.6a shows a complex crust with over four orders of magnitude variation in resistivity from <10 to 10,000 Ωm.

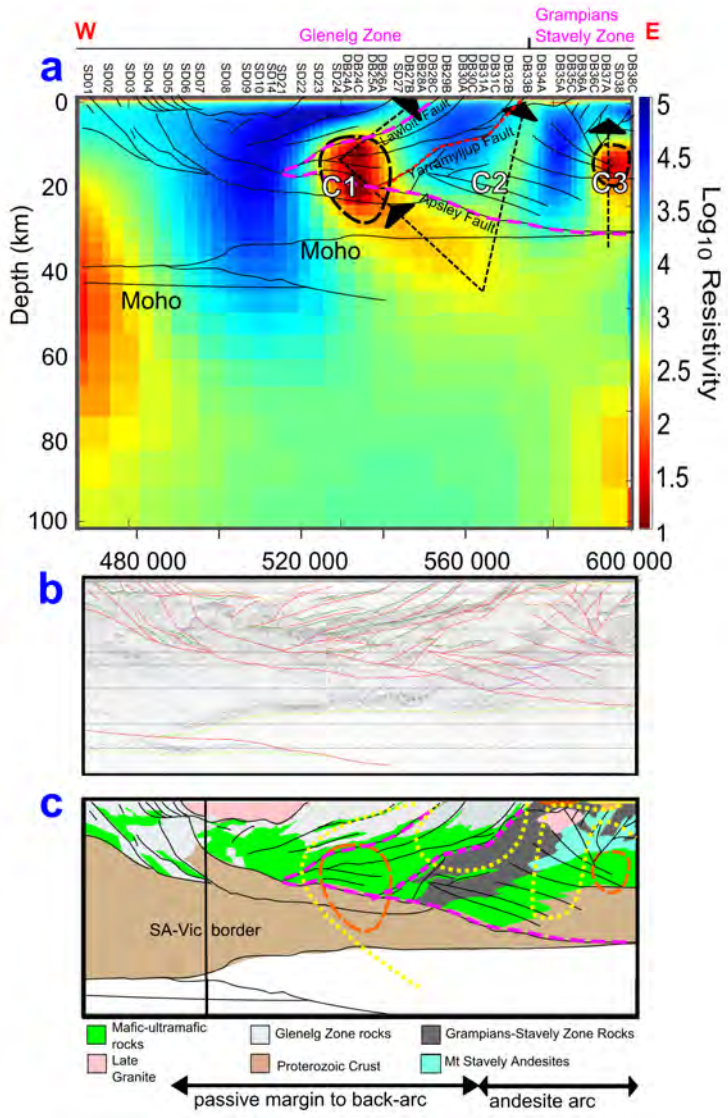

Figure 2.6: Occam2D smooth model resulting from inversion of all data from the 68 stations of the Southern Delamerian transect. Note not all stations are labelled. Red regions are conductive, blue are resistive. a) Modelling of both the transverse electric and the transverse magnetic modes. C1, C2 and C3 are low resistivity regions. The data were rotated by an angle of 49 ° west of North before inversion. The root mean squared value achieved was 1.95 with a model roughness of 197. Error floors for the inversion were 20% for the apparent resistivity and 10% for the phase. Black arrows show general trends of fluid movement. b) Reflection seismic image with fault interpretations overlain. Conductive anomalies are coincident with reflective regions in the seismic. c) The preliminary geological interpretation based on data from the seismic reflection profile and gravity and magnetic forward modelling of Cayley et al. (2011b). The yellow and orange dashed lines again represent the conductive regions of a.

A thin low resistivity layer comprises the top few hundred metres of the model, representing conductive sediments. West of station SD22 (the western part of the Glenelg Zone) is a resistive block of crust, ~10,000 Ωm, with the exception of an anomalously low resistivity region at the edge of the profile, at depths of 20-80 km.

The region east of station SD22 has a complex crustal resistivity structure consisting of highly conductive regions interspersed with resistive blocks. At a depth of about 40 km (the base of the crust), the conductor branches into three distinct regions: C1, C2 and C3, each one extending to the surface.

The main conductor, C1, is eastward-dipping and extends upward from the branch with resistivity values of about 300 Ωm until the most conductive region (ρ_a ~10 Ωm) spanning depths of 10-30 km. Above this depth, the conductor becomes west-dipping,with higher resistivities of about 1000 Ωm. The slightly west-dipping conductor, C2 (ρ_a ~300 Ωm), is much more resistive than C1, but still less than the surrounding crustal resistivity (~10,000 Ωm). The conductor C3 has similar resistivity values to C1, and it too increases greatly in resistivity upwards of 10 km depth, but is about half the width.

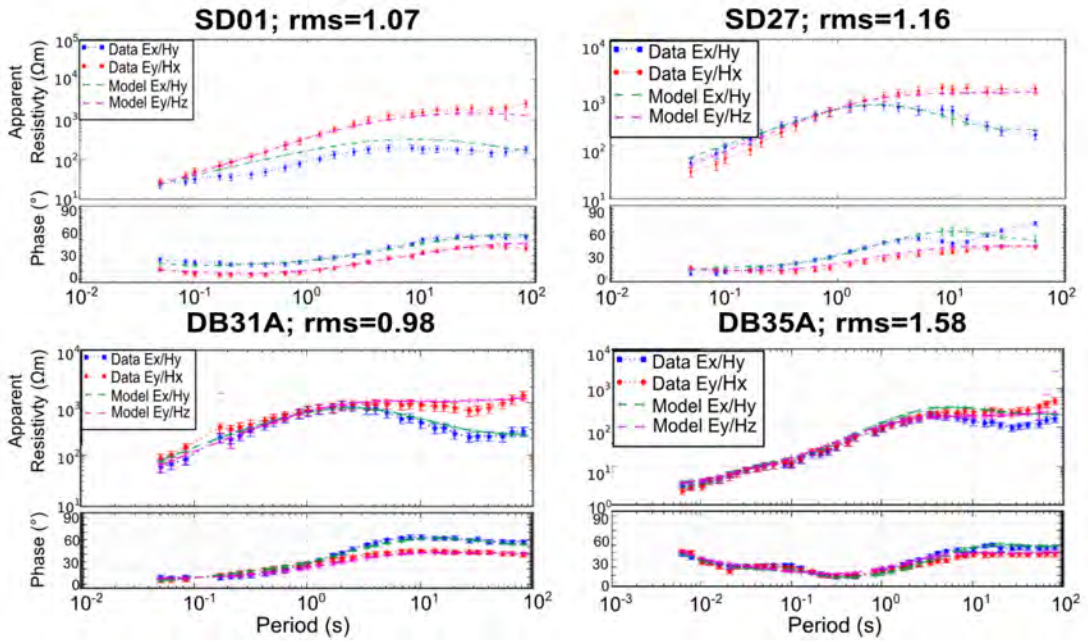

Figure 2.7: Plots showing the phases and apparent resistivities for periods ranging from 0.0064 s to 81.92 s for stations SD01, SD27, DB31A and DB35A along the 2D MT transect. Locations of these sites are shown in Fig. 2.2. The TE mode is in blue and the TM mode is in red. The green and purple lines indicate the data fit of the Occam 2D inversion results. The RMS values are listed in the title for each station.

2.4.2 Model robustness

Model sensitivity analysis was conducted by repeating inversions with varying starting resistivities of 10, 100 and 1000 Ωm, with crustal features unchanging and mantle values tending to remain close to the starting values, indicating lower sensitivity to mantle resistivities. In our inversion, the mantle has an average resistivity of about 1000~Ωm, but the low sensitivity meant that we kept interpretation of mantle features to a minimum. Inversions of individual data modes (TE and TM), and joint inversions of both modes assures robustness of the main features present in this final model. Using a bootstrap method, 50 inversions were conducted of data subsets with a random 20% of the full dataset removed (Schnaidt 2014, pers. comm.). The results indicated a low uncertainty within the resistive western half of the profile and most of the conductive eastern half. Uncertain regions include the most conductive regions within C1, C2 and C3, and some of the mantle below 60 km. This testing suggests that within the final model, the majority of uncertainty lies within the absolute resistivity values, rather than the locations, of the low resistivity regions.

As can be seen in Fig. 2.7, the modelled phase closely aligns with the data phase across almost all sites, particularly at conductor C1 but also C2 and C3. The target root-mean squared value (RMS) was set to 1 for each inversion. The closer the final RMS is to this target, the better the model fit the data. After the lowest RMS was reached (in this case 1.87), the inversion was repeated, this time with the target RMS set just above this lowest RMS (1.95 for this inversion). This caused Occam to generate a much smoother model (de Groot-Hedlin and Constable, 1990), with the roughness (inverse of smoothness the smoother the model, the less structure it contains) decreasing from 332 to 197. The relatively large RMS value of 1.95 may be attributed to the dense site spacing and/or the variation in strike direction. RMS values were significantly higher for sites in the ~1.5 km spaced eastern half of the profile, than for the ~5 km spaced stations in the western half (Fig. 2.7). Specifically, for conductor C1, misfits are low, near the target of 1. For stations within the vicinity of C2, the misfits are higher, ranging from 1.4 to 3.7 across 5 stations. C3 has low misfits, ranging from 1 to 2.

2.5 Discussion

The increased resolution MT survey coincident with a full crustal seismic reflection profile, in conjunction with good age and geochemical constraints, have all contributed to a consistent and plausible explanation of the crustal conductive regions within the eastern half of the profile. These regions appear to correspond to serpentinised mafic-ultramafic rocks above the location of a Cambrian subduction zone.

2.5.1 Interpreting the Conductors

The results of the 2D inversion are shown in Fig. 2.6a, with the main faults and lithological boundaries from the seismic interpretation (Cayley et al., 2011b) superimposed. When concurrent seismic reflection and MT surveys are collected, it is often the case that electrically conductive regions coincide with seismically reflective regions (Jones, 1987; Hyndman and Shearer, 1989) and this common observation also applies to this investigation. All of the main conductive anomalies (C1, C2, and C3) occur in the mid-crust within seismically reflective packages. Less conductive pathways appear to extend downwards into the mantle from the anomalies (arrows in Fig. 2.6a) to suggest a possible mantle source for upwelling fluids which entered the crust and may have reacted with the mid-crustal rock package to make it conductive.

We interpret this low resistivity to be related to serpentinisation and magnetite creation in mafic-ultramafic rocks from fluids rising off a subducting slab and its overlying mantle wedge. These conductors all occur in the eastern half of the section above the location of the interpreted west-dipping Cambrian subduction zone that created the andesite volcanics of the Grampians-Stavely Zone. This interpretation suggests that these anomalies still record today the activity of slab fluxed fluids formed during a Cambrian subduction event.

The conductive region within the eastern mantle could be related to the Cambrian subduction zone. It may be conductive material such as graphite, created from crustal carbon that was ingested deep into the mantle, tracing the subducted slab. Further data collection to the east of the profile with longer periods would be useful in interpreting this region.

The shallow mantle anomaly in the western part of the transect could be related to heat, fluids or partial melts associated with the mantle hot spot Quaternary Newer Volcanics. This conductor extends beyond the edge of the profile and an extension of the profile to the west of the transect, and longer period data would be required to have any confidence in interpretations of the anomaly. The Mt Gambier volcanoes are 100-150 km to the south of this end of the line. A similar conductor was observed in parts of the adjacent 2006 Lachlan MT line further east, with comparable values (10-20 Ωm) and depths (~40-90 km) by Dennis et al. (2012). This feature was thought to be connected to a central Victorian thermal anomaly and mantle-derived CO_2-rich fluids related to the Quaternary Newer Volcanics, but required further thermal modelling.

2.5.2 Low resistivity mid-crustal mafic-ultramafic rocks

All of the main conductive anomalies (C1, C2 and C3) occur in the mid-crust in seismically reflective packages which are all interpreted as mafic-ultramafic rock packages. The largest anomaly C1 occurs in the westerly Glenelg Zone, within the thickest pack-

age of inferred mafic-ultramafic rocks. This thick package is interpreted as depleted mantle rocks from the original hyper-extended rift margin, being thrust-stacked into a shortened and thickened package during the later convergent Delamerian deformation. Thin reflective packages can be traced from the mid-crustal region to the surface where thrust slices of mafic-ultramafic rocks have been mapped, such as the Hummocks Serpentinite (Morand et al., 2003). The conductive pathway dips moderately eastward, aligned with the top of the continental margin block. This surface is called the Apsley Fault in the seismic and is interpreted as one of the major crustal extensional faults being reused as a major ramp during the later thrusting and crustal thickening (Cayley et al., 2011b). Such an active thrusting crustal ramp provides a pathway for the mantle fluids to migrate up through the crust until contacting the mafic-ultramafics where serpentinisation can occur. Higher in the crust the conductor changes to an east-dipping orientation aligned with the Lawloit Fault.

Conductors C2 and C3 are within the Grampians-Stavely Zone and contrary to the preliminary seismic interpretation, we argue that the hosting rock package is best interpreted as mafic-ultramafic. The preliminary seismic interpretation (Cayley et al., 2011b) has all of the mid and upper crustal reflective package in this region as part of the 500 Ma andesitic arc - consistent with the tectonic cartoon which showed the arc erupting directly on the Proterozoic continental ribbon (Foden et al., 2006). We suggest that most of the mid-crustal part of this package is instead a thick 580 Ma rift basalt package deposited onto the Proterozoic crust during the rifting and before subduction at 500 Ma, leading to the andesite package being deposited on top. In the seismic, the mid-crustal package is more reflective than the higher levels to suggest greater density as would be expected for basalts versus andesites. The andesites have been dated as 500 Ma from magmatic zircon but some samples also contained almost as many 580 Ma pristine looking magmatic grains (Stuart-Smith, 1999). We interpret these older magmatic grains as being inherited from evolved portions of the underlying 580 Ma rift basalt package as the younger andesites erupted through these rocks. Thick 580 Ma packages of rift basalts are exposed both to the north of the seismic line in western NSW and to the south on King Island with continuity through Victoria already argued (Direen and Crawford, 2003; Meffre et al., 2004). The earlier eruption of this thick rift sequence would have helped deplete the mantle so that the boninites could form in the later subduction initiation phase (Kemp, 2003, 2004, boninites only form from a depleted mantle source;).

The more resistive C2 conductor emanates up from the mantle at the same spot as the C1 conductor. It rises near vertically along the edge of the mafic-ultramafic package, becoming more resistive at the top of the package. Steep-dipping basement strike-slip faults occur in this region (such as the Mosquito Creek Fault expressed in the Grampians cover; Cayley and Taylor, 1997). Such faults were not presented in the preliminary seismic interpretation (imaging vertical faults using seismic reflection methods can be difficult), but Victorian Geological Survey work in progress demonstrates they are more widespread than thought, and cut into the Cambrian basement. A geological explanation for this conductor is alteration of the mafic-ultramafic rocks by fossil fluids

using one of these sub-vertical faults.

The C3 conductor begins as a vertical pathway through the lower continental crustal block, becoming less resistive in the mid-crustal package of reactive mafic-ultramafic rocks, and much more resistive within the andesites. This anomaly may represent the fossil pathways of fluids and melts that built the overlying andesite arc.

2.5.3 Serpentinisation with magnetite as the conductive mineral

The presence of serpentinite within subduction regions can significantly decrease resistivity. Serpentinised rock can have resistivities three to four orders of magnitude lower than an unserpentinised rock of similar composition (Stesky and Brace, 1973). Laboratory studies show considerable variation in the magnitude that resistivity varies with serpentinisation, but all agree that serpentinisation alone cannot cause the low resistivity regions we observe (1-10 Ωm). To reach such low resistivities requires the presence of an interconnected conducting phase such as magnetite (which forms during serpentinisation) or preservation of the fluids associated with serpentinisation (Stesky and Brace, 1973; Hyndman and Shearer, 1989; Zhu et al., 2001; Reynard et al., 2011; Kawano et al., 2012). Serpentinisation can be recognised geophysically by a low seismic velocity region, high seismic reflectivity, and perhaps, lower resistivity than the surrounds. Becken and Ritter (2012) suggest that low resistivity within the San Andreas Fault Zone may be an effect of serpentinite, and that fluid pathways coincide with the serpentinite crustal exhumation pathways.

Surface outcrops of serpentinite occur in faults slivers right across the region, such as the Hummocks Serpentinite in the Glenelg Zone (Morand et al., 2003) and the Williamson Road Serpentinite in the Grampians-Stavely Zone (Stuart-Smith, 1999). The Hummocks Serpentinite, exposed in a quarry 50 km south of the survey region (see green square in Fig. 2.3), has been described in the most detail (Morand et al., 2003, see Fig. 2.9). The mineralogy now consists of antigorite, chrysotile and talc, with magnetite described as common. These minerals pseudomorph the original coarse grained igneous texture of olivine, pyroxene and spinel. The magnetite is finely distributed throughout the rock and best seen in concentrations along the exsolution lamellae of the pyroxenes.

We measured the electrical conductivity of a number of hand samples to test the theory that serpentinisation (and magnetite creation) was creating resistivities contributing to the observed conductive anomalies. The Victorian Initiative for Minerals and Petroleum (VIMP) had a stratigraphic drilling programme across the Glenelg and Grampians-Stavely Zones to collect fresh rocks for dating and geochemistry (Maher et al., 1997). Hand samples were taken from the Hummocks Serpentinite quarry and slabbed dry core from various VIMP holes intersecting the major varieties of rock types present. These samples had their electrical conductivity measured by placing the flat

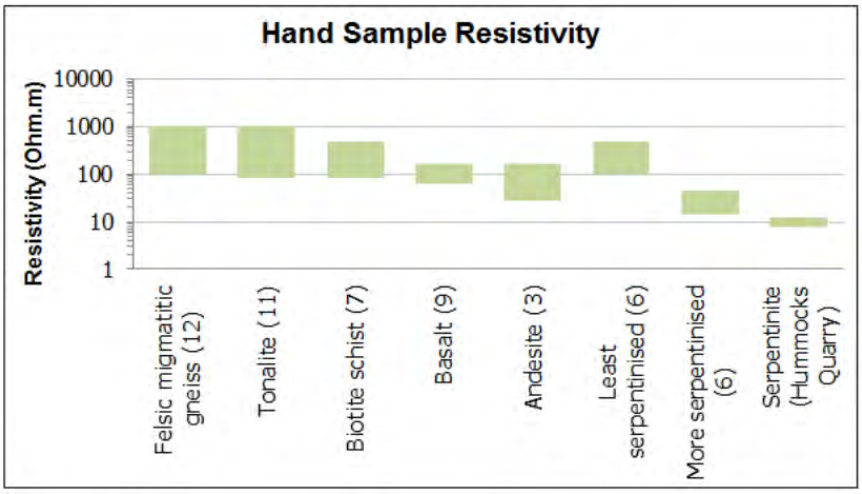

Figure 2.8: Electrical conductivity of rocks from VIMP drill holes, with the drill hole number in brackets after the rock name (with the exception of the serpentinite from the Hummocks Quarry). These values were measured on flat faces of dry slabbed cores using a Geo Instruments GCM-2 handheld conductivity meter using the 70x32 mm flat sensor plate at the 250 kHz frequency reading correctly against the check plate value. All measurements were made in mS/m corrected against a variable background air value of 212 mS/m. For comparison to our data, we have converted these values to resistivity. Serpentinised rocks show decreased electrical resistivity compared to regional values.

induction plate of a hand held meter on the samples (Fig. 2.8). Most rocks yielded typical low values of conductivity, but VIMP 6 intersected variably serpentinised mafic-ultramafic rock, with the best preserved (least altered) primary mineralogy and texture suggesting a harzburgite protolith (Maher et al., 1997). The conductivity of this rock increased with increasing serpentinisation and approached that of the pervasively serpentinised Hummocks Serpentinite.

According to Kawano et al. (2012), the presence of magnetite in amounts of 5-25% can decrease resistivity by up to an order of magnitude, and be further enhanced by shearing to improve interconnectedness by smearing out low percentages of magnetite into contact with each other. The serpentinite within the survey region outcrops in faults that can be traced to intersect the survey region. The seismically reflective region that is the mid-crustal ultramafic rocks within Fig. 2.6c is thought to have been serpentinised. The MT and seismic results show that not all of the interpreted mid-crustal mafic-ultramafic rocks exhibit low resistivity. Instead the anomalies only appear where they link with the pathways to the mantle. We suggest that long-lived fluid movement focused through these areas has created pockets of intensely altered serpentinite with abundant magnetite (more than the measured hand samples). The faults providing the fluid pathways have possibly further decreased resistivity with associated shearing. Laboratory experiments show that shearing of magnetite-rich serpentinite can create interconnected electrical pathways which decrease resistivity by several orders of magnitude (Kawano et al., 2012), like we see in Fig. 2.6a.

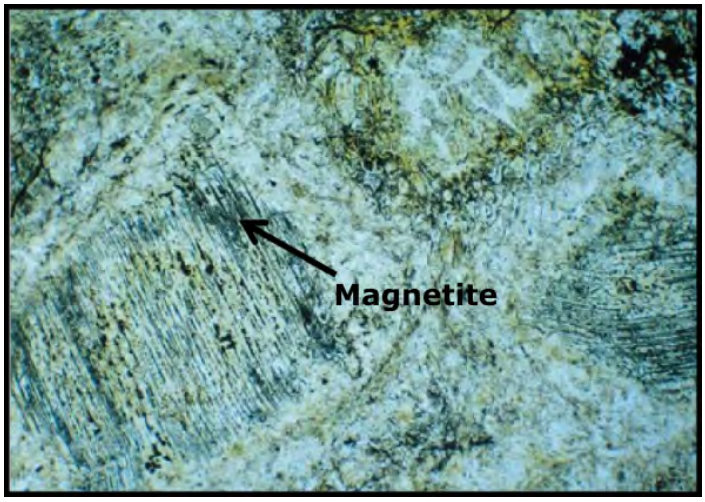

Figure 2.9: Figure showing a thin section from the Hummocks Serpentinite (Photo: Morand et al., 2003, width 4 mm in PPL). Black grains are magnetite grown in the exsolution lamellae of large relic pyroxene grains replaced by chrysotile. Note that these samples are taken south of the transect and the degree of serpentinisation within survey region can only be speculated.

2.5.4 Other potential sources of the conductors

Whilst we suggest a Cambrian subduction-related process as the fluid-generation mechanism, we note here for completeness several other possibilities which we consider less likely.

Since this is an ancient subduction zone which ceased approximately 500 Ma, it is unlikely that low resistivity slab dehydration fluids, or the magmatism these fluids may have induced, still exist within the crust today, making the presence of fluids or partial melts an unlikely explanation for the conductors. The main conductors lie above the region where the thick Adelaide geosyncline sediments lay between enclosing Proterozoic continental blocks, before they were pushed back adjacent to each other (see Fig. 2.1). Metamorphic fluids in the lower crust from this central zone of greatest crustal thickening may have been driven up the fault network that developed concurrently. The apparent continuation of the conductors down into the mantle, however, argues against a purely crustal source for the fluids.

There are also some much younger possibilities for mantle fluid sources to have affected this region. The Cretaceous southern rift margin of Australia-Antarctica breakup about 90-40 Ma (Gaina et al., 1998) is about 150 km to the south. Lithospheric thinning and magmatic underplating has already been suggested from seismic tomography (Rawlinson and Fishwick, 2012). Fluids or magnetite-bearing magma related to this underplating may be leaking into the crust, as interpreted for similar crustal conductors seen in MT on the Cretaceous rift margin in Western Australia (Myer et al., 2013). The Quaternary Newer Volcanic Province of hot spot volcanism over the last 8 Ma (Price

et al., 1997) lies about 100 km to the south and south east of this region (Fig. 2.2. It could be possible that low resistivity seen in the section is some far-field leakage of this same young source, rather than anything related to the actual Cambrian Delamerian Orogeny. However both of these potential events and sources are at least 100 km to the south of the MT transect.

2.6 Conclusions

Regions of low resistivity are well documented in many modern subduction settings. The preservation of similar observations in this Cambrian system is probably because orogenesis moved rapidly away from this region once subduction ceased, with little tectonic activity since.

Anomalous low resistivity crustal pathways occur beneath the Delamerian Orogen, observed in the eastern half of the 2D inversion of the 68 station magnetotelluric profile. The pathways appear to extend from the upper mantle and are interpreted to relate to fluids released during the west dipping Cambrian subduction that initiated the orogenesis. Crustal faults associated with crustal thickening during orogenesis, identified in a coincident seismic reflection profile, appear to have been the pathways for much of the fluid movement toward the surface. Pockets of anomalous low resistivity occur where these pathways intersect a seismically reflective mid-crustal package interpreted to be variably serpentinised mafic-ultramafic rocks. The large decrease in resistivity only at the fluid pathway intersections suggests major alteration (serpentinisation) encouraged the growth of minerals such as magnetite, beyond a critical threshold to attain electrical interconnectedness and become much less resistive than adjacent regions. Specifically, crustal Apsley and Lawloit Faults which pass through the expected serpentinised rocks have been identified as fluid pathways, with their seismic-interpreted locations coinciding with the conductors.

In addition to suggesting fluid pathways through the vertical crust, the MT has also added support to the geological domains identified by mapping. The Lawloit Fault marks a boundary between two domains of different electrical structure (phase tensor), as does the Yarramyljup Fault which is the geological boundary between the Glenelg and Grampians-Stavely Zones.

Seismic and MT have long been known to add complementary value to each other. Our study supports this case, with a mid-crustal reflective package seen in the seismic reflection being supported by the MT to be an extensive ultramafic package partially serpentinised where subduction related fluids passed through. In petroleum investigations, deep drilling can used to calibrate and validate seismic interpretations but this cannot be done for full crustal scale seismic profiles. MT can instead be used as one tool for greater confidence in interpreting unreachable rocks. Many regional MT lines are collected at approximately 5 km spacing but this study shows that spacing

down to 1.5 km over complex geology may be necessary so that the MT anomalies can be imaged in sufficient resolution to add complementary value to seismic reflection surveys.

Acknowledgments

We gratefully acknowledge funding and field support for this project from the Geological Survey of Victoria and the University of Adelaide. Logistical support was also provided by DMITRE SA and Geoscience Australia. Instrumentation was provided by the AuScope National MT Facility, and access was provided by ANSIR. We would also like to thank Jared Peacock and Sebastian Schnaidt for fieldwork and processing assistance, Lars Krieger for technical assistance and Goran Boren for equipment preparation. Thank you to Jonathan Ross, Hamish Adam and Lauren Howard for the initial deployments and data processing in 2010. This contribution formed TRaX Record 301.

CHAPTER

THREE

THE LITHOSPHERIC STRUCTURE OF THE TRANSITION BETWEEN THE DELAMERIAN AND LACHLAN OROGENS: NEW INSIGHTS FROM 3D MAGNETOTELLURIC IMAGING

Robertson, K.[1], Heinson, G.[1], Taylor, D.[2], Thiel, S.[3]

[1] Electrical Earth Imaging Group, Department of Earth Sciences,
School of Physical Sciences, University of Adelaide, Adelaide SA 5005, Australia
[2] Geological Survey of Victoria, Department of Economic Development, Jobs, Transport and Resources, Melbourne, Victoria 3001, Australia
[3] Geological Survey of South Australia, Department of State Development,
Adelaide SA 5000, Australia

Statement of Authorship

Title of Paper	The lithospheric structure of the transition between the Delamerian and Lachlan Orogens: New insights from 3D magnetotelluric imaging
Publication Status	☐ Published ☐ Accepted for Publication ☑ Submitted for Publication ☐ Unpublished and Unsubmitted work written in manuscript style
Publication Details	Robertson, K.E., Heinson, G.S. and Thiel, S. (2016). The lithospheric structure of the transition between the Delamerian and Lachlan Orogens: New insights from 3D magnetotelluric imaging. Manuscript submitted to Australian Journal of Earth Sciences.

Principal Author

Name of Principal Author (Candidate)	Kate Robertson
Contribution to the Paper	Performed data collection, processed, modelled and interpreted data. Wrote the manuscript and acted as corresponding author.
Overall percentage (%)	80 %
Certification:	This paper reports on original research I conducted during the period of my Higher Degree by Research candidature and is not subject to any obligations or contractual agreements with a third party that would constrain its inclusion in this thesis. I am the primary author of this paper.
Signature	Date 8/9/16

Co-Author Contributions

By signing the Statement of Authorship, each author certifies that:

i. the candidate's stated contribution to the publication is accurate (as detailed above);

ii. permission is granted for the candidate in include the publication in the thesis; and

iii. the sum of all co-author contributions is equal to 100% less the candidate's stated contribution.

Name of Co-Author	Graham Heinson
Contribution to the Paper	Supervised development of work, helped in data interpretation and manuscript evaluation.
Signature	Date 8 SEPT 2016

Name of Co-Author	David Taylor
Contribution to the Paper	Assisted with field data collection, helped with geological interpretation of data and manuscript evaluation.
Signature	Date 12/9/16

Name of Co-Author	Stephan Thiel
Contribution to the Paper	Supervised development of work, helped in data interpretation and manuscript evaluation.
Signature	Date 12/09/16

SUMMARY

The method of magnetotellurics (MT) was used to image the crust and upper mantle beneath the Delamerian and Lachlan Orogens in western Victoria, Australia. In the Cambrian this region changed from being the extended passive margin of Proterozoic Australia into an Andean-style convergent margin that progressively began to accrete younger oceanic terranes. Several broadband MT transects collected in stages along deep crustal seismic lines have now been combined to create a continuous 500 km east-west transect over this region. We present the electrical resistivity structure of the lithosphere using both 3D and 2D inversion methods. Additionally, long-period AusLAMP MT data on a 55 km spaced grid were used to provide 3D constraints for the starting model. The transect crossed the transitional crustal boundary between the Delamerian and Lachlan orogens in the Stawell Zone. This boundary coincides with the Mortlake Discontinuity which marks an isotopic discontinuity, with the Lachlan Orogen enriched in strontium relative to the Delamerian Orogen. Phase tensor ellipses of the MT data reveal a distinct change in electrical resistivity structure near the location of the Mortlake Discontinuity. Results of 3D and 2D inversions along the MT profile image a more conductive lower crust and upper mantle beneath the Lachlan Orogen than the Delamerian Orogen. Increased conductivity is often ascribed to mantle enrichment and thus supports the notion that the isotope enrichment of the basalts at least partially reflects an enriched mantle source rather than crustal contamination. Fault slivers of the lower crust from the Lachlan region expose boninites and island arc andesites indicative of subduction, a process that can enrich the mantle isotopically and also electrically by introducing carbon (graphite) and water (hydrogen).

3.1 Introduction

A series of Palaeozoic orogenic belts, the Tasmanides (Coney et al., 1990), were accreted onto the margin of Proterozoic Australia in various stages from the Cambrian to the Carboniferous by subduction-related convergence. The oldest part of the Tasmanides occurs in western Victoria as the Cambrian Delamerian Orogen, which youngs eastward towards the Siluro-Devonian Lachlan Orogen (Miller et al., 2005; Foden et al., 2006). Changes in mapped geology have allowed the region to be divided into a number of geological zones (e.g. VandenBerg et al., 2000) with the Glenelg and Grampians-Stavely zones in the west (Delamerian), the Stawell Zone in the middle (transitional) and the Bendigo and Melbourne zones in the east (Lachlan). Deep crustal seismic reflection data have been collected across this region to give good constraint on the crustal geometry (Cayley et al., 2011a,b) but do not yield much information on the mantle. The MT data were collected along the seismic lines to provide a complementary view for additional understanding that comes from seeing the electrical structure, with this passive source technique capable of imaging into the mantle.

Mantle seismic tomography studies suggest that the transition from the Proterozoic to Palaeozoic mantle occurs beneath the Stawell Zone of western Lachlan Orogen where P-wave speeds decrease to the east (Rawlinson et al., 2011, 2014b). Models of Re-Os isotope data from enclaves in the recently erupted continental basalts across this region also suggest that Proterozoic mantle extends at least as far east as the town of Mortlake in the transitional Stawell Zone (Handler et al., 1997, Figure 3.1).

Magnetotellurics (MT) is a passive electromagnetic technique that uses naturally occurring electromagnetic signals from lightning strikes and solar winds to determine the electrical resistivity structure of the Earth (Tikhonov, 1950; Cagniard, 1953). Broadband MT (1000 Hz-0.001 Hz) transects are ideal for imaging the crust and shallow upper mantle where seismic reflection data lose resolution. Existing transects in western and central Victoria (Dennis et al., 2011b, 2012; Robertson et al., 2015) and a new transect across the Delamerian to Lachlan transition were combined, resulting in a 500 km transect of 179 sites with stations generally spaced 2-3 km apart. Due to complex geoelectric strike which varies across the transect, a total of 80 MT sites were modelled in 3D for the first time using the ModEM 3D inversion code (Egbert and Kelbert, 2012; Kelbert et al., 2014). A higher resolution inversion of 110 sites was performed using the 2D inversion code WinGLink (Rodi and Mackie, 2001) and focused on the Delamerian-Lachlan transition region. The resultant model provides good support for the major features revealed in the 3D model, although with a more complex upper crustal structure than imaged from the lower-resolution 3D model, with fossil fluid pathways now evident.

This paper presents the results of the new modelling of the electrical structure of the crust and lithospheric mantle across the transition between the Delamerian and Lachlan Orogens. The 2D and 3D models show a change in mantle character beneath the Stawell Zone along the Delamerian-Lachlan transition. The location of this transition coincides with changes in other properties determined from pre-existing seismic tomography models and isotopic data, reflecting that this region marks the change from the edge of the Proterozoic Australian cratonic margin to a more outboard region of accreted oceanic Palaeozoic terranes. The Delamerian lithospheric mantle is more resistive as typical for depleted mantle beneath Proterozoic continental crust. The Lachlan lithospheric mantle is more conductive and this is typical of mantle enriched by subduction processes (with such processes having operated during the accretion of this region). The lower crust of the Lachlan Orogen is also more conductive and this may reflect that it contains electrically conductive material such as altered mafic oceanic crust (magnetite) and black shales (carbon-graphite).

3.2 MT Theory

Naturally occurring, time-varying external magnetic fields induce magnetic and electric field variations within Earth, which can be measured at the surface using the passive electromagnetic technique of MT (Tikhonov, 1950; Cagniard, 1953). In the

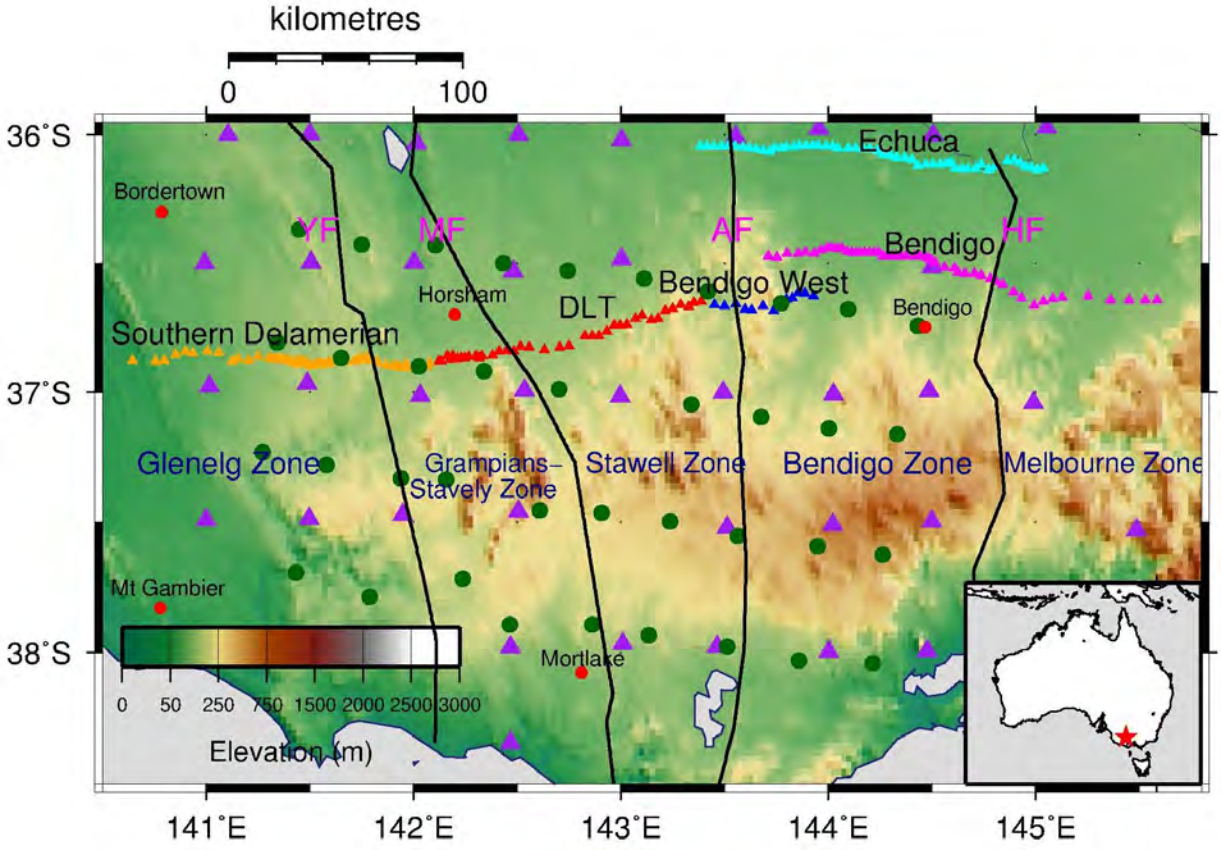

Figure 3.1: MT site locations with black lines depicting tectonic boundaries. Orange sites are of the Southern Delamerian transect (Robertson et al., 2015), red: Delamerian-Lachlan Transition transect; blue: Bendigo West (Dennis et al., 2011b); pink: Bendigo (Dennis et al., 2011b); blue: Echuca (Dennis et al., 2011a); purple: AusLAMP sites (Duan et al., 2016) and green circles: Newer Volcanic Province array (Aivazpourporgou et al., 2015). YF=Yarramyljup Fault, MF=Moyston Fault, AF=Avoca Fault, HF=Heathcote Fault.

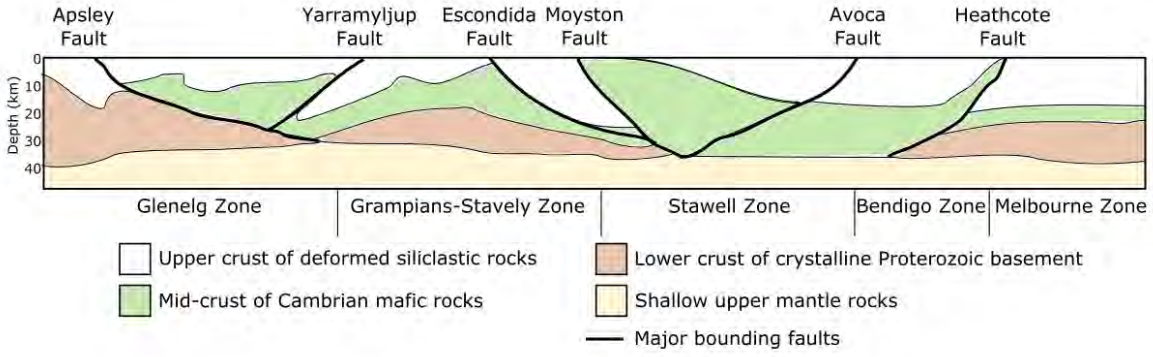

Figure 3.2: Illustration of the geology beneath the transect from interpretations of deep reflection seismic profiles (Cayley et al., 2011a,b). Depths on side are approximate.

frequency domain, complex ratios known as impedances are derived, describing the natural variations of the electric (**E**) and magnetic fields (**H**) at a particular frequency. The impedance tensor **Z** is defined as follows:

$$\begin{pmatrix} E_x \\ E_y \end{pmatrix} = \begin{pmatrix} Z_{xx} & Z_{xy} \\ Z_{yx} & Z_{yy} \end{pmatrix} \begin{pmatrix} H_x \\ H_y \end{pmatrix} . \tag{3.1}$$

The impedance tensor can be simplified for 1D and 2D cases. For a 1D resistivity structure, the diagonal components $Z_{xy} = -Z_{yx} = Z$, $Z_{xx} = Z_{yy} = 0$. For a 2D resistivity structure, rotation of the impedance tensor to the geo-electric strike will eliminate Z_{xx} and Z_{yy}, with the electric field parallel to the strike for the transverse electric (TE) (Z_{xy}) mode and the magnetic field parallel to the strike for the transverse magnetic (TM) (Z_{yx}) mode.

The apparent resistivity ($\rho_{a_{xy}}(\omega)$ where $\omega = 2\pi f$ is the angular frequency) is the depth-weighted average resistivity for the volume of Earth penetrated by a particular MT sounding period, T ($T = \frac{1}{f}$).

The phase of **Z**, Φ_{xy}, is the phase difference between the recorded electric and magnetic fields (Chave and Jones, 2012, and references therein). In this paper, the phase tensor, Φ, (where $\mathbf{\Phi} = \mathbf{X^{-1}Y}$) is represented in figures by an ellipse (Caldwell et al., 2004). The orientations of the phase tensor reflect lateral gradients in the resistivity structure. The ellipses are shaded by the minimum phase angle, with angles greater than 45° indicating a decrease in resistivity with depth, and angles less than 45° representing an increase in resistivity with depth. For an ellipse to appear circular, the resistivity structure must be one-dimensional. If elliptical, the resistivity is indistinguishable between a 2D or 3D resistivity structure.

3.3 Method and Results

In 2007 the Bendigo broadband MT data were collected along a shorter transect of 14 stations (Bendigo West, MT07-b) and a longer profile of 53 sites (Bendigo, MT07; Figure 3.1) offset to the north from Bendigo West by about 10 km (Dennis et al., 2011b, 2012). Further north, the Echuca profile (MT08) was collected (Dennis et al., 2011a), but is excluded from this study. In 2010, 29 stations at 5 km spacing were collected in an east-west direction (Southern Delamerian, SD01) and 10 sites in a north-south direction (Southern Delamerian, SD02) and were infilled in 2012 with a further 39 stations on its eastern two-thirds over the area of greatest complexity, reducing site spacing to ~1.5 km (Robertson et al., 2015). Lastly, the gap between the Southern Delamerian and the Bendigo West transects was bridged in 2014, with the 44 sites of the Delamerian-Lachlan Transition profile collected at spacings of 5 km in the east to ~1.5 km in the west. Separately, an array of long period MT sites was collected across all of Victoria as part of AusLAMP (Australian Lithosphere Architecture Magnetotelluric Project) (Duan et al., 2016), suited to imaging the entire lithosphere. Combining the MT transects (Echuca and AusLAMP array excluded) results in a continuous transect of 179 sites almost 500 km in length that traverses western Victoria (Figure 3.1).

Most of the data were processed to MT impedance responses in the frequency domain using the robust processing software, BIRRP (Chave and Thomson, 2004) with the remaining sites already processed to a suitable standard for this work. The data were firstly displayed as phase tensor ellipses to illuminate changes in electrical structure, followed by 3D inversion of the full 500 km transect using a subset of the total sites at 5 km spacing. Results from 2D inversions focusing on the Delamerian to Lachlan transition supported the results from 3D inversion at a higher resolution.

3.3.1 Phase tensor ellipses

Imaging data as a pseudosection of all periods prior to modelling using phase tensor ellipses reveals some major features in the data (Figure 3.3). A common characteristic of phase tensor ellipses at faults are that ellipses are oriented parallel to the fault strike on one side of a fault and perpendicular to the fault strike on the other side. This phenomenon is observed at several of the zone boundaries in this study, such as at the Heathcote Fault between the Bendigo and Melbourne zones at periods of 0.1-1 s and at the Yarramyljup Fault between Glenelg and Grampians-Stavely Zone at 0.001-1 s to the west of the fault, and 0.1-1 s to the east of the fault. The boundary between the Grampians-Stavely and Stawell Zone is delineated by the Moyston Fault and is also approximated as the transition between the Delamerian and Lachlan Orogens. Data quality is diminished here, which explains the missing ellipses in the Stawell Zone; however, all but three of these sites extend to periods of 1000 s. Phase tensor ellipses indicate a mostly resistive upper crust with periods less than 1 s exhibiting low phase angles (blue) across the entire transect, becoming slightly less resistive at periods longer than 10 s within the Delamerian Orogen, and a large change to ellipses of high phase angles (red) in the Lachlan Orogen, which return to low phase angles at long periods (~1000 s) showing that the subsurface eventually becomes more resistive.

Figure 3.4 shows the ellipses at a period of 100 s over grey-scaled total magnetic intensity (TMI) data. This period approximately corresponds to mid-crustal depths. The most striking feature that the ellipses image in Victoria is a strong change in minimum-phase angle across the transition from the Delamerian Orogen (<45°; blue) to the Lachlan Orogen (>45°; pink to red). White ellipses can be thought of as the transitional phase- and this transition happens over a relatively small distance (~50 km), roughly centred on the Moyston Fault. Slightly further to the east of the Moyston Fault, a rapid change in the orientation and shape of the ellipses occurs, from more circular (and white) in the west, to narrow, NNE oriented, red-shaded ellipses in the east. MT sites in the Otway Basin in the SW of the survey region have low minimum phase angles and are almost circular, showing a simple, almost one-dimensional resistivity structure.

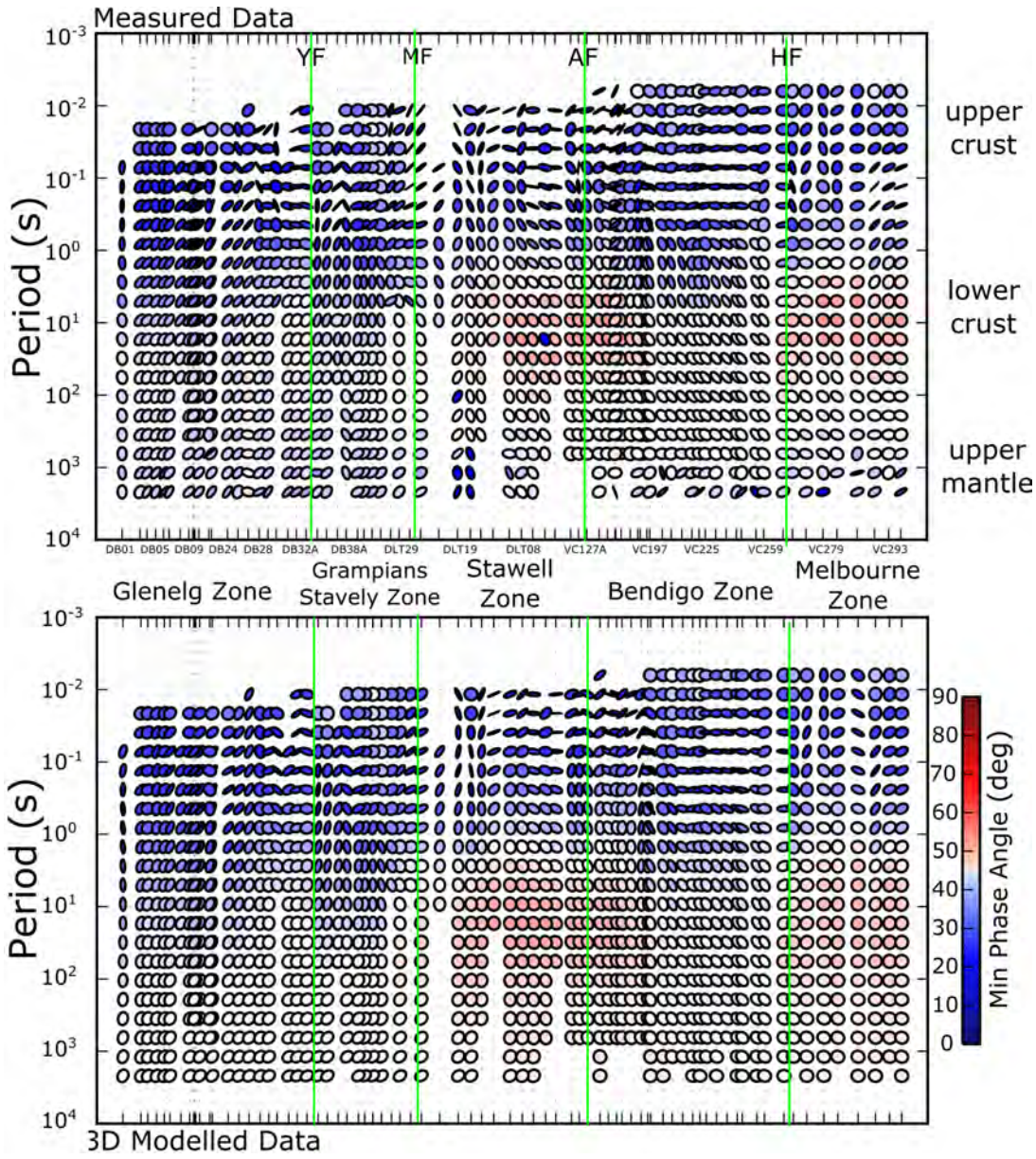

Figure 3.3: Phase tensor ellipse pseudosection for the measured data (top) and the modelled responses from the ModEM 3D inversion (bottom). Note not all stations are labelled. The surface locations of boundaries between major tectonic zones have been projected vertically down (green vertical lines) through the entire period range, despite some of these boundaries actually being represented by dipping faults. YF=Yarramyljup Fault, MF=Moyston Fault, AF=Avoca Fault, HF=Heathcote Fault.

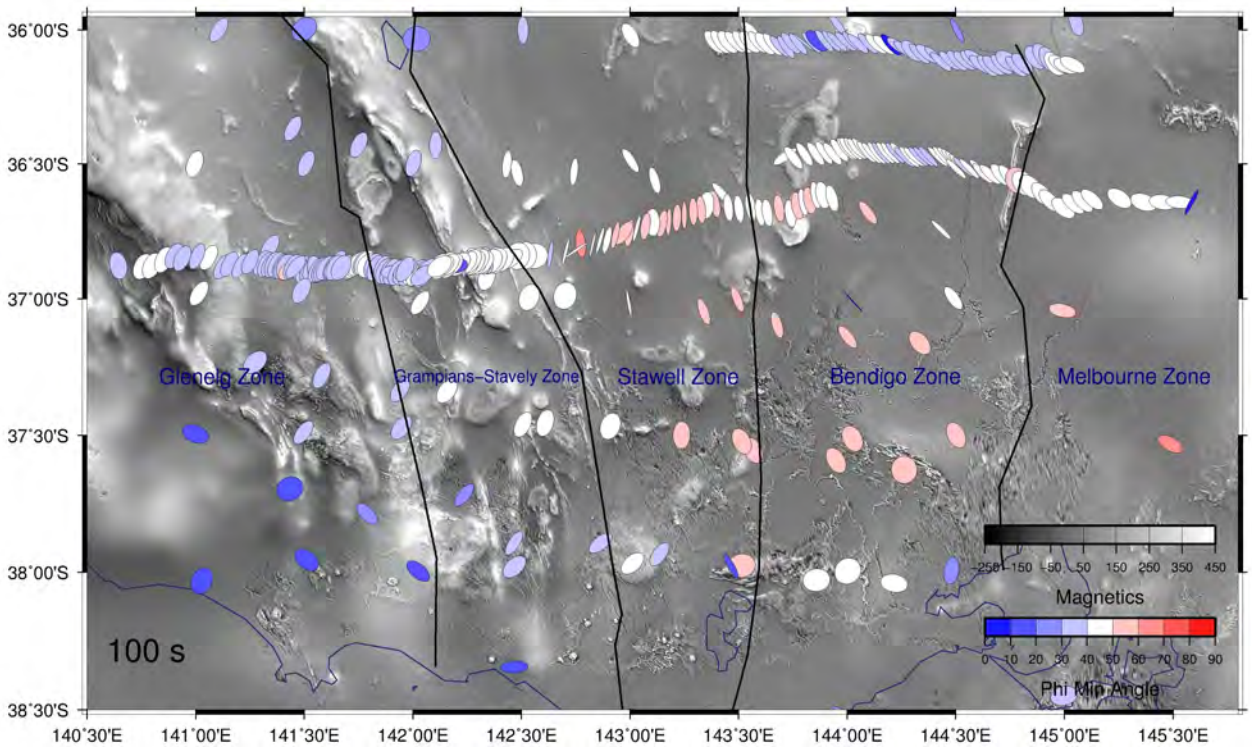

Figure 3.4: Phase tensor ellipses at a period of 100 s, overlaying total magnetic intensity data.

3.3.2 Data Inversion

Individually, each of the transects have previously been inverted using 2D inversion codes (either Occam2D; Constable et al. (1987) or WinGLink; Rodi and Mackie (2001). Dimensionality analysis of each of the individual transects indicated that the data were mainly 2D, with some 3D stations mainly at longer periods, which were masked prior to inversion. However, when the three profiles are combined, the electrical resistivity structure across the entire 500 km profile is complex, with changes in geo-electric and geological strikes across the transect making a single 2D inversion of the entire profile less reliable. In addition, the strike varies with depth, as discussed in Robertson et al. (2015). To address these complexities, first we present a 3D inversion of the 500 km transect, using a subset of evenly-spaced sites approximately 5 km apart. Results of the 3D inversion are supported by higher resolution 2D inversions of the transect, focusing on the Delamerian-Lachlan transition, and split into two profiles with the western profile axes north-west striking and the eastern profile axes north-east striking.

3.3.3 3D Inversion

Modelling of a transect using a three-dimensional inversion code can be complex, but when used carefully, it can be an ideal method if strike direction varies and can provide better off-profile resistivity characterization if all four components of the impedance

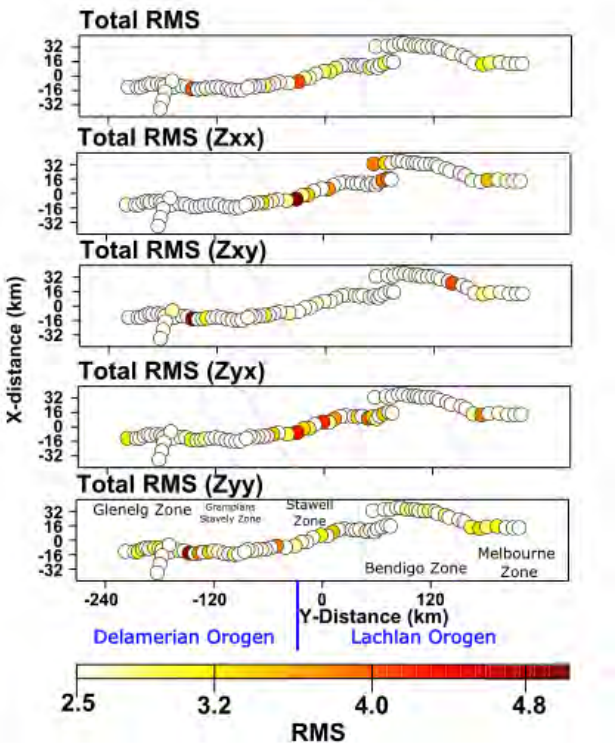

Figure 3.5: RMS values from the 3D model. Sites with RMS lower than 2.5 were deemed good quality (overall RMS of inversion is 2.3) and only sites with RMS larger than 2.5 are coloured. Magenta lines are tectonic boundaries as defined in Figure 3.1.

tensor are modelled (Zxx, Zxy, Zyy and Zyx; Siripunvaraporn, 2012). The pitfall for a long profile containing many stations is that 3D inversion is computationally slow. Thus to obtain models in a reasonable amount of time, the model is more coarse than for the 2D mesh, incorporating a subset of stations and fewer frequencies. Each of these factors will affect the resolving capabilities of the inversion.
For our transect, an evenly spaced (5 km) subset of 80 sites were inverted over 22 periods spanning 0.006 s to 2170 s. Included in these 80 stations were 14 sites of the Bendigo transect and four sites from the small north-south Southern Delamerian transect (Figure 3.1). The full impedance tensor was inverted, with error floors of 5%. Vertical magnetic field data were not inverted, as this data-type was only collected for the Bendigo and Bendigo West transects.

Numerous inversions were run using the 3D inversion code ModEM (Egbert and Kelbert, 2012; Kelbert et al., 2014) for the entire profile, varying starting resistivities, mesh size and covariance parameters. A tendency of the inversion code was to resist placing resistivity structures directly beneath the profile, instead mainly positioning conductive features away from the profile, which resulted in geologically unreasonable models. Various methods were investigated to attempt to model the resistivity structure directly beneath the profile such as decreasing the covariance parameter (a smoothing parameter described in Kelbert et al., 2014) for the shallow upper crust, or performing

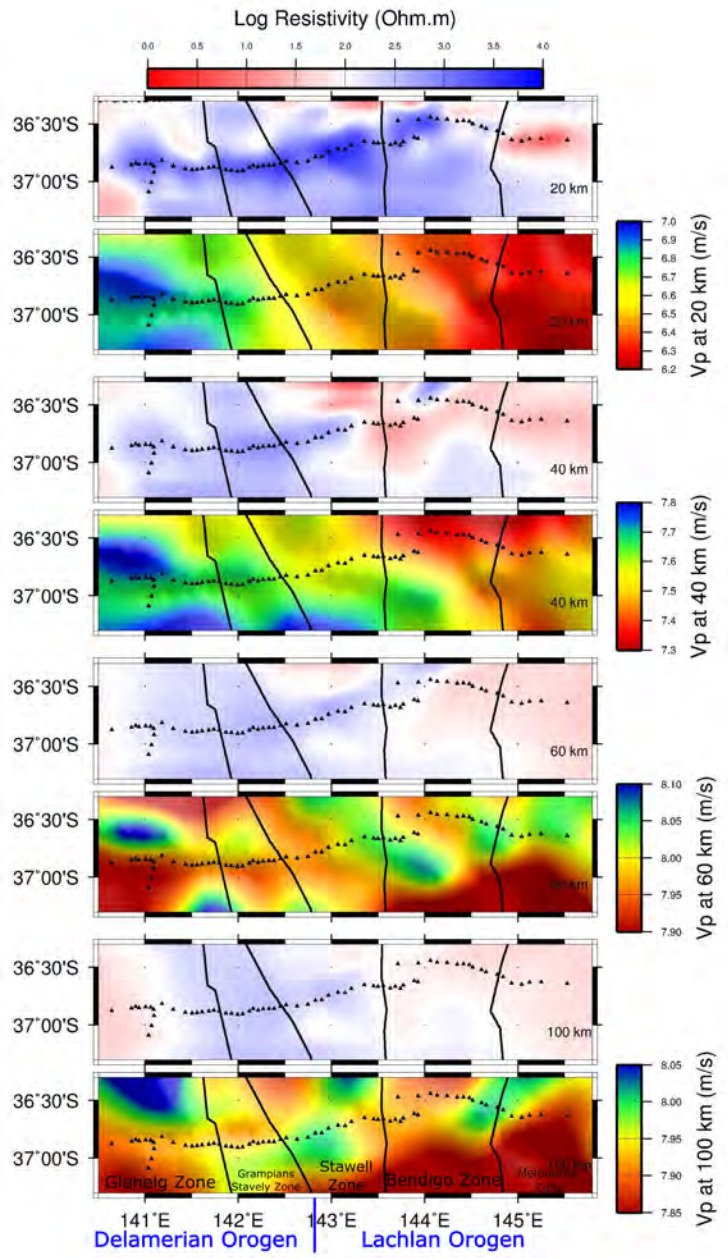

Figure 3.6: Electrical resistivity depth slices from 3D MT model (red regions conductive, blue resistive) and P-wave velocity slices from Wombat model (blue fast, red slow) at 20, 40, 60 and 100 km (Rawlinson et al., 2014b). Black boundaries are tectonic zones from Figure 3.1. Note that scale for velocity changes for each depth slice to highlight changes across the survey region.

the 'nested' approach, which involves low-resolution modelling over a large area including the ocean, followed by a calculation of the electric field boundary solutions for a smaller 'zoomed in' region, which are then used for quicker calculations of a finer mesh within the zoomed region.

The method that was most successful, however, involved varying the starting model from the general half-space approach. One-dimensional inversions were performed on the determinant of the impedance tensor using the Dipole1D (Key, 2009) modelling code for each of the 80 sites on the profile. In this step an additional 41 sites from the AusLAMP array (~55 km site spacing) were also used to provide some initial off-profile constraints and to better constrain the real-world 3D geometry. An interpolation was performed on the 1D resistivity models to obtain a smooth starting model for the 3D inversion. The presented model had the Dipole1D interpolated resistivity structure incorporating ocean regions (with a resistivity of 0.3 Ωm) in the starting model. The model space was 1000 (north-south) x 1500 (east-west) x 3000 km (vertical) kilometres and a covariance of 0.2 and horizontal cell size of 2.5 x 2.5 km were used.

Despite containing less crustal features than the 2D inversions (as expected with lower resolution capabilities and larger site spacing), the resultant 3D model fit the data well (see Figures 3.3,3.5), encompassing each of the datasets with changing strike. The final RMS obtained was 2.3. Figure 3.3 (bottom) shows the ModEM modelled data responses as phase tensor ellipses. In general, the 3D model fits the major features of the data, including the Lachlan Orogen conductive region, and the upper crustal low phase angle (dark blue) ellipses, and the changes in responses across faults. The long period ellipses are modelled with a slightly higher minimum-phase angle than the measured data. Another way of imaging the quality of the ModEM model fit is by viewing the site-by-site RMS misfits (Figure 3.5). As the overall RMS of the model was 2.3, an RMS of less than 2.5 has been deemed a good fit. Sites with a misfit larger than 2.5 are coloured for the full impedance tensor (Full Z), and the individual components of Z (Zxx, Zxy, Zyx and Zyy). In general, the Stawell and Bendigo Zones contain the sites with the highest RMS, which is to be expected due to the more complex resistivity structure indicated in the phase tensor ellipses and poorer data quality in this region (Figure 3.3).

The presented model (Figures 3.6 and 3.7) reveals a mainly resistive upper crust (~10 000 Ωm) with the exception of the Melbourne Zone (~1000-2000 Ωm with some pathways less than 50 Ωm). The lower crust is much more conductive beneath the Lachlan Orogen (~20-100 Ωm) than the Delamerian Orogen (~100-5000 Ωm). A conductive band (less than 100 Ωm, labelled as C1 in Figure 3.10d) intersects the profile near the Yarramyljup Fault, with its location in rough agreement with crustal conductors observed in Robertson et al. (2015). The change in resistivity between the Delamerian and Lachlan lithospheres occurs east of the Moyston Fault and is shown by the green dashed line in Figure 3.10d. A resistive salient juts into the Lachlan Orogen at profile latitudes, labelled as R1 in Figure 3.10d.

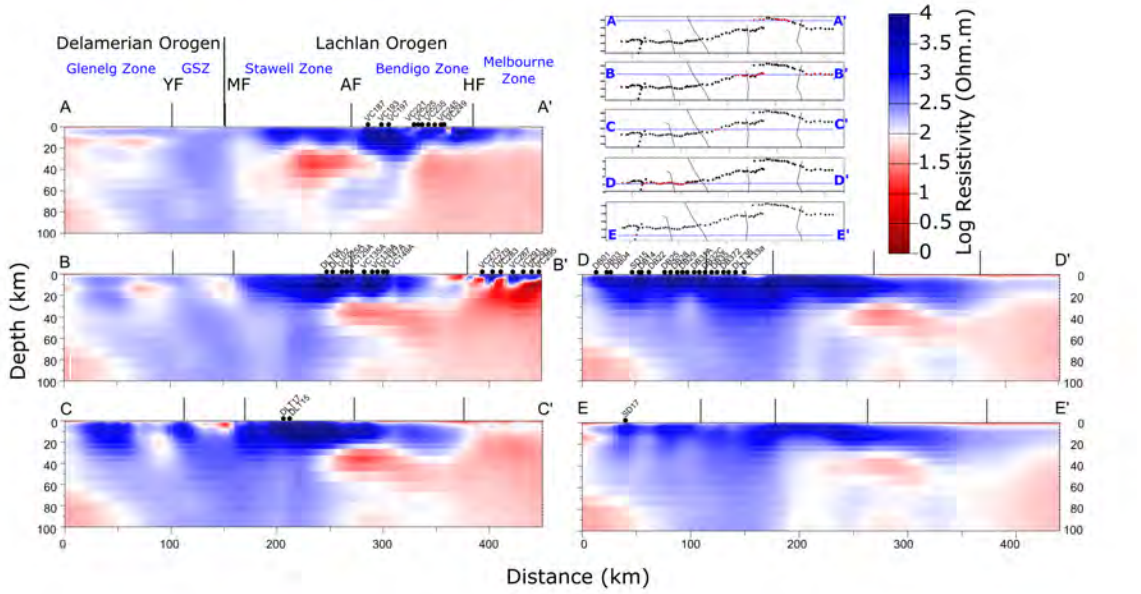

Figure 3.7: Vertical slices taken from the ModEM 3D Model. YF=Yarramyljup Fault, MF=Moyston Fault, AF=Avoca Fault, HF=Heathcote Fault, GSZ=Grampians-Stavely Zone.

3.3.4 2D Inversion

2D inversion is useful as models can be inverted at a higher resolution with a finer mesh than in a 3D inversion and in less time. The Bendigo transect (Dennis et al., 2011b) was excluded from the 2D inversion due to its 10 km offset from the rest of the transect. Given the complications with strike variance along the transect, data were rotated to a strike that suits sites within the transition zone between the Delamerian and Lachlan Orogen, as this was the region of most interest. The strike changes at around the location of the transition, so west of site DLT22 (in the Delamerian-Lachlan transition transect) the profile was rotated to 60 degrees west of North, and to the east of site DLT22 the profile was rotated to 75 degrees east of North, resulting in two profiles that meet in a shallow v-shape. The off-diagonal components of the impedance tensor for each site were modelled in WinGLink (Rodi and Mackie, 2001) using error floors of 2.5% for the TE and TM phase, 5% for the TM resistivity and 50% for the TE resistivity to allow for out-of-plane galvanic effects. The resultant model fit the data well with a final RMS of 2.18 using a tau value of 1 (tau is a trade-off parameter between data fit and model smoothness, with smoother models having a higher tau value). Flexibility was given during the inversion process to allow the code to adjust the apparent resistivity values to account for any static shift effects (an inherent problem of the MT method involving scaling of apparent resistivity curves caused by near surface local anomalies; see Jones, 1988). Additionally, having a very fine mesh near the surface alleviated static shift effects.

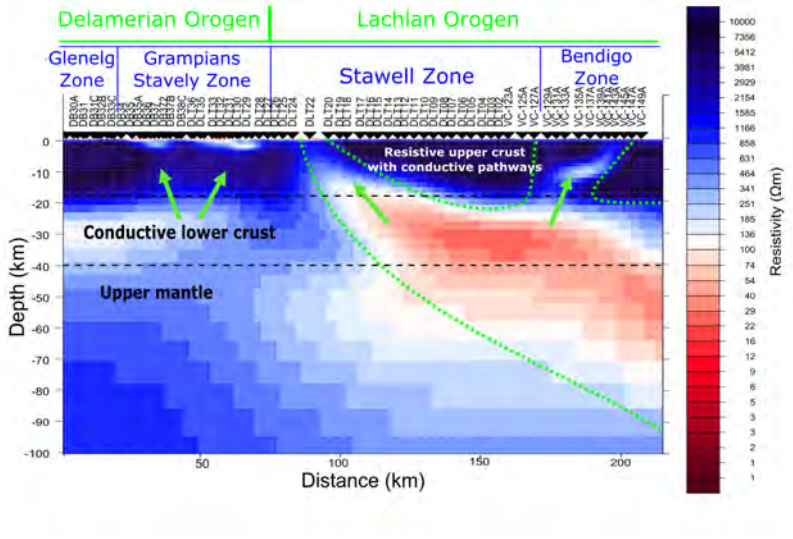

Figure 3.8: 2D Inversion of MT data using WinGLink from the Southern Delamerian, Delamerian-Lachlan Transition and Bendigo West transects. Red regions are low resistivity (or conductive) and blue regions are resistive. Note not all MT sites are labelled. Green arrows indicate direction of fluid movement and green dotted lines outline conductive crust of the Lachlan Orogen. Black horizontal dashed lines approximately mark the transitions between the upper crust, lower crust and upper mantle.

The resultant inversion (Figure 2.6) shows a heterogeneous lithosphere; the western half of the profile resides within the more resistive Delamerian Orogen, and the eastern half within the more conductive Lachlan Orogen. The shallow upper crust has a thin conductive layer of sediments (~10-60 Ωm), thinning to the east. The mid-upper crust is much more resistive (10 000-20 000 Ωm). Traversing this resistive zone are conductive pathways of a few hundred to a thousand Ωm extending from mid-crustal to upper mantle depths, often connecting to the surface. The base of most of these conductors resides in the lower crust to upper mantle, where a change in resistivity across the Delamerian to Lachlan transition is apparent. The boundary appears to be east dipping, slightly east of the Moyston Fault at site DLT22. Within the Lachlan Orogen, the lower crustal resistivity is as low as 10 Ωm (range ~ 10-50 Ωm), and is up to an order of magnitude less resistive than the adjacent Delamerian Orogen's lower crust (50-100 Ωm). Within the Lachlan Orogen, the lower crustal conductor may extend into the upper mantle to a depth of around 80 km, but it is difficult to resolve the bottom of lower crust/upper mantle conductors as MT signal is attenuated within a conductor (Jones and Ferguson, 2001).

3.4 Discussion

3.4.1 Delamerian lithosphere and Lachlan lithosphere

The most striking feature in both the 2D and 3D inversions is the west-to-east gradient in electrical resistivity of the lower crust and upper mantle near the transition from the Delamerian to the Lachlan Orogens in the Stawell Zone (Miller et al., 2005). This large change in resistivity occurs approximately at the location of the Mortlake Discontinuity. The Mortlake Discontinuity was initially identified by Price et al. (1997) from a distinct change in strontium and lead isotopic ratios in Newer Volcanic basalts across a north-northwest boundary zone spanning 35 km. The Lachlan Orogen is enriched in strontium relative to the Delamerian Orogen, and contains the highest $^{87}Sr/^{86}Sr$ ratios in the province (up to 0.7058), with much more variation, and the mean ratio is higher than is observed in the Delamerian Orogen. These changes were attributed to either a change in the mantle source of the basalts on either side of the discontinuity, or a variation in the crustal contamination that occurred to the magma on its ascent. A seismic velocity gradient also occurs across the Mortlake Discontinuity to depths greater than 200 km (Rawlinson et al., 2014b). The combination of the resistivity gradient spanning mid crustal to upper mantle depths, a discontinuity in the phase tensor ellipses down to periods of at least ~1000 s, and the deep-reaching velocity gradient suggest a shallow upper mantle explanation for the Mortlake Discontinuity.

3.4.2 Comparison of 2D and 3D Inversion of a transect

Despite the differences between the 2D and 3D datasets there is good agreement of models, particularly at lower crust to upper mantle depths, as shown in Figure 3.9. For the 3D model the transition between the more resistive subsurface of the Delamerian Orogen and the more conductive Lachlan Orogen varies for different latitudes. Its most easterly location occurs at site DLT06 in the eastern Stawell Zone at latitudes similar to the transect. Its most westerly extent is in the western Stawell Zone at site DLT17, around 20 km east of the Moyston Fault, as can be seen in Figure 3.7. A resistive salient (R1: Figure 3.10d) is imaged in the 3D model and is a feature that could not be observed from 2D modelling. For the 2D inversion, the location of the transition occurs near the western-most extent of the boundary as imaged in the 3D inversion. This is likely a result of performing a 2D inversion on a profile with complex non-2D resistivity structure, which has placed off-profile conductors to the north and south (above and below the resistive salient), at profile latitudes. The transition in the 2D inversion is located near the western edge of the Stawell Zone at site DLT20, and extends from 10 km to 80 km depth.

The upper crust shows a greater degree of heterogeneity in the 2D models, with conductive pathways extending from the mid-crust to the surface, such as those imaged in Robertson et al. (2015) and Dennis et al. (2011b, 2012). The larger mesh size and lower number of MT sites of the 3D inversion inevitably leads to less resolving power, thus making the narrow conductors imaged in the 2D model difficult to resolve in the

3D inversion. Comparing the two models at 10 km depth reveals small decreases in resistivity in the 3D model at the locations of the crustal conductors that appear much more pronounced in the 2D models (Figure 3.9). These absolute resistivities may differ as the 3D inversion code can distribute the conductance amongst a 3D volume whilst the 2D inversion code can only distribute conductance within a 2D area. The 2D inversion resolves the base of the lower crustal to upper mantle conductor of the Lachlan Orogen better than the 3D inversion, which is still imaging a conductive mantle at 100 km depth, although the inversion sensitivity decreases beneath the conductor. Phase tensor ellipses in Figure 3.3 for the Lachlan Orogen show that at longer periods the upper mantle has a rise in resistivity, although the depth at which this should occur is undetermined.

3.4.3 Comparison with seismic velocity

A comparison of seismic wavespeeds and resistivity may be helpful as an enriched lithosphere is commonly thought to exhibit lower resistivities (due to expected high hydrogen concentrations Selway (2014)) and lower velocities (due to Fe-enrichment) than a depleted lithosphere (Griffin et al., 2013). More often than not, however, a simple correlation is not possible as seismic wavespeeds depend on a large number of factors including mineral composition, temperature, pressure and pore-space geometry (Muñoz et al., 2010), whereas resistivity in the lower crust and upper mantle is primarily controlled by interconnected minor conducting phases, hydrogen and partial melt.

In Figure 3.6, there is a change in wavespeeds in the Delamerian Orogen (faster) than the Lachlan Orogen at crustal depths. At a depth of 20 km, a transition from lower P-wavespeeds in the Lachlan Orogen to higher P-wavespeeds in the Delamerian Orogen occurs at the Moyston Fault. At this depth, a change is not yet observable in the resistivity, which occurs onlt at depths exceeding 20 km, and further east than the seismic-defined transition. There is a good agreement between the seismological and MT models at 40 km, with the Lachlan region containing lower resistivities and lower wavespeeds than the west, suggesting an enriched lithopsheric mantle composition. By 60 km the seismic model becomes reasonably complex, and it is difficult to make comparisons until a depth of 100 km where the Bendigo and Melbourne zones both have low resistivities and low velocities, thus suggesting a compositional variation between the Bendigo and Melbourne zones.

3.4.4 Comparison with Moho depths

A notable feature within the 3D inversion is the correlation between resistive regions at 37 km depth and shallower Moho depths (Figure 3.10). The eastern part of the model is conductive, as is the far west of the model region. These regions coincide with greater Moho depths exceeding 37 km, and are therefore imaging conductive lower crust at this depth. The more resistive western part of the model has Moho depths less than 37 km and is imaging resistive upper mantle within the Delamerian Orogen.

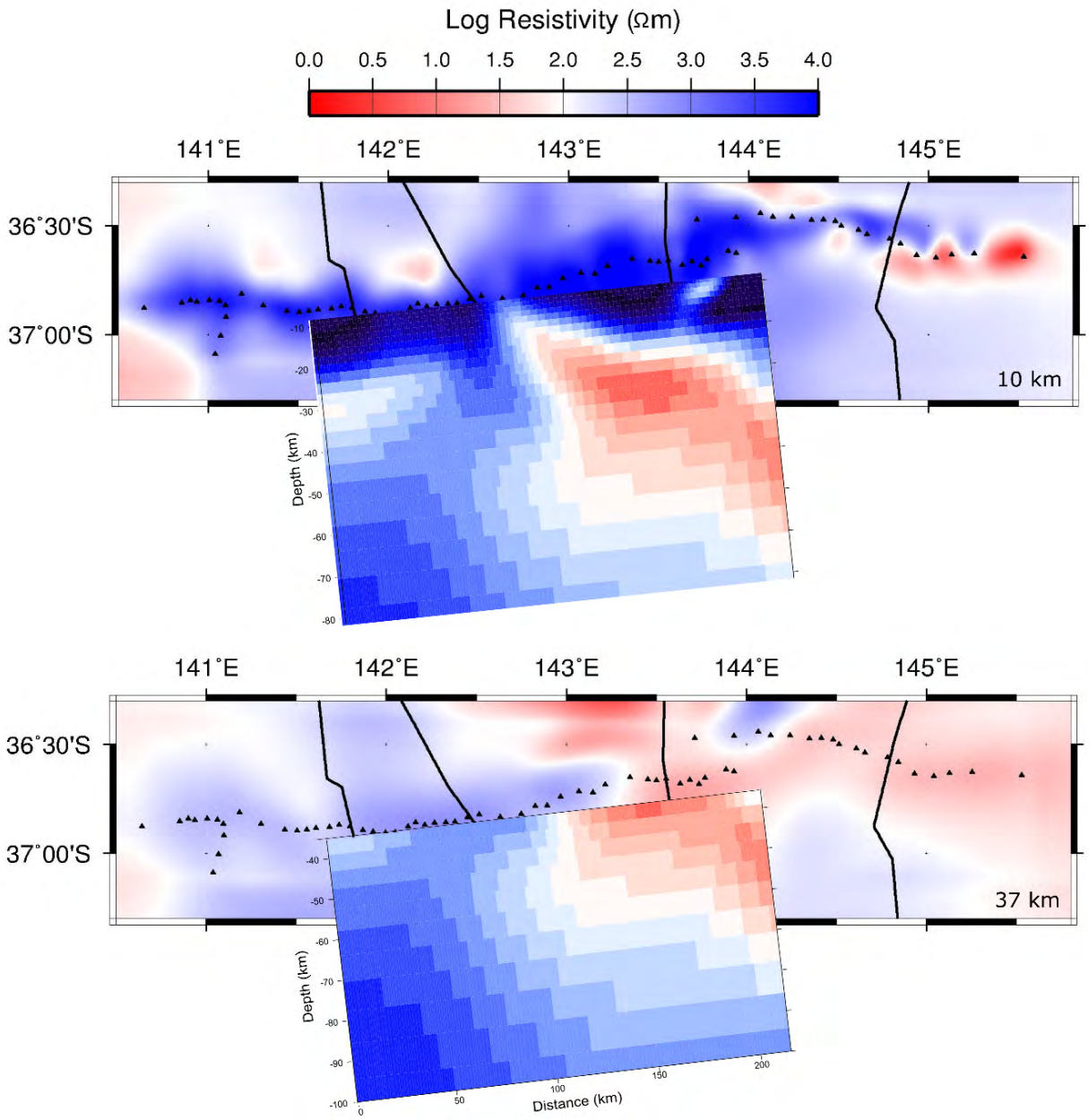

Figure 3.9: 2D WinGLink model overlying the 3D ModEM model.
Top: 10 km depth slice of 3D model with the 2D slice for depths 10-80 km.
Bottom: 37 km depth slice of 3D model with the 2D slice for depths 37-100 km.

The Moho depths are reasonably well constrained within the survey region, as Moho picks come from seismic reflection profiles coinciding with the MT transects (Kennett et al., 2011; Salmon et al., 2013; Kennett et al., 2015). The gradient of Moho depths varies from being NE-SW oriented in the west, to N-S in the east which has a notable correlation with geo-electric strike from phase tensor ellipses (Figures 3.3 and 3.4).

3.4.5 Geological explanation for resistivity variation

Resistivity trends of the crust emerge across the globe, with porous and clay rich crustal sediments of low electrical resistivity (~1-100 Ωm), a resistive upper-mid crust (1000-50 000 Ωm), which sometimes transitions to a conductive lower crust varying from around ten to a few hundred Ωm. Laboratory studies of commonly occurring crustal rocks are unable to explain the low resistivities in the lower crust, and thus conductors are often attributed to the presence of minor conducting phases such as graphite, hydrogen or fluids (Jones, 1992; Guo et al., 2015; Glover, 2015). In a stable environment, fluids do not have a long residence in the lower crust before being consumed in interactions with wall rocks, however hydrogen in nominally anhydrous minerals can reside for hundreds of millions of years provided there is an absence of high temperature events (Demouchy, 2010), and graphite will remain stable if temperatures remain below 900 °C (Mathez, 1987).

The eastern end of the transect is within the mostly conductive Bendigo Zone. Exposures of Cambrian basalts in this region include island arc andesites and boninites that formed above an oceanic subduction zone (Crawford et al., 1984). Newer Volcanics Province enriched mantle to the east of the Mortlake Discontinuity has also been argued as a possible relict subduction effect (Price et al., 1997). Subduction processes can enhance conductivity from the release of hydrogen into nominally anhydrous minerals from dehydration reactions (Sleep, 2009). At the absence of partial melting events, this hydrogen can remain for hundreds of millions years (Demouchy, 2010). Resistivity can also be decreased by carbon from subduction related melts and fluids (Sleep, 2009; Plank and Langmuir, 1998) which may precipitate out as conductive grain boundary graphite films (Glover, 1996; Mathez, 1987). Three-dimensional forward modelling of MT data from Palaeozoic orogens in the Ossa Morena Zone in Portugal detected a lower crustal conductor that extends laterally for hundreds of kilometres which the authors interpret as a combination of interconnected graphite in grain boundary films and graphite aggregates in movement planes of deep seated decollements (Muñoz et al., 2008).

The Precambrian Selwyn Block in the Melbourne Zone exhibits unusually low resistivity for lithosphere of this age. Generally, Precambrian lithosphere is more resistive than younger lithosphere such as most of the Palaeozoic lithosphere surrounding the Selwyn Block in Victoria, however this does not seem to be the case here. Although seemingly unusual, this is certainly not unique within Precambrian lithosphere, with two examples in South Australia alone. Within the Archaean Gawler Craton, Thiel and Heinson (2013) reveal a mantle conductor possibly related to a subduction-modified

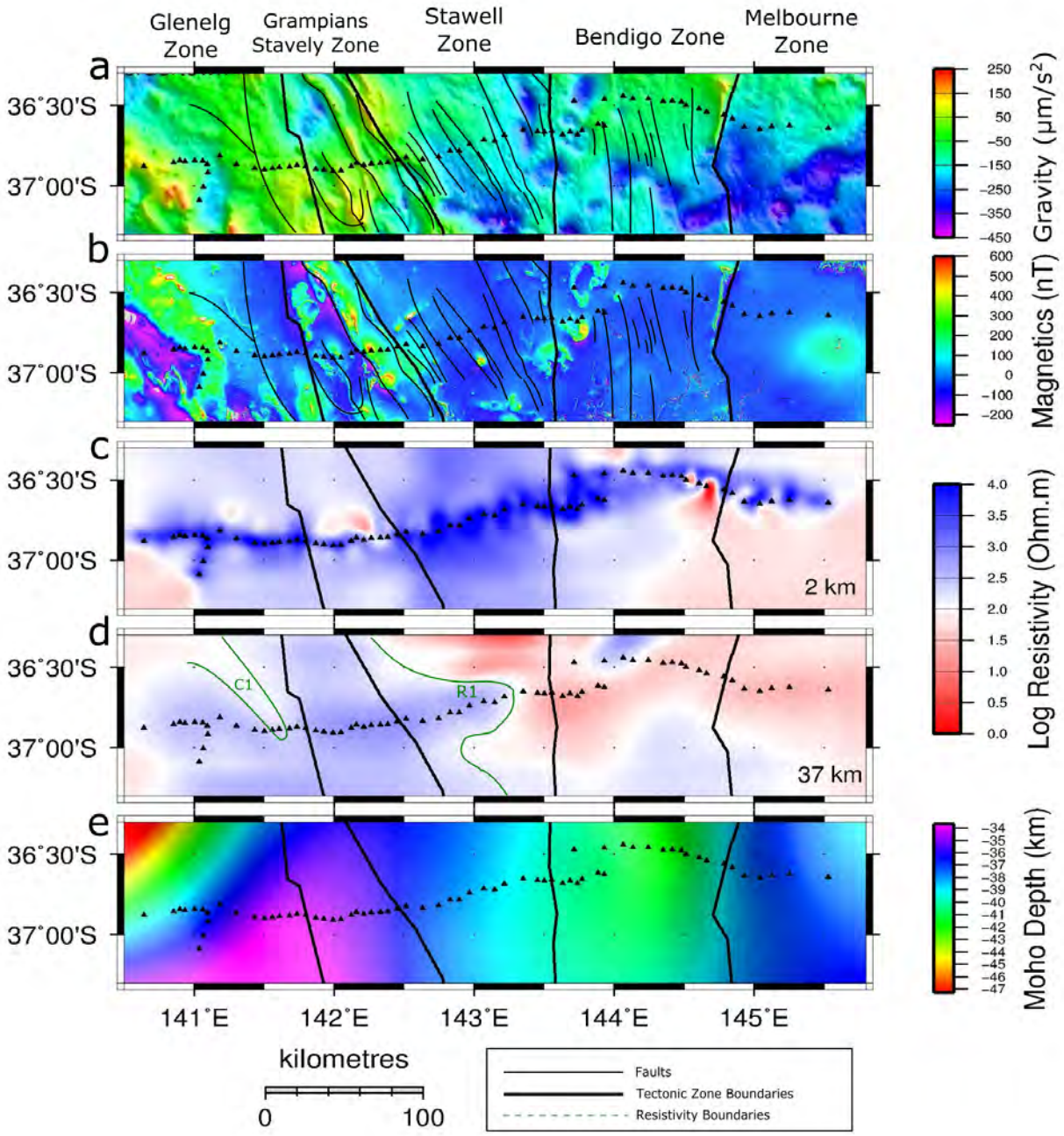

Figure 3.10: a) Gravity data with faults overlain. b) TMI data with faults overlain. c) 1 km electrical resistivity depth slice from 3D inversion. d) 37 km electrical resistivity depth slice from 3D inversion. e) Moho depths from AusMoho (Kennett et al., 2011; Salmon et al., 2013).

mantle plume event, and Robertson et al. (2016b) and Thiel et al. (2016) image crustal conductors related to fluid movement within the Paleo-Mesoproterozoic Curnamona Province. Robertson et al. (2016b) also observe conductors within the Neoproterozoic Ikara-Flinders Ranges, and interpret these to relate to past alterations associated with kimberlite intrusions. A similar scenario may be occurring here, with north-east-southwest trending conductors correlating with the trend of Devonian granitic intrusions being observed in the regional scale AusLAMP MT data (Duan et al., 2016).

3.5 Conclusion

The crust and upper mantle beneath western Victoria were imaged using magnetotellurics, traversing the transition between the Delamerian to the Lachlan Orogen. The east-west transect is almost 500 km in length, and its location revealed a more conductive lower crust and upper mantle beneath the Lachlan Orogen than in the Delamerian Orogen. Within the Lachlan Orogen, the Stawell Zone is conductive in parts, but the Bendigo and Melbourne Zones are more so. The Stawell and Bendigo Zones were formed above a subduction zone. Hydrogen and/or carbon precipitated from dehydration reactions of the subducting plate and from subduction-related melts may have served to enhance conductivity. The Melbourne Zone contains the Proterozoic microcontinent of the Selwyn Block, and is more conductive than expected for Proterozoic lithosphere.

If the change from resistive to conductive lower crust/upper mantle is taken to be an indication of the location of the Delamerian-Lachlan transition, then this transition occurs as an undulating NNW-SSE-trending boundary, with a salient of resistive Delamerian lithosphere jutting across the Stawell Zone. The western most extent of the transition within the survey region occurs near the Moyston Fault and its eastern most location occurs closer to the Avoca Fault, near the boundary between the Stawell and Melbourne Zones.

The lithosphere beneath the Delamerian Orogen is resistive with higher seismic velocities at crustal depths. Small low resistivity regions are imaged within the crust and are attributed to fossil fluid pathways. Recent collection of a 100 km MT transect 50 km south will allow better lateral constraint on the continuity of the resistivity gradient near the Delamerian-Lachlan transition.

Additionally, we found that the method of performing 1D inversion on the determinant of the impedance tensor and interpolating between these 1D models to use as a starting model for 3D inversion resulted in a more geologically plausible final model than simply using a half-space. In particular, inclusion of the 55 km spaced AusLAMP sites within a few hundred kilometres of the survey region in the initial 1D interpolation starting model also provided better off-profile constraints without increasing computational time by having to include these off-transect sites in the 3D inversion.

Acknowledgments

Thank you to the many personnel that contributed to the collection of the MT data throughout the 5 different surveys this paper uses. Many thanks to Zara Dennis, Michael Stepan for making their data available, and to Geoscience Australia and the Geological Survey of Victoria for making the Victorian AusLAMP dataset available. Figures were produced using GMT (Wessel et al., 2013), MTpy (Krieger and Peacock, 2014), and 3D grid (kindly provided by Naser Meqbel). Thank you to Alison Kirkby for providing scripts for the 1D interpolation, and to Phil Skladzien for providing geophysical maps for the project. Thank you to AuScope for providing the equipment, and Goran Boren for maintaining the equipment. Funding was generously provided by AuScope, the University of Adelaide and the Victorian Geological Survey.

CHAPTER

FOUR

LITHOSPHERIC REWORKING AT THE PROTEROZOIC-PHANEROZOIC TRANSITION OF AUSTRALIA IMAGED USING AUSLAMP MAGNETOTELLURIC DATA

Robertson, K.[1], Heinson, G.[1], Thiel, S.[2]

[1]Electrical Earth Imaging Group, Department of Earth Sciences,
School of Physical Sciences, University of Adelaide, Adelaide SA 5005, Australia
[2] Geological Survey of South Australia, Department of State Development,
Adelaide SA 5000, Australia

Published on 15th October, 2016 as:
Robertson, K., Heinson, G. and Thiel, S. (2016). Lithospheric reworking at the Proterozoic-Phanerozoic transition of Australia imaged using AusLAMP Magnetotelluric data. *Earth and Planetary Science Letters*, 452:27-35. doi: 10.1016/j.epsl.2016.07.036

Statement of Authorship

Title of Paper	Lithospheric reworking at the Proterozoic–Phanerozoic transition of Australia imaged using AusLAMP Magnetotelluric data
Publication Status	☑ Published ☐ Accepted for Publication ☐ Submitted for Publication ☐ Unpublished and Unsubmitted work written in manuscript style
Publication Details	Robertson, K., Heinson, G. and Thiel, S. (2016). Lithospheric reworking at the Proterozoic–Phanerozoic transition of Australia imaged using AusLAMP Magnetotelluric data. Earth and Planetary Science Letters, 452, 27-35.

Principal Author

Name of Principal Author (Candidate)	Kate Robertson
Contribution to the Paper	Performed data collection, processed, modelled and interpreted data. Wrote the manuscript and acted as corresponding author.
Overall percentage (%)	85 %
Certification:	This paper reports on original research I conducted during the period of my Higher Degree by Research candidature and is not subject to any obligations or contractual agreements with a third party that would constrain its inclusion in this thesis. I am the primary author of this paper.
Signature	Date 8/9/16

Co-Author Contributions

By signing the Statement of Authorship, each author certifies that:

i. the candidate's stated contribution to the publication is accurate (as detailed above);

ii. permission is granted for the candidate in include the publication in the thesis; and

iii. the sum of all co-author contributions is equal to 100% less the candidate's stated contribution.

Name of Co-Author	Graham Heinson
Contribution to the Paper	Supervised development of work, helped in data interpretation and manuscript evaluation.
Signature	Date 8 SEPT 2016

Name of Co-Author	Stephan Thiel
Contribution to the Paper	Supervised development of work, helped in data interpretation and manuscript evaluation.
Signature	Date 12/09/16

SUMMARY

Seventy-four stations from the long-period Australia-wide AusLAMP (Australian Lithospheric Architecture Magnetotelluric Project) dataset were used to image the electrical resistivity beneath the Neoproterozoic Ikara-Flinders Ranges and adjacent Palaeo-Mesoproterozoic Curnamona Province. Results from 3D inversions using ModEM show a relatively resistive Ikara-Flinders Ranges, with two parallel arcuate conductors at 20 to 80 km depth in the Nackara Arc. There is a good correlation of diamondiferous kimberlites occurring over conductors, which we interpret as evidence for these conductors to be residing on large lithospheric structures that have been conduits for partial melt and volatile movement in the Jurassic. The Curnamona Province is remarkably conductive for a region that is thought to have a cratonic core, with Delamerian reworking only at its edges. The conductor covers most of the province at depths of 10-40 km, and its presence at lower crustal depths suggests that conductive sediments can not entirely explain it. Fluids associated with subduction may have pervasively modified the crust in the past, resulting in an enrichment of carbon, enhancing the conductivity. Additionally, we conclude that the notion of a single continuous arcuate Flinders Conductivity Anomaly is unlikely and that the anomalous response observed is instead a result of the combined response of three separate anomalies: the Curnamona Province Conductor and the two Nackara Arc Conductors.

4.1 Introduction

Electrical conductivity anomalies have been observed in Australia and around the world. Utilising naturally occurring electromagnetic fields, large zones of anomalous conductivity have been identified using induction vectors. Within Australia, several major regional conductivity anomalies have been defined, most extending for hundreds of kilometres. These include; the Eyre Peninsula Anomaly, the Carpentaria Anomaly, the Tamar Anomaly, the Southwest Queensland Anomaly, the Canning Basin Anomaly, the Otway Anomaly and the Flinders Conductivity Anomaly (see Wang et al., 1997, for a summary of anomalies).

Each of these anomalies was first identified using Geomagnetic Depth Sounding (GDS) data, as early as 1972 when the enigmatic Flinders Conductivity Anomaly (FCA) was first observed (Gough et al., 1972). The FCA is a well known but little understood anomalous electrical resistivity region that runs through the Palaeo-Mesoproterozoic Curnamona Province and the Neoproterozoic Ikara-Flinders Ranges. With each new dataset collected, interpretations of the anomaly have changed in terms of shape, size and origin. The FCA is roughly situated at the ancient eastern margin of Gondwana, at the transition from Precambrian Australia in the west to the Phanerozic accreted orogenic belts to the east. Gough et al. (1972) initially suggested the presence of a north-south conductor in the upper mantle, alongside a possible east-west crustal conductor north of the Ikara-Flinders Ranges. Since then, the FCA was interpreted as a single NW-SE trending line running north of the Ikara-Flinders Ranges (Tammemagi

and Lilley, 1973). By 1985, a southward extension of the FCA into the Flinders Ranges was made possible with new GDS sites through the Central Ikara-Flinders Ranges (Chamalaun, 1985), with successive studies all having a shape similar to that in Wang and Chamalaun (1995). The interpreted depth of the anomaly varied between studies, ranging from upper crustal to shallow upper mantle, with a minimum thickness of 10 km. Interpretations of the FCA have focussed on two main theories: a crustal interpretation based on buried saline-filled sediments (Lilley and Tammemagi, 1972; Tammemagi and Lilley, 1973; Chamalaun, 1985; White and Polatajko, 1985; Wang and Chamalaun, 1995; Milligan et al., 2012) or a mantle cause such as a mantle step or postulated plate boundary (Gough et al., 1972; Tammemagi and Lilley, 1973; Paul, 1994).

The Australian Lithosphere Architecture Magnetotelluric Project (AusLAMP) commenced in late 2013 with the collection of long-period magnetotelluric data at 0.5 degree intervals across the Ikara-Flinders Ranges, which is intended to eventually expand to image the entire Australian lithosphere in three dimensions. The new addition of our array provided an excellent opportunity to help determine the nature of the FCA. The AusLAMP dataset has enabled this enigmatic and anomalous region to be illuminated in full 3D detail with results from inversions of 74 long period MT sites showing that the FCA is more likely to be the combined effect of three separate conductors, one within the crust of the Curnamona Province and two parallel conductors within the Nackara Arc, rather than one continuous conductor.

4.2 Geological Background

Within South Australia sits the north-south trending Neoproterozoic Ikara-Flinders Ranges, dividing the two tectonically stable provinces of the Archaean-Proterozoic Gawler Craton to the west and the Palaeo-Mesoproterozoic Curnamona Province to the east. The Ikara-Flinders Ranges form most of the Adelaide Rift Complex, a region that has undergone at least five rift cycles, the earliest from ~827 Ma. Rifting was incomplete with only early stage magmatism occurring during most cycles. In the Cambrian, tectonics switched to a compressive regime, with the Delamerian Orogeny (514-490 Ma) and associated subduction affecting the Ikara-Flinders Ranges. The Ikara-Flinders Ranges are comprised of thick Neoproterozoic sediments, divided into five different tectonic zones by Rutland et al. (1981), based mostly on the type of Delamerian-associated deformation that occurred; The Northern Flinders Zone, the Central Flinders Zone, the Nackara Arc, the Fleurieu Arc and the Torrens Hinge Zone.

More recently in the Jurassic, magmatic events have included the eruption of kimberlites in the Ikara-Flinders Ranges, predominantly within the Nackara Arc at Monk Hill (depth range- mantle lithosphere, 50-180 km; Tappert et al., 2011) and Eurelia (depth range-lower mantle >670 km; Tappert et al., 2009). To the west lies the Gawler Craton, where any major reworkings ceased about 1.5 Ga (Hand et al., 2007). To the east, the Benagerie Volcanics, part of the Ninnerie Supersuite, are the Curnamona Province's equivalent to the Gawler Range Volcanics, both erupting within 10 Ma of each other at

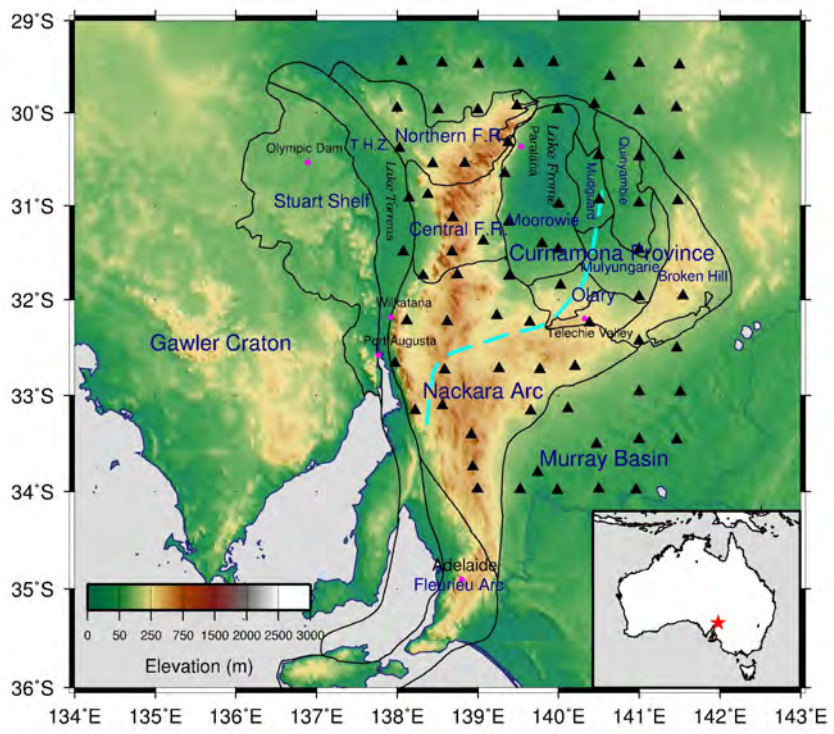

Figure 4.1: Station Locations AusLAMP MT site locations over topography with tectonic zones of the Ikara-Flinders Ranges, and domains of the Curnamona Province, outlined in black. The cyan dashed line shows the previous estimate of the Flinders Conductivity Anomaly, which differs to the outcomes of this paper.

1595 Ma (Wade et al., 2012). The Curnamona Province has been reworked at its edges by the Delamerian Orogeny and can be divided into separate domains based mostly on metamorphic assemblages (Dutch et al., 2005; Rutherford et al., 2006, as labelled in Figure 4.1).

The Ikara-Flinders Ranges, in its locality near the transition between Proterozoic to Phanerozoic Australia, undoubtedly holds clues to the tectonic history, formation and evolution of Australia. It has relatively high seismicity for an intraplate deformation region and an explanation to satisfy both the deformation and seismicity is difficult. The South Australian Heat Flow Anomaly (SAHFA) runs through the Ranges, with average heat flow measurements of 92 ± 10 mW/m^2 (Neumann et al., 2000), resulting in deeper earthquakes occurring in ductile lower crust. Many explanations have been put forward for the deformation and seismicity ranging from a thermally weakened crust (Holford et al., 2011) to various types of mechanically weakened crust (Célérier et al., 2005; Dyksterhuis and Müller, 2008; Pilia et al., 2013). More recently, Balfour et al. (2015) suggest high pore fluid pressure in the lower crust is required to account for the earthquakes which occur in the ductile lower crust.

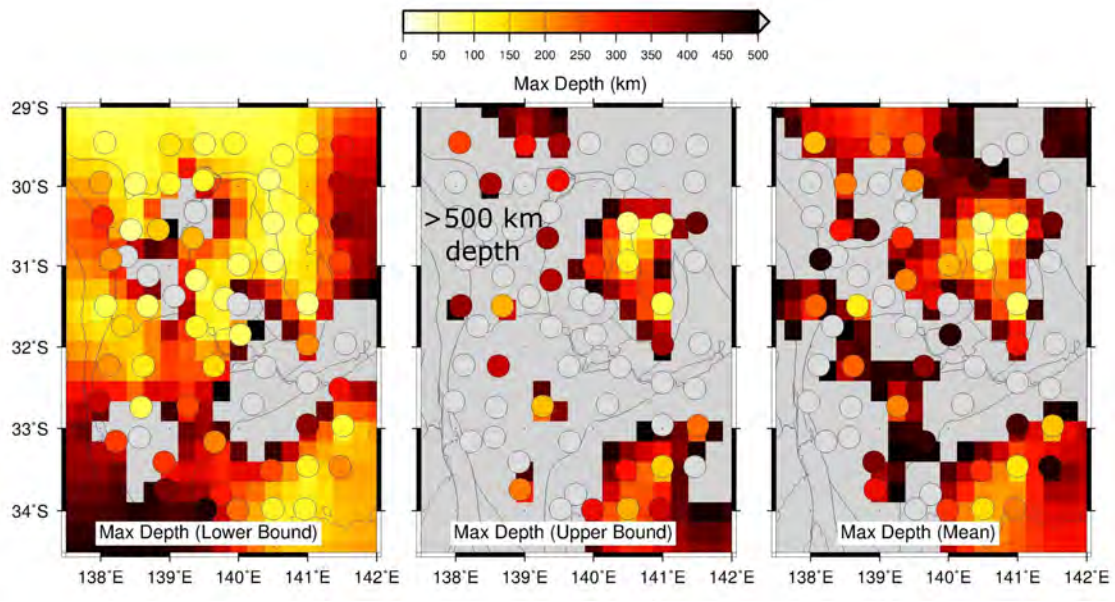

Figure 4.2: Estimate of depth of MT signal penetration using a Niblett-Bostick transformation. This figure shows estimates for penetration depth of the longest period data at each site. The lower estimates represent those of the Zxy component, the upper estimates represent those of the Zyx component, and mean shows the average of the two depths. Regions in grey image deeper than 500 km.

4.3 Method and Results

In November 2013, 29 long-period MT sites were collected using AuScope instruments covering the entire Ikara-Flinders Ranges, commencing AusLAMP. An additional 47 stations were collected in June, 2015 to expand the dataset northward, and eastward into western New South Wales (Figure 4.1). The resulting dataset encompasses the entire Ikara-Flinders Ranges and Curnamona Province. Data were processed using the robust remote processing algorithm BIRRP (Chave and Thomson, 2004) and sites were referenced to neighbouring sites that were recording simultaneously or to the Canberra geomagnetic observatory to improve signal-to-noise ratio and responses at short periods. Data were processed to a period range of ~2 to 17 000 s. Longer periods correspond to greater depths, dictated by the skin depth equation which relates the skin depth δ(T) (in m) to period T by $\delta(T) \sim 500\sqrt{\rho_a T}$ where ρ_a is the equivalent average resistivity of a uniform half-space.

An estimate of the depth of signal penetration is shown in Figure 4.2, which was derived from a Niblett-Bostick transformation, which involves rotation of the impedance tensor to obtain the minimum and maximum values of the Zxy and Zyx components of the impedance tensor, from which the lower and upper bounds of the apparent resistivity can be derived. From these two values, the skin-depth can be calculated, giving the lower and upper bounds, respectively, on the maximum depth of penetration of the MT

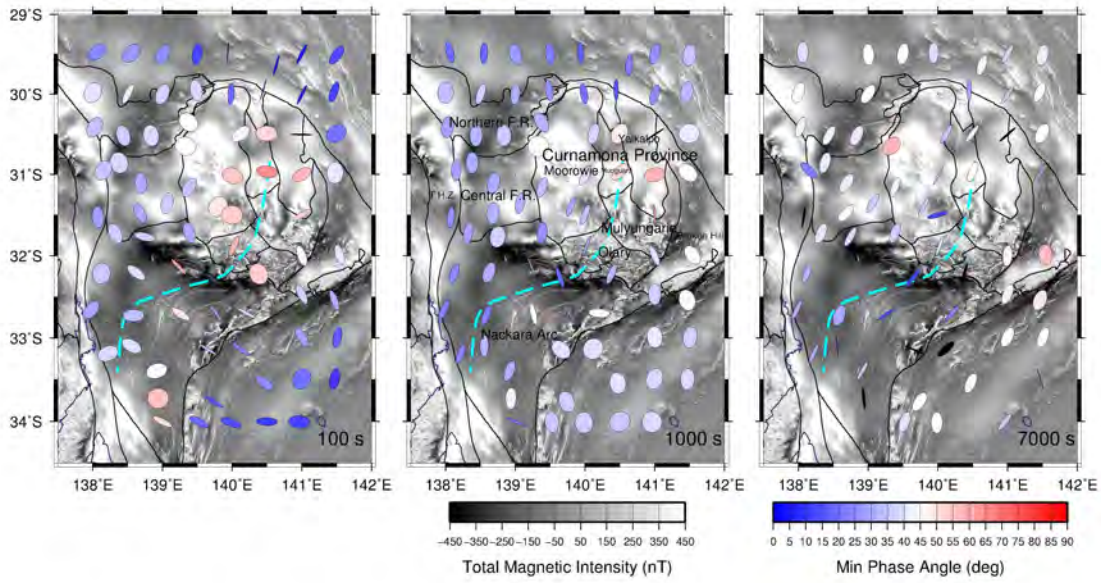

Figure 4.3: Phase tensor ellipses over TMI Phase tensor ellipses for periods of 100, 1000 and 7000 s corresponding to lower crust and upper mantle depths over greyscale Total Magnetic Intensity. Cyan dashed line shows previous interpretation of the FCA.

signal. In most cases the average estimated penetration depth is 200 km or greater, with grey regions indicating an estimated depth exceeding 500 km.

Phase tensor ellipses shown in Figure 4.3 are shaded with the minimum phase angle, which gives an indication of how the resistivity changes with depth; angles greater than 45°, or a shade of red, show that the structure is becoming more conductive with depth. Conversely, angles less than 45°, or ellipses shaded blue, are representative of increasing resistivity with depth. Phase tensor ellipses within the centre of the Curnamona Province at periods of 100, 500 and 1000 s are red indicating there is a more conductive region within the Curnamona Province, as are the ellipses in the southern Nackara Arc (Figure 4.4). Blue ellipses in the north of the model region and in the southeast represent shallow sediments of the Arrowie/Cooper Basins and the Murray Basin, respectively, overlying basement. From the ellipses it is apparent that the eastern margin of the Nackara Arc forms an electrical boundary, with the minimum phase lower, and the ellipses more circular, in the Murray Basin than the Nackara Arc.

At a period of 7000 s, corresponding to upper mantle depths, ellipses are all oriented in a similar direction, with the major axis aligned in a NE-SW direction, similar to the present direction of motion of the Australian-Indian tectonic plate. This phenomenon has been observed before by Thiel and Heinson (2013), and can be explained by anisotropy within hydrous olivine in the upper mantle (Karato, 1990).

4.3.1 3D Modelling

The three-dimensional inversions were performed using the ModEM algorithm of Egbert and Kelbert (2012) and Kelbert et al. (2014). Many inversions were run to investigate the effect of varying parameters such as the model covariance (a smoothing factor that penalizes deviations from a prior resistivity model- see Kelbert et al., 2014), the half-space starting resistivity, model dimensions, cell size, number of layers and the method of error calculation. Some of these tests are discussed further in the Supplementary Information, but the features within our preferred model are robust features that have withstood this testing.

A starting resistivity of 100 Ωm was used with a model covariance factor of 0.3 in all directions, and error floors of 5% for the impedance tensor and 3% for the tipper error. We inverted the full impedance tensor at 23 periods from ~2 s to 17 000 s, and the tipper at only 21 periods ranging from ~1 s to 8000 s, as the planar wave approximation fundamental to the magnetotelluric theory breaks down at longer periods. The model fits the data well, with the starting RMS (RMS here is the ratio of the difference between the measured data and the modelled data, and the data error) of 15.05 reducing to a final RMS of 1.33. Almost all modelled responses fit the data well, with Supplementary Figure A.3 highlighting the few sites which have an RMS larger than 2. The similarity of the phase tensor ellipses for the measured and the modelled data indicate that the model fits the data well (Figure 4.4). The ellipses shown for a period of 4000 s differ from the data ellipses more than shorter periods, and in general the data fit is slightly poorer. This is expected within MT data due to the diffusive nature of MT signal with depth. Additionally, the model is less sensitive to deep features, especially if situated beneath a highly conducting region. From Figure 4.2 it can be seen that even within the highly conducting Curnamona Province, the penetration depth estimates are at least 100 km.

The three-dimensional electrical resistivity model that we present in Figure 4.5 comprises a mainly resistive Ikara-Flinders Ranges, with resistivity varying from 1000-5000 Ωm in the crust, reducing to about 1000-2000 Ωm by 60 km. At a depth of 1 km, the model is resistive (~1000-3000 Ωm), with the exception of the Murray Basin in the southeast, and the Cooper Basin in the north, which are both very conductive (~10 Ωm). Within the Nackara Arc of the Ikara-Flinders Ranges, the 3D model delineates two roughly parallel, arcuate conductors (~1-50 Ωm) that follow the curve of the arc (labelled the Western Nackara Arc Conductor-WNAC and the Eastern Nackara Arc Conductor-ENAC; Figure 4.5). The main conductor of the ENAC spans depths of about 20 to 60-70 km, and the WNAC from 20 to 80 km. These conductors extend further into the mantle with a lower conductivity, however in the MT method, resolution decreases significantly beneath large conductors, creating a downward smearing effect. The Curnamona Province exhibits a complex resistivity structure, with a very resistive Broken Hill Domain on the eastern third of the province (~2000 to 10 000 Ωm). The western two-thirds of the province are host to a large conductor (the Curnamona Conductor- CC, ~1-50 Ωm), spanning a depth of about 5-40 km. The CC starts at a depth of about 5 km in the northern two-thirds of the Curnamona Province, although we cannot eliminate the possibility of a connection to the surface, and at about 10 km

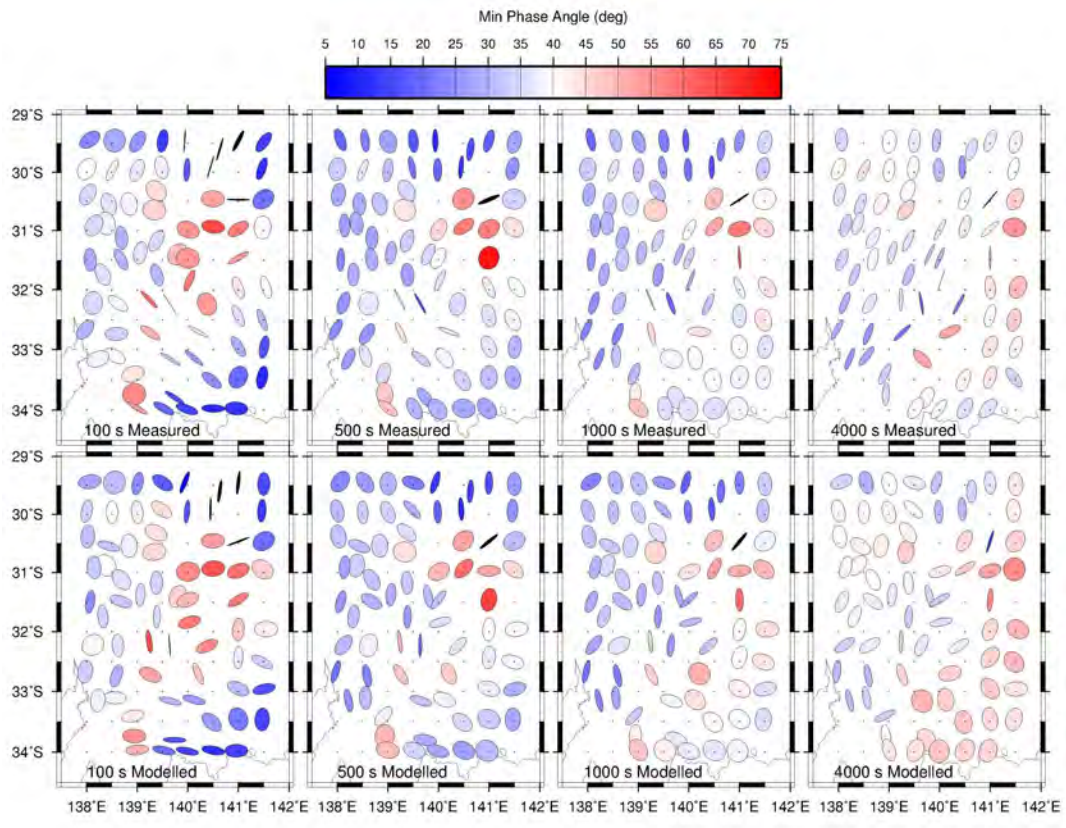

Figure 4.4: 3D Inversion Data fit Top row: Phase tensor ellipses for the MT data at periods of 100, 500, 1000 and 4000 s. Bottom row: Phase tensor ellipses for the same periods, but using the ellipses taken from the data as modelled using ModEM.

in the southern third of the Curnamona Province. At 10 km depth, the CC is elongated in the north-south direction, 250 km long by 100-150 km wide, residing almost entirely within the Quinyambie Domain of the Curnamona Province. The conductor dips steeply westward, and by 20 km almost covers the Mudguard and Moorowie Domains. At 30 km, the shape of the CC has altered, forming an upside-down T-shaped conductor, until it disappears almost entirely by about 40 km.

4.4 The Flinders Conductivity Anomaly

It seems unlikely that the observed anomalous features in the GDS and MT surveys summarised in the introduction are all highlighting one single conductor. Results from three-dimensional inversion of the AusLAMP data subset indicate the presence of three separate conductive anomalies, whose combined responses create the observed effect from induction arrows. Figure 4.6 shows induction arrows at a period of 1000 s over a 10 km and a 30 km depth slice, with the previous best estimate of the FCA indicated by the cyan dashed line. Within the northern half of the array, most induction arrows

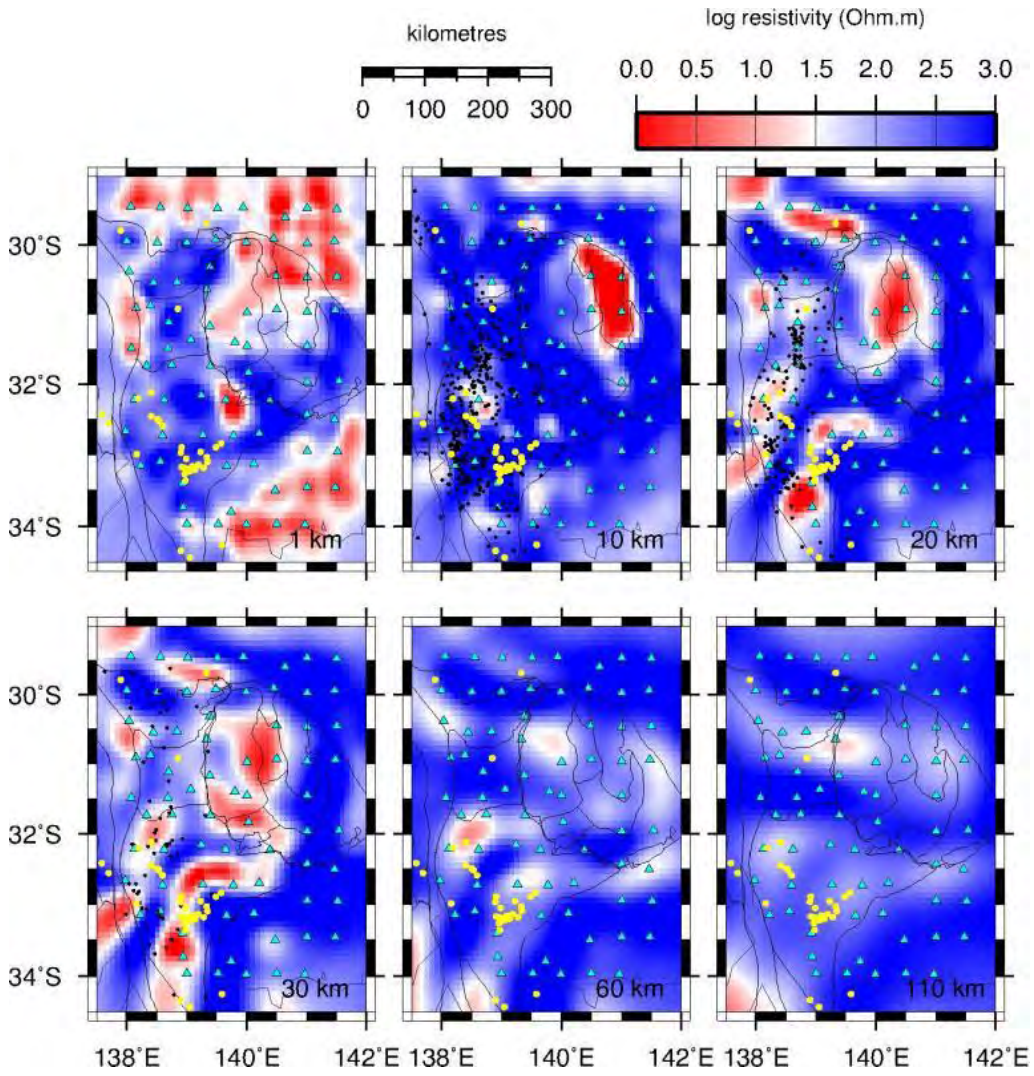

Figure 4.5: 3D Inversion Depth Slices Resistivity depth slices with earthquake hypocentres plotted with black circles. Earthquakes within ±1 km, ±2 km and ±3 km are projected on the 10 km, 20 km and 30 km resistivity slices respectively. Yellow circles are discovered diamonds. CC=Curnamona Conductor, WNAC=Western Nackara Arc Conductor, ENAC=Eastern Nackara Arc Conductor. Shape of Nackara Arc conductors depicted by green lines for the 30 km depth slice.

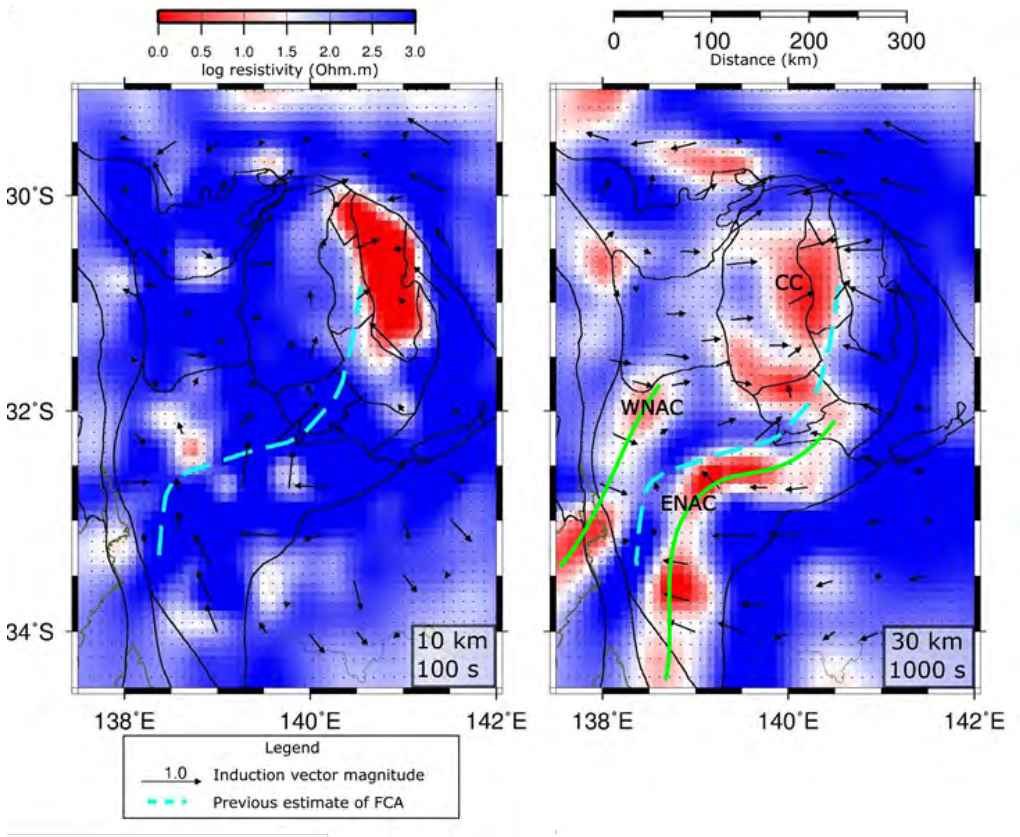

Figure 4.6: Flinders Conductivity Anomaly Induction vectors shown at a period of 100 s and 1000 s for each MT station point in the direction of increasing conductivity. Vectors are overlaying 10 km and 30 km depth slices, and zone boundaries in black are as labelled in Figure 4.1. The cyan dashed line shows the previous interpreted location of the FCA.

arrays point toward the Curnamona Conductor, which spans depths of about 5-40 km. Moving southward from the Curnamona Province into the Nackara Arc, the notion of a continuous conductor now seems unlikely. The arrows all point toward the previous estimate of the FCA, however instead of seeing one conductor on this cyan line, we instead observe two large conductors on either side of the line. It appears that within this resistive band nested between the ENAC and WNAC, the induction vectors are almost cancelled out due to the superimposed responses from the conductors on either side. Thus we can deduce that the 'FCA' can be split into three different conductors, the Curnamona Conductor at ~5-40 km and the Eastern and Western Nackara Arc Conductors at 30-80 km, and hereon the FCA refers to the Flinders Conductivity Anomalies. Our interpretation for these conductors differs slightly from the north to the south. We discuss in more detail possible causes of the Flinders Conductivity Anomalies in the next sections.

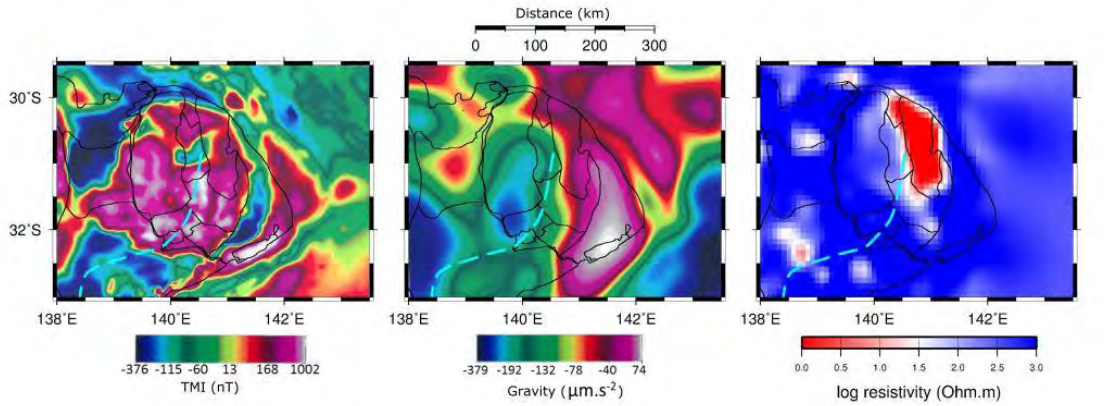

Figure 4.7: The Curnamona Province Left: Total magnetic intensity, reduced to the pole with an upward continuation of 5 km. Middle: Bouguer Gravity with a 50 km low-pass filter applied. Both from (Milligan et al., 2000). Right: Electrical resistivity depth slice at 10 km for the Curnamona Province.

4.4.1 Curnamona Province Conductor

The Curnamona Province is a relatively tectonically stable province, which has only undergone three thermal events in the last 1.6 Ga (Dutch et al., 2005). The first, and most significant event was the Olarian Orogeny which occurred 1620-1585 Ma and included the development of the (mainly S-type) granites of the Ninnerie Supersuite during the late stages of the orogeny. Most features of the Curnamona Province today are derived from this orogeny, during a period of high heat flow and compression. The cause of the second, a Grenvillian event (~1200-1100 Ma), is speculatively related to reactivation and/or formation of shear zones. The third and most recent thermal event is associated with the subduction and subsequent uplift of the Delamerian Orogeny which has reworked the province, mainly at its edges, and has resulted in the formation of the greenschist to amphibolite grade shear zone metamorphic assemblages (Dutch et al., 2005).

The Curnamona Province has remarkably high conductivities for a stable province. A craton generally exhibits high resistivities, due to the decrease in temperature and depletion of conductive phases over time (Selway, 2014). The thermal and structural reworking of the Curnamona Province during the Delamerian Orogeny may have resulted in the conductive province interior. Much of the mid-lower crust of the Curnamona Province exhibits very low resistivities. At these depths, possible explanations for high conductivity involve the presence of interconnected conducting phases including graphite, sulphides, magnetite, free fluids or partial melt. Seismic tomography results indicated the presence of a high velocity region beneath the Curnamona Province (Rawlinson et al., 2014b) at upper mantle depths. Resolution decreases at crustal depths, but the high velocity zone appears to extend upward into the crust, indicating that partial melt is unlikely within this stable province. Whilst there are sulphides in economic amounts within the province, they are unlikely to explain a conductor that

covers such a large area and depth range.

The Curnamona Province is divided up into domains based on age, sedimentary facies and thickness, magmatism and metamorphism (Figure 4.1). At 10 km depth, the conductor resides almost entirely within the Quinyambie Domain, which is covered by the Yalkalpo Subbasin. Due to the thick cover sequence, little is known about the geology of the Quinyambie Domain, but from total magnetic intensity (TMI) data it is defined by deep-seated magnetic granites, indistinguishable from the neighbouring Erudina Domain (Fricke et al., 2004). The conductor dips westward and shifts to the Mudguard, Olary, Mulyungarie and Erudina Domains to depths of about 35 km. The Broken Hill Domain is the only domain to remain resistive at all depths, further supported by two independent 2D profiles of long period MT data in a NS and an EW orientation through the Broken Hill and Olary Domains (Gill, pers. comms, 2002). The Broken Hill Domain hosts numerous deposits, most notably the Broken Hill Pb-Ag-Zn deposit (about 200 million tonnes with 50 million tonnes of lead and zinc and 20 000 tonnes of silver), but a number of other Pb-Ag-Zn and Cu deposits. Conductive crustal pathways are often observed at the location of mineral occurrences, usually marking the prevailing alteration from fossil fluid movement through zones of weakness in the crust (e.g. Heinson et al., 2006; Robertson et al., 2015; Dennis et al., 2011b).

The boundary between the Broken Hill Domain and the rest of the Curnamona Province appears to be a very significant lithospheric feature in electrical resistivity but also in geochemistry (Rutherford et al., 2006) and potential field data (Milligan et al., 2000). Figure 4.7 shows potential field data in the Curnamona Province, filtered to highlight deep-seated features. The reduced to the pole TMI data with an upward continuation of 5 km, show a large change from west to east, from a magnetic high, to a large dip of magnetic low at the transition to the Broken Hill Domain, coinciding with the eastern boundary of the Curnamona Conductor at 10 km depth. The low stretches ~50 km across and then changes back to a magnetic high. The Bouguer gravity with a 50 km low-pass filter applied changes from a gravity low in the west to a gravity high in the east (at about 141 °E) coinciding with the western boundary of the Curnamona Conductor at 10 km depth in Figure 4.7.

Using trace element geochemistry of metabasites from the Broken Hill and Olary domains, Rutherford et al. (2006) interpret that lithospheric thinning in the Broken Hill Domain resulted in the incorporation of more primitive and depleted melts into the partial melt region. In contrast, the westerly neighbouring Olary Domain's lithospheric mantle has undergone less thinning, and is thought to have been refertilised from sediment or fluids from a subducting slab (Rutherford et al., 2006), probably during the period of 1.8 and 1.6 Ga, when a convergent boundary along the southern margin of eastern Proterozoic Australia was proposed by Giles et al. (2002). Subduction refertilisation can re-introduce conductive minor phases to the lithosphere, such as graphite or interconnected magnetite within serpentinite (Robertson et al., 2015), both of which can enhance conductivity. Graphite is known to exist at shallow depths within parts

of the Curnamona Province, such as within the Plumbago Formation and the Alconie Formation (Conor and Preiss, 2008).

Lilley and Tammemagi (1972); Wang and Chamalaun (1995) and Milligan et al. (2012) all suggest that conductive, possibly saline-filled, sediments may contribute to the enhanced conductivity of the FCA. The Ikara-Flinders Ranges are host to thick (up to 15 km) Adelaidean marine sediment sequences (Preiss and Forbes, 1981) and the Curnamona Province is host to Neoproterozoic sediments and the Palaeoproterozoic Willyama Supergroup. Wet sedimentary rocks can have resistivities in an approximate range of 5-50 Ωm and the presence of interconnected saline water can further reduce resistivities to the range of 0.1-1 Ωm (Nesbitt, 1993). Shallow (<5 km) sedimentary rocks in the Cooper and Otway basins have low resistivities ranging from 1-30 Ωm based on broadband MT surveys and well resistivity logs (Kirkby et al., 2015; Didana, 2016). Low resistivities in sedimentary rocks can result from the presence of interconnected pore space containing saline fluids or the presence of clay minerals, which are usually conductive. However, the anomaly is located deeper than 5 km and is therefore less likely to have significant connected pore space. Fluid-filled fractures may be a source of enhanced conductivity but these would have to be open, which is dependent on age and stress field, and the presence of fluids in a tectonically stable region is unlikely, although it has been suggested by Balfour et al. (2015) to explain the seismicity of the Ikara-Flinders Ranges. Measurements taken from several springs in the western Great Artesian Basin Springs contain high $^{3}He/^{4}He$ isotope ratios that are interpreted to be derived from mantle carbon beneath the springs (Keppel et al., 2013, K. Karlstrom & A. Love, pers. comms. 2015). This suggests that there are crustal conduits for fluids nearby to the Curnamona Province.

Two examples of lithospheric structures in the survey region that could be used as crustal fluid pathways include the Paralana escarpment (Célérier et al., 2005), and Wilkatana, north of Port Augusta on the western Ikara-Flinders Ranges (Williams, 1973). Clark et al. (2005) also present evidence for crustal fluid flow in the Telechie Valley shear zone in the Olary Domain, with fluids originating from metamorphic dehydration of the Willyama Supergroup Metasediments and the shear zones acting as pathways for fluid movement to shallow levels.

4.4.2 Eastern Nackara Arc Conductor

The Nackara Arc is a mechanically weakened zone from numerous rift sequences since the Neoproterozoic (Preiss, 2000). Phase tensor ellipses (Figure 4.3) show a change in resistivity structure from the Eastern Nackara Arc Conductor into the Murray Basin for periods of 100 s and 1000 s. The arcuate boundary is interpreted to be the transition from Proterozoic Australia in the west to Phanerozoic Australia in the east. Using ambient noise tomography, Rawlinson et al. (2014a) show that the fast axis of anisotropy aligns in a curvilinear north-south direction with the western edge of the Murray Basin, that sweeps around to follow the eastern boundary of the Curnamona Province, roughly coinciding with the eastern limit of Precambrian basement. Results

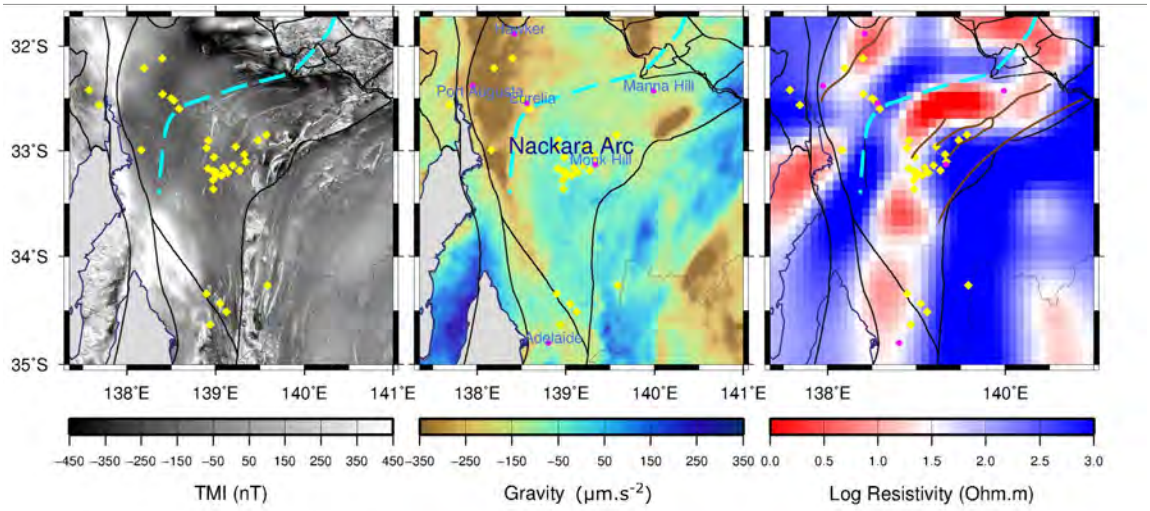

Figure 4.8: The Nackara Arc The Nackara Arc of the Flinders Ranges, from left to right: Total Magnetic Intensity (TMI), bouguer gravity, and electrical resistivity. The brown lines on the resistivity image show 'macrofaults' from Lindsay Curtis (2003). Black boundaries are as described in Figure 4.1.

of Rawlinson et al. (2014b) reveal high velocities within the mantle of the Curnamona Province as expected, with a change from fast velocities to slower velocities moving into Phanerozoic Australia, the likely boundary of East Gondwana. Gough et al. (1982) suggested from his study on the North American Central Plains resistivity structure, that conductivity anomalies may be related to ancient plate margins. The presence of diamondiferous kimberlites that were erupted in the Jurassic have been found within the conductive region encompassed by the Nackara Arc Conductors, indicating that in the past there have been major pathways spanning the lithosphere vertically to sub-vertically (Figure 4.8). These kimberlites are suggested to have been derived from subducted remnants of the proto-Pacific plate (Tappert et al., 2009). We suggest that mantle-sourced fluids or partial melt have moved through the lithosphere in the past, altering the subsurface and depositing conductive phases such as grain-boundary graphite films, similar to the interpretation proposed by Jones et al. (2001) in the Slave Craton. The orientation of the Nackara Arc Conductors follow that of complex along strike so-called macro-structures that spatially coincide with mafic intrusions and kimberlite pipes (Lindsay Curtis, 2003).

4.4.3 Western Nackara Arc Conductor

The WNAC at its locality on the western edge of the Ikara-Flinders Ranges, is more likely to be related to the rifting cycles. A continuous, major melting event will gradually lead to depletion of the lithospheric mantle in incompatible elements such as Fe, H, Na and Al, which would result in a resistive mantle. However, during each rifting cycle in the Ikara-Flinders Ranges, only early stage magmatism occurred, therefore

it is likely that asthenospheric fluids and melt were introduced to the lithosphere at the commencement of rifting, with only some of these incompatible elements actually ascending into the crust. The rifting would have left behind a mechanically weakened mantle, that has since been metasomatised at its base (Tappert et al., 2011). Metasomatism by fluids or melts may refertilize depleted lithosphere, if enriched in incompatible elements. To the west lies the Gawler Craton, which is for the most part, resistive as expected, but preserves a large conductor at 80 km depth beneath the 1595 Ma Gawler Range Volcanics, with its cause still in debate (Thiel and Heinson, 2013).

Modern analogues of rifting can help to better understand the ancient rifting. A study by Jiracek et al. (2013) found that in regions of active rifting around the world, the subsurface tends to exhibit low resistivity (less than or equal to 50 Ωm) at depths less than 30 km. A ~20 km thick crustal conductor (~10-30 Ωm) sits in the Baikal Rift in southeast Russia, in a depth range of 20-50 km. In the East African Rift, a highly conducting zone (~10 Ωm) was imaged in the upper crust (0-15 km). In the Rhine Graben lies a narrow very conductive (~3 Ωm) layer at 30 km. The cause of these conductors is variously attributed to pore fluids in an elevated geothermal gradient resulting in partial melting, interconnected amphibole and hydrothermal alteration products. With the right conditions, these conductive zones can be preserved. Ritz (1984) image a conductive zone in Senegal, West Africa, which they interpret to be a remnant of a failed ancient rift zone. The resistivity of the WNAC varies from about 1-50 Ωm and the main body of the conductor occurs at depths of 20 km to 50 km, within the range of the active rift conductors in Jiracek et al.'s 2013 comparative study.

4.4.4 Comment on fluids as a source of seismicity

The Ikara-Flinders Ranges experience unusually high levels of seismicity for an intraplate deformation region, at depths that are normally considered ductile. Various explanations have been called upon to explain the cause of these earthquakes, most recently that of Balfour et al. (2015) who suggest high pore fluid pressure in the lower crust as a cause for the relatively high levels of intraplate seismicity experienced in the Ikara-Flinders Ranges. Indeed, some western Great Artesian Basin springs to the north of our study region have been measured, recording elevated $^{3}He/^{4}He$ ratios, indicating that ascent of mantle fluids up lithospheric scale structures may still occur today. Figure 4.5 shows the locations of earthquakes within the Ikara-Flinders Ranges for upper, mid and lower crustal depths. The presence of pore fluids would potentially enhance conductivity unless these pores are disconnected. Mantle derived carbon residing in isolated fluid inclusions will not enhance conductivity. As we do not see a correlation of high conductivity and locations of earthquakes, either the pore spaces are discrete, i.e. not connected within the crust or the hypothesis of high pore fluids causing the earthquakes may be incorrect.

4.5 Conclusions

The Ikara-Flinders Ranges are mostly quite resistive (1000-5000 Ωm), with the exception of a very conductive crust within the Curnamona Province, which we label the Curnamona Conductor, and interpret to be the result of conductive sediments and refertilisation from subduction associated fluids and sediments. Despite induction arrows from electromagnetic studies over the last 45 years suggesting that there exists a single continuous conductor of length ~400 km running from the Curnamona Province and down through the Nackara Arc, we observe another two distinctly separate conductors occurring in the Nackara Arc. The Western Nackara Arc sits at the boundary between the Ikara-Flinders Ranges and the Torrens Hinge Zone and is attributed to rift-related mechanical weakness forming ancient fluid pathways. The Eastern Nackara Arc conductor is a significant lithospheric structure, situated at the approximate location of the transition from Proterozoic to Phanerozoic lithosphere. The conductor coincides with diamondiferous kimberlites erupted in the Jurassic, indicating that this region has had pathways stemming down into the lower mantle. We suggest that a conductive phase, perhaps grain-boundary graphite films, may have been deposited during the ascent of partial melt or fluids, enhancing the conductivity, a signature still retained in the lithosphere today.

Acknowledgments

We would like to thank AuScope for use of the instruments, and Goran Boren for continued technical expertise. Thanks to the many field personnel and to Geoscience Australia for logistical assistance. Thanks to Andy Love for assistance with contacting landholders, and to the landholders and traditional owners themselves for granting permission to their lands. Thanks to Peter Milligan, Wolfgang Preiss and Anthony Reid for helpful discussions. Thankyou to Nasar Meqbel for making 3D grid available for constructing input files for ModEM. All figures were produced using GMT, and 3D inversions were performed on eResearchSA supercomputers. We thank two anonymous reviewers for their valuable feedback resulting in an improved manuscript. Funding was from the Department for State Development, South Australia. KR was funded by an Australian Postgraduate Award. This publication is TRaX record number 356.

CHAPTER

FIVE

SUMMARY AND CONCLUSION

5.1 Summary

This thesis involves a study of the electrical resistivity of the lithosphere beneath southeastern Australia. Chapter 1 introduces the method of MT, the survey region and the motivation for this work. Chapter 2 outlines the processing, 2D modelling and interpretation of the 150 km Southern Delamerian broadband transect across the Delamerian Orogen. The outcome is a high resolution image of the resistivity of the crust (Robertson et al., 2015). Chapter 3 considers western Victoria in a regional 3D context, with the Southern Delamerian broadband transect combined with other existing transects in the region to create a continuous 500 km transect. Modelling of the transect was performed in both 3D and 2D, and has been submitted to the Australian Journal of Earth Science (Robertson et al., 2016a). Chapter 4 includes results from a subset of the AusLAMP array over the Ikara-Flinders Ranges and Curnamona Province. The study involved the collection, processing, 3D modelling and interpretation of the data (Robertson et al., 2016b).

5.2 The resistivity of southeast Australian lithosphere

By comparing the results from two survey regions (Figure 5.1) within southeast Australia at two very different resolutions with very different aged lithospheres, conclusions and generalisations can be made.

- The top few kilometres of the crust is mostly dominated by sedimentary basins and regolith. The primary control on resistivity here is permeability and porosity, with these unconsolidated shallow layers having low resistivities in the models (e.g. Otway Basin (Figure 3.10) and Cooper, Arrowie and Murray Basin (Figure 4.5)).

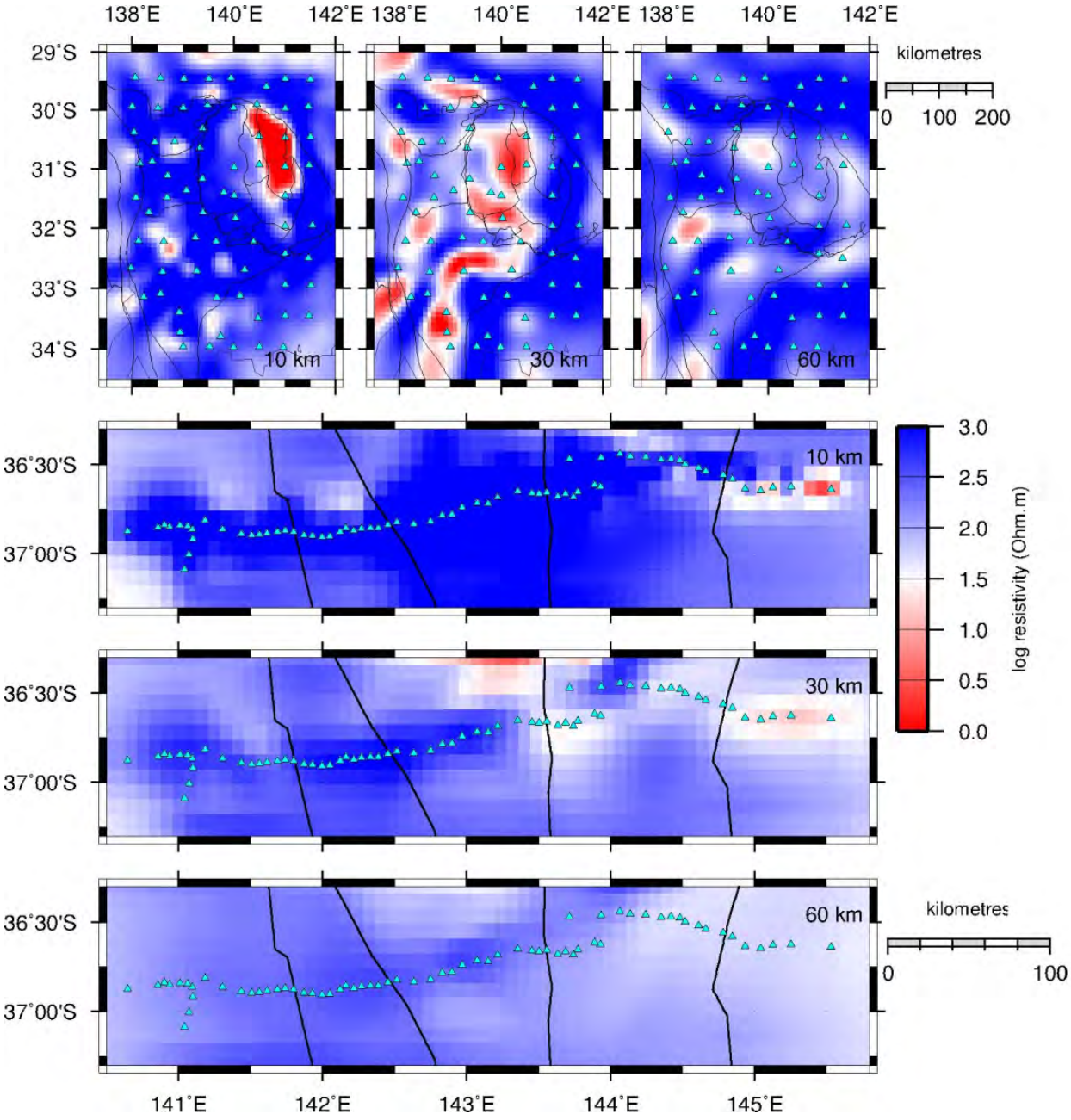

Figure 5.1: Comparison of the Ikara-Flinders Ranges/Curnamona Province 3D inversion (Chapter 4; top) and the western Victoria 3D inversion (Chapter 3; bottom), on the same colour scale for 10, 30 and 60 km.

- The upper crust extends to the brittle-ductile transition, whose depth varies with temperature and rheology (often ~15 km). Resistivity is generally larger than 1000 Ωm, with those regions of lower resistivity deemed anomalous (see e.g. conductors C1, C2 and C3 in Chapter 2). There is some evidence for narrow (brittle-permeable) low-resistivity zones in locations where there is <5 km spaced broadband. These narrow low-resistivity zones typically do not match known faults. Finer resolution surveys may delineate these features more, but it is not clear as to how laterally continuous they are.

- The lower crust has regions of high-resistivity (~1000 Ωm) but can be as low as ~10 Ωm. At the brittle-ductile transition there are some instances of very low-resistivity zones (~1-10 Ωm) that appear much more focused. At deeper levels (~20-40 km) the lower crustal conductors are broad (>100 km in extent). This suggests either (a) a formation event (e.g. subducted oceanic crust that forms an eclogite layer at the base of the crust) or (b) a thermal/fluid event that may have occurred at the same time (e.g. subduction-related melting) or later (plume, large igneous event etc.). The lower crust of the Ikara-Flinders/Curnamona region exhibits much lower resistivities along the Flinders Conductivity Anomalies regions than the western Victoria lower crust (Figure 5.1).

- The upper mantle resistivity generally varies between 100-1000 Ωm and is strongly affected by the tectonothermal history of the region. For example, the conductive Lachlan Orogen (~50 Ωm) retains signatures of subduction-related enrichment, and the Ikara-Flinders Ranges is resistive (~1000 Ωm) having undergone numerous rift events.

Although there are some apparent correlations with mapped crustal-scale faults and boundaries, the pattern of lower crustal conductors and strike of the MT data do not readily conform to the dominant strike and location of major boundaries. Secondary thermal/fluid resetting of the lower crust appears to be occurring, with enhanced conductivity due to either deposition of grain boundary graphite through fluid-based CO_2 from deeper mantle sources (perhaps melting of carbonates) and/or formation of magnetite-rich serpentinite.

5.3 Geological Observations

The Curnamona Province has seen almost no major reworkings since the Olarian Orogeny at 1.6 Ga, with the exception of reworking at its edges during the Delamerian Orogeny at ~500 Ma. However, the results of this work reveal a highly conductive crust within the Curnamona Province. Questions arise from these results regarding the enrichment event that must have occurred here, and what it means for prospectivity. A major contribution that continuation of AusLAMP will provide is the ability to identify prospective zones for mineral deposits. Parts of the Curnamona Province are known to host mineral deposits, with the large low resistivity zone in the crust highlighting a region of interest for mineral exploration. The Broken Hill Domain of

the Curnamona Province is imaged as completely resistive (with the 50 km resolution, despite the domain hosting the world-class Broken Hill Deposit.

The Flinders Conductivity Anomaly was previously thought to be one continuous conductor. A full 3D view such as that provided from this study was required to fully delineate the Flinders Conductivity Anomaly. The results were surprising, with the anomaly actually a combined effect of three separate conductors: the Curnamona Conductor, the Western Nackara Arc Conductor and the Eastern Nackara Arc Conductor. More surprising is that the depth spans vary considerably between the Curnamona Province and the Nackara Arc, indicating different causes of the conductors. Where the Curnamona Conductor is fully constrained to the crust, the Nackara Arc Conductors do not begin until 20 km depth, and appear to extend to at least 60-80 km depth, probably deeper.

The Delamerian-Lachlan transition is delineated by a change in resistivity within the Stawell Zone. The lower crust of the Lachlan Orogen is an order of magnitude less resistive than the adjacent Delamerian Orogen, and also than the lower crust of the Ikara-Flinders Ranges. Further modelling of the transects incorporating AusLAMP data and a newly collected transect further south of the main transect (Merrett, pers. comms. 2016) will provide information on the lateral continuity of this resistivity gradient.

5.4 Future Directions

Magnetotellurics has progressed considerably in the ~60 years since its development. This is due to a number of reasons- a better understanding of the magnetotelluric method, improved laboratory studies on the conductivities of minerals to aid interpretation of MT-derived conductivities, improved instrumentation, the continuous development of new and improved inversion codes, and largely, the increase in computer power making once impossible tasks such as 3D inversion possible. Results produced from the early stages of AusLAMP have been very beneficial in highlighting anomalous resistivity regions, opening up the opportunity to infill broad-scale surveys across these anomalous zones. However, incorporating closely space broadband MT sites into a model containing AusLAMP data is difficult with the huge variation in site spacing (50 km vs. <5 km). An increased speed of performing 3D inversions will enable better incorporation of high resolution surveys (such as those presented in Chapter 2 and 3) into a low resolution survey such as AusLAMP (Chapter 4) and make a fine model mesh over a large area possible. It will also allow larger subsets of AusLAMP to be inverted, a requirement that must be fulfilled over the next 5-10 years if AusLAMP is to be realised to its full extent- an eventual trans-lithospheric resistivity model of the entire country.

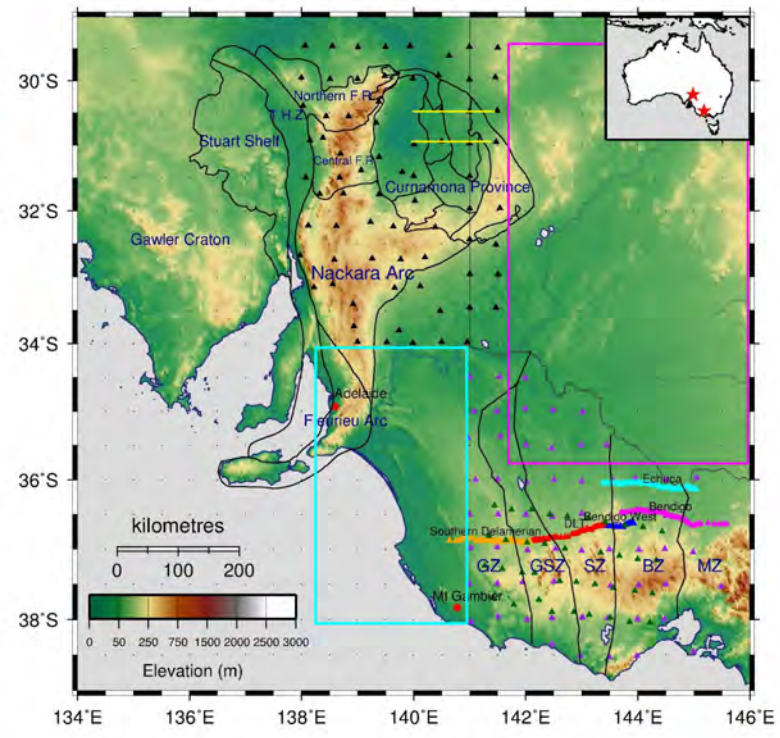

Figure 5.2: Regions are highlighted that are suggested for future studies. Suggestions: Extension of AusLAMP into NSW with collection of new sites (magenta box); extend 3D modelling of AusLAMP (Duan et al., 2016) to include existing AusLAMP SA sites (blue box); Collect new parallel transects in the Curnamona Province (yellow lines).

- Extend AusLAMP into the Lachlan Orogen in NSW to determine the relationship of the Curnamona Province with the Delamerian and Lachlan Orogens to test the models of Moresi et al. (2015); Cayley (2011).

- Extend 3D modelling of western Victoria into South Australia using existing AusLAMP data.

- Test the concept of the mid-crustal conductor in the Curnamona Province by collecting two dense broadband MT lines to highlight upper crustal pathways.

- Compare continental seismological models (e.g. Kennett and Salmon, 2012; Rawlinson et al., 2014b) with expanding AusLAMP dataset.

APPENDIX

A

SUPPORTING INFORMATION FOR CHAPTER 4

A.1 Model mesh parameters

Mesh dimensions were 70 x 54 x 70 cells in the x (north-south), y (east-west) and z directions respectively. The dimensions of the survey area were 500 km in the x direction by 400 km in the y direction. Including padding, the model dimensions were 1230 km in the x direction, 800 km in the y direction, and 1353 km deep. Cell sizes were 10 x 10 km, and z layers began with 50 m thickness, and increased by a factor of 1.125 for each layer. Topography and bathymetry were included in the model. Layers were included beneath the ocean to account for sediments, with resistivity linearly increasing from 0.3 Ωm immediately beneath the ocean (which was fixed at 0.3 Ωm), to 30 Ωm at 8 km below sea level.

A.2 Testing the presence of the conductors

To test the sensitivity of the MT data to the presence of the Curnamona Conductor, a forward model was calculated with the Curnamona Conductor replaced with 1000 Ωm, the approximate resistivity of the cells surrounding the conductor. This generated a major increase in RMS of each site within the locality of the conductor and had a major effect on the overall RMS which increased from 1.33 to 6.15, indicating that a conductive anomaly is required by the data (as evident from phase tensor ellipses and induction arrows; Figure 3 and 6 respectively). The same process was followed to test the dependence of the model to the Nackara Arc Conductors. Although this did not have as large an impact as removing the Curnamona Conductor, the overall RMS still increased significantly from 1.33 to 3.01. The model responses for individual sites within the Nackara Arc then fit the data poorly, again indicating the requirement of the conductors by the data.

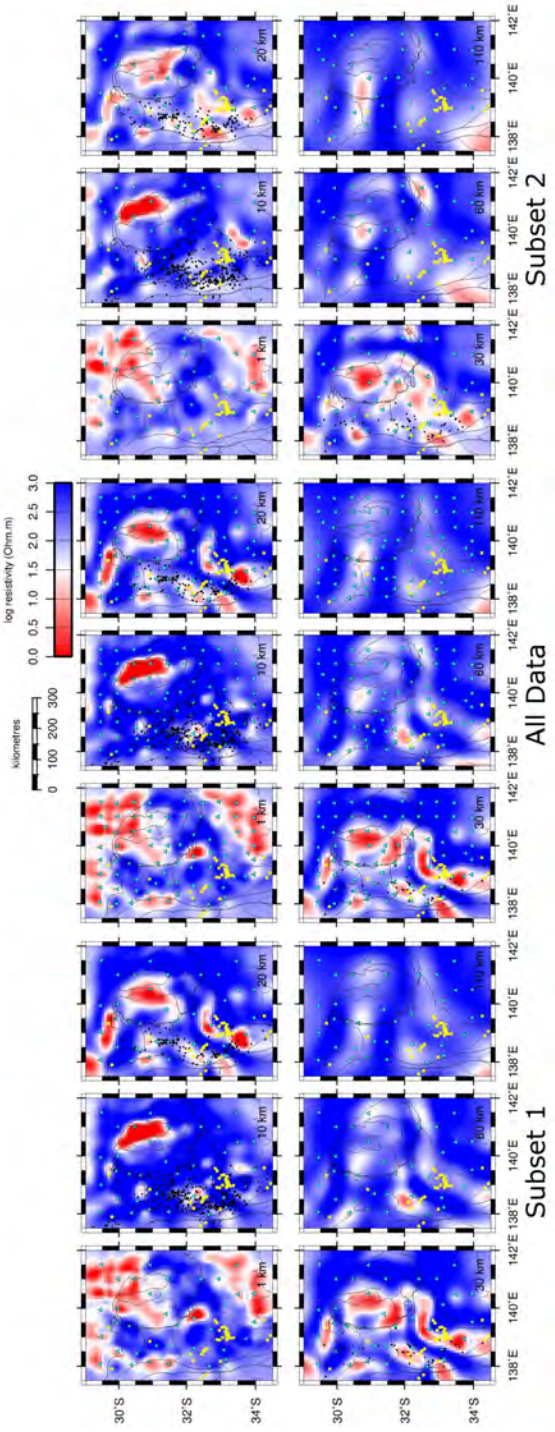

Figure A.1: Subsets of data Inversion results using the same modelling parameters as the presented model, but with the dataset of 74 stations divided into two subsets containing half of the total sites, to test the dependence of the model features on the data. The sites included for each of the three inversions are shown as blue triangles. The middle inversion is the presented model with all sites included, for comparison.

A.3 Dependence of the final model on the starting model

Three different inversions were conducted, using exactly the same model mesh, data and model parameters, but starting with a half space of 50, 500 and 1000 Ωm. (compared to our presented model with a starting half space of 100 Ωm). The below table indicates the convergence of the different models, with 100 Ωm converging the best, and thus the most appropriate starting resistivity of the half space.

Table A.1: Test of Starting Model

Starting resistivity (Ωm)	Starting RMS	Final RMS
50	10.65	1.37
100	15.05	1.33
500	36.7	1.56
1000	53.45	1.82

A.4 Testing the dependence of the data for the presented model

To test the models dependence on the data, the original 74 sites were divided into two subsets of data that still provided a roughly even coverage of the survey area. For each of these two subsets an inversion was run using only the 36 sites, with the final iteration of the presented model used as the starting model. The results indicate that the Curnamona Conductor is very robust at 10 km depth, and its presence until 40 km depth occurs in all models, although shape changes slightly at lower crustal depths. Large site spacing makes the narrow Nackara Arc conductors difficult to resolve when the site spacing is doubled for the subset data. However, the first subset of data resolves the conductors very well. The second subset of data show conductors within the Nackara Arc, but these are not connected in the same way as our presented model, thus making the location and connectedness of these conductors in our model less reliable than that of the Curnamona Conductor.

A.5 Data fit per site

Supplementary Figure A.3 highlights those stations that have an RMS of larger than 2.0, as stations with an RMS below this value were determined to fit the model well. It can be seen that overall there are no regions where the model is unable to fit the data reasonably well.

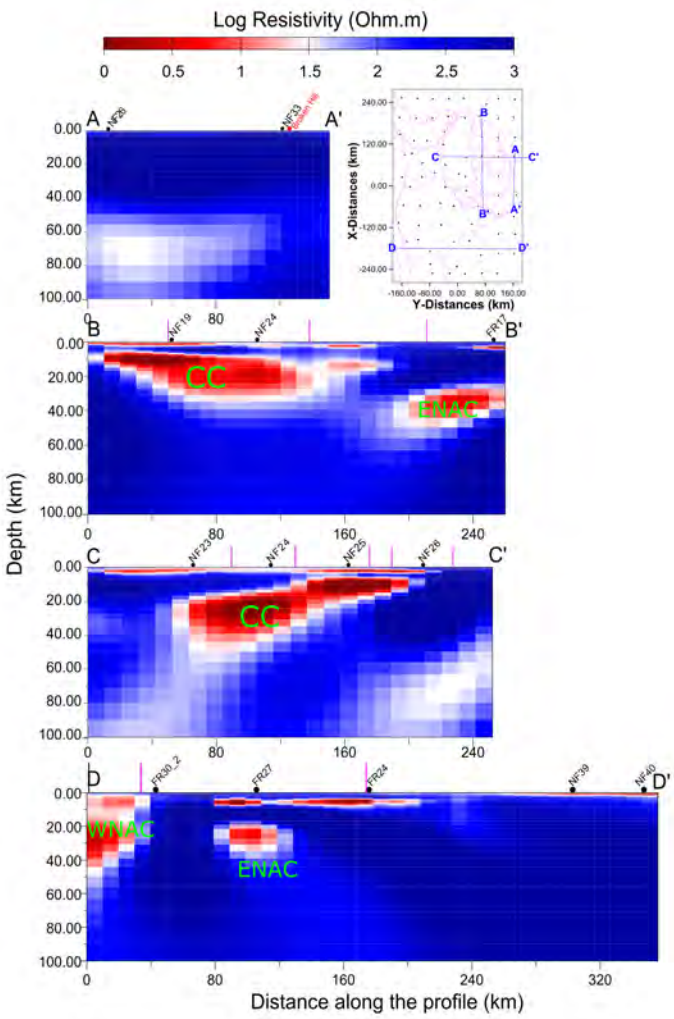

Figure A.2: Vertical Resistivity Slices Cross sections of the final resistivity model taken at the locations shown by blue lines on the map. CC, WNAC and ENAC are the Curnamona Conductor, Western Nackara Arc Conductor and the Eastern Nackara Arc Conductor, respectively.

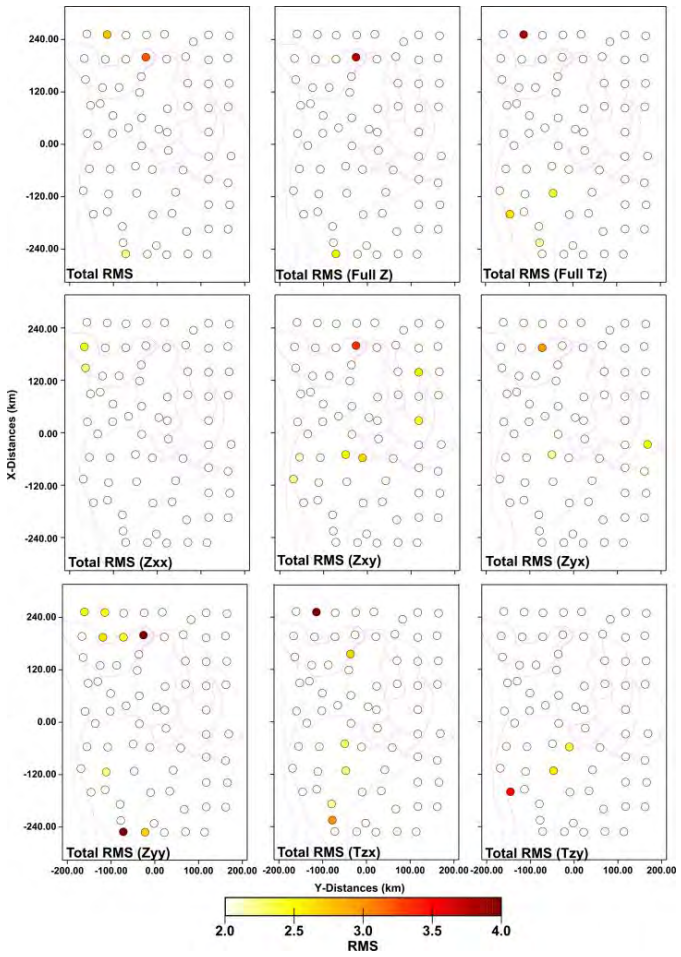

Figure A.3: RMS of stations Circles for each MT station, coloured according to RMS of the final model. White circles have an RMS of less than 2, and were deemed to fit the data well. RMS misfits are shown for each component of the impedance tensor **Z**: Zxy, Zyx, Zyy and Zyy, and for each component of the tipper, **T**: Tzx, Txy, as well as the overall RMS, and the RMS of the full impedance tensor and the full tipper.

BIBLIOGRAPHY

Aitken, A., Altinay, C., and Gross, L. (2015). Australia's lithospheric density field, and its isostatic equilibration. *Geophysical Journal International*, 203(3):1961–1976.

Aitken, A., Salmon, M., and Kennett, B. (2013). Australia's Moho: A test of the usefulness of gravity modelling for the determination of Moho depth. *Tectonophysics*, 609:468–479.

Aitken, A. R. (2010). Moho geometry gravity inversion experiment (MoGGIE): A refined model of the Australian Moho, and its tectonic and isostatic implications. *Earth and Planetary Science Letters*, 297(1-2):71–83.

Aivazpourporgou, S., Thiel, S., Hayman, P. C., Moresi, L. N., and Heinson, G. (2015). Decompression melting driving intraplate volcanism in Australia: Evidence from magnetotelluric sounding. *Geophysical Research Letters*, 42(2):346–354.

Australian Academy of Science (2012). UNCOVER. Technical report, Australian Academy of Science, Canberra ACT.

Balfour, N., Cummins, P., Pilia, S., and Love, D. (2015). Localization of intraplate deformation through fluid-assisted faulting in the lower-crust: The Flinders Ranges, South Australia. *Tectonophysics*, 655:97–106.

Becken, M. and Ritter, O. (2012). Magnetotelluric Studies at the San Andreas Fault Zone: Implications for the Role of Fluids. *Surveys in Geophysics*, 33(1):65–105.

Bedrosian, P. and Feucht, D. (2014). Structure and tectonics of the northwestern United States from EarthScope USArray magnetotelluric data. *Earth and Planetary Science Letters*, 402:275–289.

Betts, P. G., Giles, D., Lister, G. S., and Frick, L. R. (2002). Evolution of the Australian lithosphere. *Australian Journal of Earth Sciences*, 49(4):661–695.

Bibby, H. M., Caldwell, T. G., and Brown, C. (2005). Determinable and non-determinable parameters of galvanic distortion in magnetotellurics. *Geophysical Journal International*, 163(3):915–930.

Booker, J. R. (2014). The magnetotelluric phase tensor: A critical review. *Surveys in Geophysics*, 35(1):7–40.

Brun, J. and Beslier, M. (1996). Mantle exhumation at passive margins. *Earth and Planetary Science Letters*, 142:161–173.

Cagniard, L. (1953). Basic theory of the magnetotelluric method of geophysical prospecting. *Geophysics*, 18:605–635.

Caldwell, T. G., Bibby, H. M., and Brown, C. (2004). The magnetotelluric phase tensor. *Geophysical Journal International*, 158(2):457–469.

Cayley, R. (2011). Exotic crustal block accretion to the eastern Gondwanaland margin in the Late Cambrian-Tasmania, the Selwyn Block, and implications for the Cambrian-Silurian evolution of the Ross, Delamerian, and Lachlan orogens. *Gondwana Research*, 19(3):628–649.

Cayley, R., Korsch, R., Kennett, B., Skladzien, P., Jones, L., Morand, V., G.Gibson, Rawling, T., and Betts, P. (2011a). Results of deep seismic reflection imaging of the eastern Delamerian Orogen, South Australia and western Victoria, Australia. *GeoScience Department of Primary Industries, Victoria*, Data CD version: 4 March, 2011(4).

Cayley, R., Korsch, R., Moore, D., Costelloe, R., Nakamura, A., Willman, C., Rawling, T., Morand, V., Skladzien, P., and O'Shea, P. (2011b). Crustal architecture of central Victoria: results from the 2006 deep crustal reflection seismic survey. *Australian Journal of Earth Sciences*, 58(2):113–156.

Cayley, R. and Taylor, D. (1997). Grampians special map area geological report. Technical report, Geological Survey of Victoria Report 107, Melbourne, Victoria.

Célérier, J., Sandiford, M., Hansen, D. L., and Quigley, M. (2005). Modes of active intraplate deformation, Flinders Ranges, Australia. *Tectonics*, 24(6). TC6006.

Chamalaun, F. (1985). Geomagnetic deep sounding experiment in the central Flinders Ranges of South Australia . *Physics of the Earth and Planetary Interiors*, 37(23):174–182.

Chamalaun, F. and Barton, C. (1993). Electromagnetic induction in the Australian crust: results from the Australia-wide array of geomagnetic stations. *Exploration Geophysics*, 24(2):179–186.

Chave, A. and Jones, A., editors (2012). *The Magnetotelluric Method: Theory and Practice*. Cambridge University Press.

Chave, A. and Thomson, D. (2004). Bounded influence magnetotelluric response function estimation. *Geophysical Journal International*, 157(3):988–1006.

Clark, C., Mumm, A. S., and Faure, K. (2005). Timing and nature of fluid flow and alteration during Mesoproterozoic shear zone formation, Olary Domain, South Australia. *Journal of Metamorphic Geology*, 23(3):147–164.

Collins, W. (2002). Hot orogens, tectonic switching and creation of continental crust. *Geology*, 30:535–538.

Coney, P., Edwards, A., Hine, R., Morrison, F., and Windrim, D. (1990). The regional tectonics of the Tasman orogenic system, eastern Australia. *Journal of Structural Geology*, 12(5-6):519–543.

Connolly, J. A. D. and Podladchikov, Y. Y. (2004). Fluid flow in compressive tectonic settings: Implications for midcrustal seismic reflectors and downward fluid migration. *Journal of Geophysical Research: Solid Earth*, 109(B4):B04201.

Conor, C. and Preiss, W. (2008). Understanding the 1720-1640 Ma Palaeoproterozoic Willyama Supergroup, Curnamona Province, southeastern Australia: implications for tectonics, basin evolution and ore genesis. *Precambrian Research*, 166(1-4):297–317.

Constable, S. (1990). Electrical Studies of the Australian Lithosphere. In Drummond, B., editor, *The Australian Lithosphere*, volume 17, pages 121–140. Geological Society of Australia Special Publications.

Constable, S. (2006). SEO3: A new model of olivine electrical conductivity. *Geophysical Journal Interntational*, 166:435–437.

Constable, S., Parker, R., and Constable, C. (1987). Occam's inversion; a practical algorithm for generating smooth models from electromagnetic sounding data. *Geophysics*, 52(3):289–300.

Constable, S., Shankland, T. J., and Duba, A. (1992). The electrical conductivity of an isotropic olivine mantle. *Journal of Geophysical Research: Solid Earth*, 97(B3):3397–3404.

Crawford, A., Cameron, W., and Keays, R. (1984). The association boninite low-ti andesite-tholeiite in the heathcote greenstone belt, Victoria; ensimatic setting for the early lachlan fold belt. *Australian Journal of Earth Sciences*, 31(2):161–175.

Crawford, A., Cayley, R., Taylor, D., Morand, V., Gray, C., Kemp, A., Wohlt, K., VandenBerg, A., Moore, D., Maher, S., Direen, N., Edwards, J., Donagy, A., Anderson, J., and Black, L. (2003). Neoproterozoic and Cambrian continental rifting, continent-arc collision and post-collisional magmatism. In: Evolution of the Palaeozoic Basement. *Geological Society of Australia, Sydney, Australia*, pages 73–92.

Dai, L. and Karato, S. (2009). Electrical conductivity of orthopyroxene: Implications for the water content of the asthenosphere. *Proceedings of the Japan Academy, Series B*, 85(10):466–475.

Dai, L., Li, H., Hu, H., Shan, S., Jiang, J., and Hui, K. (2012). The effect of chemical composition and oxygen fugacity on the electrical conductivity of dry and hydrous garnet at high temperatures and pressures. *Contributions to Mineralogy and Petrology*, 163(4):689–700.

de Caritat, P., Cooper, M., Jaireth, S., and Bastrakov, E. (2011). National Geochemical Survey of Australia: Preliminary Implications for Energy and Mineral Exploration. Technical report, Geoscience Australia. Record 2011/29, 78 pp.

de Groot-Hedlin, C. D. and Constable, S. C. (1990). Occam's inversion to generate smooth, two-dimensional models from magnetotelluric data. *Geophysics*, 55(12):1613–1624.

Debayle, E. and Kennett, B. (2000). Anisotropy in the Australasian upper mantle from Love and Rayleigh waveform inversion. *Earth and Planetary Science Letters*, 184(1):339–351.

Demouchy, S. (2010). Hydrogen diffusion in spinel grain boundaries and consequences for chemical homogenization in hydrous peridotite. *Contributions to Mineralogy and Petrology*, 160(6):887–898.

Dennis, Z., Moore, D., and Cull, J. (2011a). A geological interpretation of the Echuca magnetotelluric survey, Victoria. *Australian Journal of Earth Sciences*, 58(6):587–597.

Dennis, Z., Moore, D., and Cull, J. (2011b). Magnetotelluric survey for undercover structural mapping, Central Victoria. *Australian Journal of Earth Sciences*, 58(1):33–47.

Dennis, Z., Thiel, S., and Cull, J. (2012). Lower crust and upper mantle electrical anisotropy in southeastern Australia. *Exploration Geophysics*, 43(4):228–241.

Didana, Y. L. (2016). *Magnetotellurc imaging of conventional and unconvential geothermal resources*. PhD thesis, The University of Adelaide.

Direen, N. G. and Crawford, A. J. (2003). The Tasman Line: Where is it, what is it, and is it Australia's Rodinian breakup boundary? *Australian Journal of Earth Sciences*, 50(4):491–502.

Duan, J., Taylor, D., Chopping, R., and Cayley, R. (2016). AusLAMP MT over Victoria. New insight from the 3D grid highlights regions of anomalously conductive mantle and unexpected linear trends in the crust. *ASEG Conference Extended Abstracts*.

Duba, A., Huengest, E., Nover, G., Will, G., and Jödicke, H. (1988). Impedance of black shale from Münsterland 1 borehole: an anomalously good conductor? *Geophysical Journal International*, 94(3):413–419.

Dutch, R. A., Hand, M., and Clark, C. (2005). Cambrian reworking of the southern Australian Proterozoic Curnamona Province: constraints from regional shear-zone systems. *Journal of the Geological Society*, 162(5):763–775.

Dyksterhuis, S. and Müller, R. (2008). Cause and evolution of intraplate orogeny in Australia. *Geology*, 36(6):495–498.

Egbert, G. D. and Kelbert, A. (2012). Computational Recipes for Electromagnetic Inverse Problems. *Geophysical Journal International*, 189:251–267.

Evans, R. L., Jones, A., Garcia, X., Muller, M., Hamilton, M., Evans, S., Fourie, C. J. S., Spratt, J., Webb, S., Jelsma, H., and Hutchins, D. (2011). Electrical lithosphere beneath the Kaapvaal craton, southern Africa. *Journal of Geophysical Research: Solid Earth*, 116(B4).

Foden, J., Barovich, K., Jane, M., and O'Halloran, G. (2001). Sr-isotopic evidence for Late Neoproterozoic rifting in the Adelaide Geosyncline at 586 Ma: Implications for a Cu ore forming fluid flux. *Precambrian Research*, 106:291–308.

Foden, J., Elburg, M., Dougherty-Page, J., and Burtt, A. (2006). The timing and duration of the Delamerian orogeny: Correlation with the Ross Orogen and implications for Gondwana assembly. *Journal of Geology*, 114(2):189–210.

Foster, D. and Gray, D. (2000). Evolution and structure of the Lachlan fold belt of eastern Australia. *Annual Review of Earth and Planetary Sciences*, 28:47–80.

Freeze, R. and Cherry, J. (1979). *Groundwater*. Prentice-Hall.

Fricke, C., Preiss, W., and Neumann, N. (2004). The Curnamona Province: a Palaeo- to Mesoproterozoic time slice. PDF published online https://d28rz98at9flks.cloudfront.net/70435/ 04CurnamonaProvinceGeologyByFrickeEtAl.pdf.

Frogtech (2014). Phanerozoic OZ SEEBASE v2 GIS. Bioregional Assessment Source Dataset. Viewed 14 June 2016. http://data.bioregionalassessments.gov.au/dataset/26e0fbd9-d8d0-4212-be52-ca317e27b3bd.

Frost, B., Fyfe, W., Tazaki, K., and Chan, T. (1989). Grain-boundary graphite in rocks and implications for high electrical conductivity in the lower crust. *Nature*, 340:134–136.

Fuji-ta, K., Katsura, T., and Tainosho, Y. (2004). Electrical conductivity measurement of granulite under mid- to lower crustal pressure-temperature conditions. *Geophysical Journal International*, 157(1):79–86.

Gaina, C., Müller, D., Royer, J., Stock, J., Hardebeck, J., and Symonds, P. (1998). The tectonic history of the Tasman Sea: a puzzle with 13 pieces. *Journal of Geophysical Research*, 103(12):413–433.

Gamble, T. D., Goubau, W. M., and Clarke, J. (1979). Error analysis for remote reference magnetotellurics. *Geophysics*, 44(5):959–968.

Giles, D., Betts, P., and Lister, G. (2002). Far-field continental backarc setting for the 1.80-1.67 Ga basins of northeastern Australia. *Geology*, 30:823–826.

Glen, R. A. (2005). The Tasmanides of eastern Australia. *Geological Society, London, Special Publications*, 246(1):23–96.

Glover, P. (1996). Graphite and electrical conductivity in the lower continental crust; a review. *Physics and Chemistry of the Earth*, 21:279–287.

Glover, P. (2015). Comment on 'Electrical conductivity of albite-(quartz)-water and albite-water-NaCl systems and its implication to the high conductivity anomalies in the continental crust' by Guo, X., Yoshino, T. & Shimojuku, A. *Earth and Planetary Science Letters*, 423:244–245.

Gough, D. (1986). Seismic reflectors, conductivity, water and stress in the continental crust. *Nature*, 323:143–144.

Gough, D., Lilley, F. E. M., and McElhinny, M. W. (1972). A polarization-sensitive magnetic variation anomaly in South Australia. *Nature Physical Science*, 239:88–91.

Gough, D. I., Bingham, D. K., Ingham, M. R., and Alabi, A. O. (1982). Conductive structures in southwestern Canada: a regional magnetometer array study. *Canadian Journal of Earth Sciences*, 19(8):1680–1690.

Graeber, F., Houseman, G. A., and Greenhalgh, S. (2002). Regional teleseismic tomography of the western Lachlan Orogen and the Newer Volcanic Province, southeast Australia. *Geophysical Journal International*, 149(2):249–266.

Gray, C., Kemp, A., Anderson, J., Bushell, D., Ferguson, D., Fitzherbert, J., and Stevenson, M. (2002). Delamerian Glenelg tectonic zone, western Victoria: geology and metamorphism of stratiform rocks. *Australian Journal of Earth Sciences*, 49(2):187–200.

Gregori, G. P. and Lanzerotti, L. J. (1980). Geomagnetic depth sounding by induction arrow representation: A review. *Reviews of Geophysics*, 18(1):203–209.

Griffin, W., O'Reilly, S. Y., and A., S. (1988). Mantle metasomatism beneath western Victoria, Australia: II. Isotopic geochemistry of Cr-diopside lherzolites and Al-augite pyroxenites. *Geochimica et Cosmochimica Acta*, 52(2):449–459.

Griffin, W. L., Begg, G., and O'Reilly, S. (2013). Continental-root control on the genesis of magmatic ore deposits. *Nature Geoscience*, 6(11):905–910.

Guo, X., Yoshino, T., and Shimojuku, A. (2015). Electrical conductivity of albite-(quartz)-water and albite-water-NaCl systems and its implication to the high conductivity anomalies in the continental crust. *Earth and Planetary Science Letters*, 412:1–9.

Haak, V. and Hutton, R. (1986). Electrical resistivity in continental lower crust. *Geological Society, London, Special Publications*, 24(1):35–49.

Hand, M., Reid, A., and Jagodzinski, L. (2007). Tectonic framework and evolution of the gawler craton, southern australia. *Economic Geology*, 102(8).

Handler, M. R., Bennett, V. C., and Esat, T. M. (1997). The persistence of off-cratonic lithospheric mantle: Os isotopic systematics of variably metasomatised southeast Australian xenoliths. *Earth and Planetary Science Letters*, 151:61–75.

Heinson, G. S., Direen, N. G., and Gill, R. M. (2006). Magnetotelluric evidence for a deep-crustal mineralizing system beneath the Olympic Dam iron oxide copper-gold deposit, southern Australia. *Geology*, 34(7):573–576.

Holford, S., Hillis, R. R., Hand, M., and Sandiford, M. (2011). Thermal weakening localizes intraplate deformation along the southern Australian continental margin. *Earth and Planetary Science Letters*, 305:207–214.

Hyndman, R. and Shearer, P. (1989). Water in the lower continental crust: modelling magnetotelluric and seismic reflection results. *Geophysics Journal International*, 98:343–365.

Jenkins, R. (1990). The Adelaide Fold Belt: Tectonic reappraisal. In Jago, J. and Moore, P., editors, *The Evolution of a Late Precambrian-Early Palaeozoic Rift Complex: The Adelaide Geosyncline*, volume 16, pages 396–420.

Jiracek, G. R., Ander, M. E., and Truman Holcombe, H. (2013). In Riecker, R., editor, *Rio Grande Rift: Tectonics and Magmatism*, chapter Magnetotelluric Soundings of Crustal Conductive Zones in Major Continental Rifts, pages 209–222. American Geophysical Union.

Jödicke, H., Jording, A., Ferrari, L., Arzate, J., Mezger, K., and Rüpke, L. (2006). Fluid release from the subducted Cocos plate and partial melting of the crust deduced from magnetotelluric studies in southern Mexico: Implications for the generation of volcanism and subduction dynamics. *Journal of Geophysical Research: Solid Earth*, 111:B08102.

Johnson, R., editor (1989). *Intraplate Volcanism in Eastern Australia and New Zealand*. Cambridge University Press, Melbourne.

Jones, A. (1988). Static shift of magnetotelluric data and its removal in a sedimentary basin environment. *Geophysics*, 53(7):967–978.

Jones, A. (1992). Electrical conductivity of the continental lower crust. In Fountain, D., Arculus, R., and Kay, R., editors, *Continental lower crust*, pages 81–143. New York, Elsevier.

Jones, A. and Ferguson, I. (2001). The electric Moho. *Nature*, 409:331–333.

Jones, A., Ledo, J., Ferguson, I., Craven, J., Unsworth, M., Chouteau, M., and Spratt, J. (2014). The electrical resistivity of Canadas lithosphere and correlation with other parameters: contributions from Lithoprobe and other programmes. *Canadian Journal of Earth Sciences*, 51(6):573–617.

Jones, A. G. (1987). MT and reflection: an essential combination. *Geophysical Journal of the Royal Astronomical Society*, 89(1):7–18.

Jones, A. G., Evans, R. L., and Eaton, D. W. (2009). Velocity-conductivity relationships for mantle mineral assemblages in Archean cratonic lithosphere based on a review of laboratory data and Hashin-Shtrikman extremal bounds. *Lithos*, 109(1-2):131–143.

Jones, A. G., Ferguson, I. J., Chave, A. D., Evans, R. L., and McNeice, G. W. (2001). Electric lithosphere of the slave craton. *Geology*, 29(5):423–426.

Jones, A. G., Fullea, J., Evans, R. L., and Muller, M. R. (2012). Water in cratonic lithosphere: Calibrating laboratory-determined models of electrical conductivity of mantle minerals using geophysical and petrological observations. *Geochemistry, Geophysics, Geosystems*, 13(6). Q06010.

Jones, A. G., Ledo, J., and Ferguson, I. J. (2005). Electromagnetic images of the trans-hudson orogen: the north american central plains anomaly revealed. *Canadian Journal of Earth Sciences*, 42(4):457–478.

Karato, S. (1990). The role of hydrogen in the electrical conductivity of the upper mantle. *Nature*, 347:272–273.

Karato, S. (2006). Remote Sensing of Hydrogen in Earth's Mantle. *Reviews in Mineralogy and Geochemistry*, 62(1):343–375.

Kawano, S., Yoshino, T., and Katayama, I. (2012). Electrical conductivity of magnetite-bearing serpentinite during shear deformation. *Geophysical Research Letters*, 39:L20313.

Kelbert, A., Meqbel, N., Egbert, G., and Tandon, K. (2014). ModEM: A modular system for inversion of electromagnetic geophysical data. *Computational Geoscience*, 66:40–53.

Kemp, A. (2003). Plutonic boninite-like rocks in an anatectic setting: Tectonic implications for the Delamerian orogen in southeastern Australia. *Geology*, 31(4):371–374.

Kemp, A. (2004). Petrology of high-Mg, low-Ti igneous rocks of the Glenelg River Complex (SE Australia) and the nature of their interaction with crustal melts. *Lithos*, 78(1-2):119–156.

Kemp, A., Gray, C., and Ellis, D. (2002). Delamerian Glenelg tectonic zone, western Victoria: characterisation and synthesis of igneous rocks. *Australian Journal of Earth Sciences*, 49:201–224.

Kemp, A., Hawkesworth, C., Collins, W., Gray, C., and Blevin, P. (2009). Isotopic evidence for rapid continental growth in an extensional accretionary orogen: The Tasmanides, eastern Australia. *Earth and Planetary Science Letters*, 284(3-4):455–466.

Kennett, B. and Saygin, E. (2015). The nature of the Moho in Australia from reflection profiling: A review. *GeoResJ*, 5:74–91.

Kennett, B. L. N. and Salmon, M. (2012). AuSREM: Australian Seismological Reference Model. *Australian Journal of Earth Sciences*, 59(8):1091–1103.

Kennett, B. L. N., Salmon, M., Saygin, E., and AusMoho Working Group (2011). AusMoho: the variation of Moho depth in Australia. *Geophysical Journal International*, 187(2):946–958.

Kennett, B. L. N., Saygin, E., and Salmon, M. (2015). Stacking autocorrelograms to map Moho depth with high spatial resolution in southeastern Australia. *Geophysical Research Letters*, 42(18):7490–7497.

Keppel, M., Karlstrom, K., Love, A., Priestley, S., Wohling, D., and De Ritter, S., editors (2013). *Allocating Water and Maintaining Springs in the Great Artesian Basin, Volume I: Hydrogeological Framework of the Western Great Artesian Basin.* National Water Commission, Canberra.

Key, K. (2009). 1D inversion of multicomponent, multifrequency marine CSEM data: Methodology and synthetic studies for resolving thin resistive layers. *Geophysics*, 74(2):F9–F20.

Kirkby, A., Heinson, G., Holford, S., and Thiel, S. (2015). Mapping fractures using 1D anisotropic modelling of magnetotelluric data: a case study from the Otway Basin, Victoria, Australia. *Geophysical Journal International*, 201(3):1961–1976.

Korsch, R. J., Barton, T. J., Gray, D. R., Owen, A. J., and Foster, D. A. (2002). Geological interpretation of a deep seismic-reflection transect across the boundary between the Delamerian and Lachlan Orogens, in the vicinity of the Grampians, western Victoria. *Australian Journal of Earth Sciences*, 49(6):1057–1075.

Krieger, L. and Peacock, J. (2014). MTpy: A Python toolbox for magnetotellurics. *Computers & Geosciences*, 72:167–175.

Kurtz., R. D., Delaurier., J. M., and Gupta., J. C. (1986). A magnetotelluric sounding across Vancouver Island detects the subducting Juan de Fuca plate. *Nature*, 321:596–599.

Lilley, F. E. M. and Tammemagi, H. Y. (1972). Magnetotelluric and Geomagnetic Depth Sounding Methods Compared. *Nature Physical Science*, 240:184–187.

Lindsay Curtis, J. (2003). The Nackara Arc: an under-explored diamond province in South Australia? - a new perspective on applied exploration. *MESA Journal*, pages 25–29.

Maher, S., Moore, D., Crawford, A., Twyford, R., and Fanning, C. (1997). Test drilling of the southern margin of the Murray Basin. Technical report, Department of Natural Resources and Environment.

Mathez, E. (1987). Carbonaceous matter in mantle xenoliths: Composition and relevance to the isotopes. *Geochimica et Cosmochimica Acta*, 51(9):2339–2347.

Maumus, J., Bagdassarov, N., and Schmeling, H. (2005). Electrical conductivity and partial melting of mafic rocks under pressure. *Geochimica et Cosmochimica Acta*, 69(19):4703–4718.

Meffre, S., Direen, N. G., Crawford, A. J., and Kamenetsky, V. (2004). Mafic volcanic rocks on King Island, Tasmania: evidence for 579 Ma break-up in east Gondwana. *Precambrian Research*, 135(3):177–191.

Miller, J., Phillips, D., Wilson, C., and Dugdale, L. (2005). Evolution of a reworked orogenic zone: the boundary between the Delamerian and Lachlan fold belts, south-eastern Australia. *Australian Journal of Earth Sciences*, 52:921–940.

Milligan, P., Dhu, T., Duan, J., and Thiel, S. (2012). New magnetotelluric data across enigmatic conductivity anomalies that span Australia north-south. *Abstract, 21st EM Induction Workshop, Darwin*.

Milligan, P., Direen, N., and Shaw, R. (2000). Geophysical Atlas of the Curnamona Province 1:2 Million Scale. *AGSO, Canberra*.

Mookherjee, M. and Karato, S. (2010). Solubility of water in pyrope-rich garnet at high pressures and temperature. *Geophysical Research Letters*, 37(3). L03310.

Moore, D. (1996). A geological interpretation of the geophysical data for the Horsham 1: 250,000 map sheet area. *Geological Survey of Victoria VIMP Report 24*.

Morand, V., Wohlt, K., Cayley, R., Taylor, D., Kemp, A., Simons, B., and Magart, A. (2003). Glenelg Special Map Area - Geological Report. Technical report, Geological Survey of Victoria, Melbourne.

Moresi, L., Betts, P. G., Miller, M., and Cayley, R. (2015). Dynamics of continental accretion. *Nature*, 508:245–249.

Muñoz, G., Bauer, K., Moeck, I., Schulze, A., and Ritter, O. (2010). Exploring the Groß Schönebeck (Germany) geothermal site using a statistical joint interpretation of magnetotelluric and seismic tomography models. *Geothermics*, 39(1):35–45.

Muñoz, G., Mateus, A., Pous, J., Heise, W., Monteiro Santos, F., and Almeida, E. (2008). Unraveling middle-crust conductive layers in Paleozoic Orogens through 3D modeling of magnetotelluric data: The Ossa-Morena Zone case study (SW Iberian Variscides). *Journal of Geophysical Research: Solid Earth*, 113(B6).

Muller, M., Jones, A., Evans, R., Grütter, H., Hatton, C., Garcia, X., Hamilton, M., Miensopust, M., Cole, P., Ngwisanyi, T., Hutchins, D., Fourie, C., Jelsma, H., Evans, S., Aravanis, T., Pettit, W., Webb, S., and Wasborg, J. (2009). Lithospheric structure, evolution and diamond prospectivity of the Rehoboth Terrane and western Kaapvaal Craton, southern Africa: Constraints from broadband magnetotellurics. *Lithos*, 112, Supplement 1:93–105. Proceedings of the 9th International Kimberlite Conference.

Myer, D., Constable, S., and Key, K. (2013). Magnetotelluric evidence for layered mafic intrusions beneath the Vøring and Exmouth rifted margins. *Physics of the Earth and Planetary Interiors*, 220:1–10.

Nesbitt, B. E. (1993). Electrical resistivities of crustal fluids. *Journal of Geophysical Research: Solid Earth*, 98(B3):4301–4310.

Neumann, N., Sandiford, M., and Foden, J. (2000). Regional geochemistry and continental heat flow: implications for the origin of the South Australian heat flow anomaly. *Earth and Planetary Science Letters*, 183:107–120.

O'Reilly, S. and Griffin, W. (1988). Mantle metasomatism beneath western Victoria, Australia: I. Metasomatic processes in Cr-diopside lherzolites. *Geochimica et Cosmochimica Acta*, 52(2):433–447.

O'Reilly, S. Y. and Griffin, W. (1985). A xenolith-derived geotherm for southeastern Australia and its geophysical implications. *Tectonophysics*, 111:41–63.

Parker, E. (1958). Interaction of the solar wind with the geomagnetic field. *Physics of Fluids*, 1:171–187.

Parkinson, W. D. (1959). Direction of rapid geomagnetic fluctuations. *Geophysical Journal of the Royal Astronomical Society*, 2:1–14.

Paul, S. (1994). *Geomagnetic Induction Study of the Adelaide Geosyncline*. PhD thesis, Flinders University of South Australia.

Peacock, S. A. (1990). Fluid Processes in Subduction Zones. *Science*, 248(4953):329–337.

Pearson, D. G., Boyd, F. R., Haggerty, S. E., Pasteris, J. D., Field, S. W., Nixon, P. H., and Pokhilenko, N. P. (1994). The characterisation and origin of graphite in cratonic lithospheric mantle: a petrological carbon isotope and Raman spectroscopic study. *Contributions to Mineralogy and Petrology*, 115(4):449–466.

Pilia, S., Rawlinson, N., Cayley, R., Bodin, T., Musgrave, R., Reading, A., Direen, N., and Young, M. (2015). Evidence of micro-continent entrainment during crustal accretion. *Scientifc Reports*, 5(8218).

Pilia, S., Rawlinson, N., Direen, N. G., Cummins, P. R., and Balfour, N. (2013). Structural controls on localized intraplate deformation and seismicity in Southern Australia: Insights from local earthquake tomography of the Flinders Ranges. *Journal of Geophysical Research Solid Earth*, 118(5):2176–2190.

Plank, T. and Langmuir, C. (1998). The chemical composition of subducting sediment and its consequences for the crust and mantle. *Chemical Geology*, 145(3-4):325–394.

Pommier, A. (2014). Interpretation of magnetotelluric results using laboratory measurements. *Surveys in Geophysics*, 35(1):41–84.

Preiss, W. (2000). The Adelaide geosyncline of South Australia and its significance in Neoproterozoic continental reconstruction. *Precambrian Research*, 100:21–63.

Preiss, W. and Forbes, B. (1981). Stratigraphy, correlation and sedimentary history of Adelaide (Late Proterozoic) basins in Australia. *Precambrian Research*, 255:255–304.

Price, R., Gray, C., and Frey, F. (1997). Strontium isotopic and trace element heterogeneity in the plains basalts of the Newer Volcanic Province, Victoria, Australia. *Geochimica et Cosmochimica Acta*, 61(1):171–192.

Rajagopalan, S. (1999). Thursdays Gossan Prospect. In *Geophysical signatures of base metal deposits in Victoria*, volume 119, pages 129–136. Geological Survey of Victoria Report.

Rawlinson, N., Arroucau, P., Musgrave, R., Cayley, R., Young, M., and Salmon, M. (2014a). Complex continental growth along the proto-pacific margin of east gondwana. *Geology*, 42(9):783–786.

Rawlinson, N. and Fishwick, S. (2012). Seismic structure of the southeast Australian lithosphere from surface and body wave tomography. *Tectonophysics*, 572-573:111–122.

Rawlinson, N., Kennett, B., Vanacore, E., Glen, R., and Fishwick, S. (2011). The structure of the upper mantle beneath the Delamerian and Lachlan orogens from simultaneous inversion of multiple teleseismic datasets. *Gondwana Research*, 19(3):788–799.

Rawlinson, N., Salmon, M., and Kennett, B. (2014b). Transportable seismic array tomography in southeast Australia: Illuminating the transition from Proterozoic to Phanerozoic lithosphere. *Lithos*, 189:65–76.

Reston, T. (2009). The structure, evolution and symmetry of the magma-poor margins of the north and Central Atlantic: a synthesis. *Tectonophysics*, 468:6–27.

Reynard, B., Mibe, K., and Van de Moortèle, B. (2011). Electrical conductivity of the serpentinised mantle and fluid flow in subduction zones. *Earth and Planetary Science Letters*, 307:387–394.

Ritz, M. (1984). Inhomogeneous structure of the senegal lithosphere from deep magnetotelluric soundings. *Journal of Geophysical Research: Solid Earth*, 89(B13):11317–11331.

Robertson, K., Heinson, G., Taylor, D., and Thiel, S. (2016a). The lithospheric structure of the transition between the Delamerian and Lachlan Orogens: New insights from 3D magnetotelluric imaging. *Submitted to Australian Journal of Earth Science*.

Robertson, K., Heinson, G., and Thiel, S. (2016b). Lithospheric reworking at the Proterozoic-Phanerozoic transition of Australia imaged using AusLAMP Magnetotelluric data. *Earth and Planetary Science Letters*, 452:27–35.

Robertson, K., Taylor, D., Thiel, S., and Heinson, G. (2015). Magnetotelluric evidence for serpentinisation in a Cambrian subduction zone beneath the Delamerian Orogen, southeast Australia. *Gondwana Research*, 28(2):601–611.

Robertson, R., Preiss, W., Crooks, A., Hill, P., and Sheard, M. (1998). Review of the Proterozoic geology and mineral potential of the Curnamona Province in South Australia. Technical Report 17:3, Australian Geological Survey Organisation, Canberra.

Rodi, W. and Mackie, R. (2001). Nonlinear conjugate gradients algorithm for 2D magnetotelluric inversion. *Geophysics*, 66(1):174–187.

Ross, J. V. and Bustin, R. (1990). The role of strain energy in creep graphitization of anthracite. *Nature*, 343(6253):58–60.

Rutherford, L., Barovich, K., Hand, M., and Foden, J. (2006). Continental ca 1.7- 1.69 Ga Fe-rich metatholeiites in the Curnamona Province, Australia: a record of melting of a heterogeneous, subduction-modified lithospheric mantle. *Australian Journal of Earth Sciences*, 53(3):501–519.

Rutland, R., Parker, A., Pitt, G., Preiss, W., and Murrell, B. (1981). Precambrian of the southern hemisphere. In Hunter, D., editor, *Developments in Precambrian Geology Series*, volume 2, pages 309–360. Elsevier, Amsterdam.

Salmon, M., Kennett, B., Stern, T., and Aitken, A. (2013). The Moho in Australia and New Zealand. *Tectonophysics*, 609:288–298.

Sandiford, M., Foden, J., Zhou, S., and Turner, S. (1992). Granite genesis and the mechanics of convergent orogenic belts with application to the southern Adelaide Fold Belt. *Earth and Environmental Science Transactions of the Royal Society of Edinburgh*, 83(1-2):83–93.

Schuster, A. and Lamb, H. (1889). The diurnal variation of terrestrial magnetism. *Philosophical Transactions of the Royal Society A*, 180:467–518.

Selway, K. (2014). On the causes of electrical conductivity anomalies in tectonically stable lithosphere. *Surveys in Geophysics*, 35(1):219–257.

Shankland, T. J. and Ander, M. E. (1983). Electrical conductivity, temperatures, and fluids in the lower crust. *Journal of Geophysical Research: Solid Earth*, 88(B11):9475–9484.

Simpson, F. and Bahr, K. (2005). *Practical Magnetotellurics*. Cambridge University Press.

Siripunvaraporn, W. (2012). Three-Dimensional Magnetotelluric Inversion: An Introductory Guide for Developers and Users. *Surveys in Geophysics*, 33:5–27.

Sleep, N. (2009). Stagnant lid convection and carbonate metasomatism of the deep continental lithosphere. *Geochemistry, Geophysics, Geosystems*, 10(11):Q11010.

Stesky, R. M. and Brace, W. F. (1973). Electrical conductivity of serpentinized rocks to 6 kilobars. *Journal of Geophysical Research*, 78(32):7614–7621.

Stuart-Smith, P. (1999). Willaura sheet 7422 victoria 1:100 000 geological report record 1999/038. Technical report, Australian Geological Survey Organisation, Canberra.

Tammemagi, H. Y. and Lilley, F. E. M. (1973). A Magnetotelluric Traverse in Southern Australia. *Geophysical Journal of the Royal Astronomical Society*, 31(4):433–445.

Tappert, R., Foden, J., Muehlenbachs, K., and Wills, K. (2011). Garnet Peridotite Xenoliths and Xenocrysts from the Monk Hill Kimberlite, South Australia: Insights into the Lithospheric Mantle beneath the Adelaide Fold Belt. *Journal of Petrology*, 52(10):1965–1986.

Tappert, R., Foden, J., Stachel, T., Muehlenbachs, K., Tappert, M., and Wills, K. (2009). Deep mantle diamonds from South Australia: A record of Pacific subduction at the Gondwanan margin. *Geology*, 37(1):43–46.

Thiel, S. and Heinson, G. (2013). Electrical conductors in Archean mantle-Result of plume interaction? *Geophysical Research Letters*, 40(12):2947–2952.

Thiel, S., Soeffky, P., Krieger, L., Regenauer-Lieb, K., Peacock, J., and G., H. (2016). Conductivity response to intraplate deformation: evidence for metamorphic devolatilization and crustal-scale fluid focussing. *Submitted: Geophysical Research Letters*.

Tikhonov, A. (1950). On determining electrical characteristics of the deep layers of the Earth's crust. *Doklady*, 73:295–297.

Turner, S., Adams, C., Flöttmann, T., and Foden, J. (1993). Geochemical and geochronological constraints on the Glenelg River Complex, western Victoria. *Australian Journal of Earth Sciences*, 40(23):275–292.

Unsworth, M. (2010). Magnetotelluric Studies of Active Continent–Continent Collisions. *Surveys in Geophysics*, 31(2):137–161.

Unsworth, M., Jones, A. G., Wei, W., Marquis, G., Gokarn, S., Spratt, J., Bedrosian, P., Booker, J., Leshou, C., Clarke, G., Shenqhui, L., Chanhong, L., Ming, D., Sheng, J., Solon, K., Handong, T., Ledo, J., Roberts, b., and INDEPTH-MT team (2005). Crustal rheology of the Himalaya and Southern Tibet inferred from magnetotelluric data. *Nature*, 438:78–81.

van der Hilst, R., Kennett, B., Christie, D., and Grant, J. (1994). Project Skippy explores lithosphere and mantle beneath Australia. *Eos Transactions. American Geophysical Union*, 75(15):177–181.

VandenBerg, A., Willman, C., Maher, S., Simons, B., Cayley, R., Taylor, D., Morand, V.J. Moore, D., and Radojkovic, A. (2000). The Tasman Fold Belt System in Victoria. In *Geological Survey of Victoria Special Publication*.

VandenBerg, A. H. M. (1978). The Tasman fold belt system in Victoria. *Tectonophysics*, 48:267–297.

Wade, C. E., Reid, A. J., Wingate, M. T., Jagodzinski, E. A., and Barovich, K. (2012). Geochemistry and geochronology of the c. 1585 Ma Benagerie Volcanic Suite, southern Australia: Relationship to the Gawler Range Volcanics and implications for the petrogenesis of a Mesoproterozoic silicic large igneous province. *Precambrian Research*, 206-207:17–35.

Wang, D., Mookherjee, M., Xu, Y., and Karato, S. (2006). The effect of water on the electrical conductivity of olivine. *Nature*, 443:977–980.

Wang, L. and Chamalaun, F. (1995). A magnetotelluric traverse across the Adelaide Geosyncline. *Exploration Geophysics*, 26:539–546.

Wang, L., Lilley, F., and Chamalaun, F. (1997). Large-scale electrical conductivity structure of Australia from magnetometer arrays. *Exploration Geophysics*, 28:150–155.

Wang, L. J. and Lilley, F. E. M. (1999). Inversion of magnetometer array data by thin-sheet modelling. *Geophysical Journal International*, 137(1):128–138.

Wannamaker, P. E., Caldwell, T. G., Jiracek, G. R., Maris, V., Hill, G. J., Ogawa, Y., Bibby, H. M., Bennie, S. L., and Heise, W. (2009). Fluid and deformation regime of an advancing subduction system at Marlborough, New Zealand. *Nature*, 460:733–737.

Wei, W. (2001). Detection of Widespread Fluids in the Tibetan Crust by Magnetotelluric Studies. *Science*, 292:716–719.

Wessel, P., Smith, Walter, H. F., Scharroo, R., Luis, J., and Wobbe, F. (2013). Generic Mapping Tools: Improved Version Released. *Eos, Transactions American Geophysical Union*, 94(45):409–410.

Whelan, J., Hergt, J., and Woodhead, J. (2007). Granite-greestone connection in western Victoria: an example from the Bushy Creek Igneous Complex. *Australian Journal of Earth Sciences*, 54:975–990.

White, A. and Polatajko, O. (1985). Electrical Conductivity Anomalies and their Relationship with the tectonics of South Australia. *Geophysical Journal of the Royal Astronomical Society*, 80:757–771.

Wiese, H. (1962). Geomagnetische Tiefentellurik Teil II: Die Streichrichtung der Untergrundstrukturen des elektrischen Widerstandes, erschlossen aus geomagnetischen Variationen [Strike direction of underground structures of electric resistivity, inferred from geomagnetic variations.]. *Pure and applied geophysics*, 52:83–103.

Wilde, S., Valley, J., Peck, W., and Graham, C. (2000). Evidence from detrital zircons for the existence of continental crust and oceans on the Earth 4.4 Gyr ago. *Nature*, 409:175–178.

Williams, G. E. (1973). Late Quaternary piedmont sedimentation, soil formation and paleoclimates in arid South Australia. *Geomorphology*, 17:102–125.

Worzewski, T., Jegen, M., Kopp, H., Brasse, H., and Taylor Castillo, W. (2011). Magnetotelluric image of the fluid cycle in the Costa Rican subduction zone. *Nature Geoscience*, 4:108–111.

Yang, X. (2011). Origin of high electrical conductivity in the lower continental crust: A review. *Surveys in Geophysics*, 32:875–903.

Yang, X., Keppler, H., McCammon, C., and Ni, H. (2012). Electrical conductivity of orthopyroxene and plagioclase in the lower crust. *Contributions to Mineralogy and Petrology*, 163(1):33–48.

Yang, X., Keppler, H., McCammon, C., Ni, H., Xia, Q., and Fan, Q. (2011). Effect of water on the electrical conductivity of lower crustal clinopyroxene. *Journal of Geophysical Research: Solid Earth*, 116(B4). B04208.

Yoshino, T. (2010). Laboratory Electrical Conductivity Measurement of Mantle Minerals. *Surveys in Geophysics*, 31:163–206.

Yoshino, T., Laumonier, M., McIsaac, E., and Katsura, T. (2010). Electrical conductivity of basaltic and carbonatite melt-bearing peridotites at high pressures: Implications for melt distribution and melt fraction in the upper mantle. *Earth and Planetary Science Letters*, 295(3-4):593–602.

Yoshino, T., Matsuzaki, T., Shatskiy, A., and Katsura, T. (2009). The effect of water on the electrical conductivity of olivine aggregates and its implications for the electrical structure of the upper mantle. *Earth and Planetary Science Letters*, 288(1-2):291–300.

Yoshino, T., Matsuzaki, T., Yamashita, S., and Katsura, T. (2006). Hydrous olivine unable to account for conductivity anomaly at the top of the asthenosphere. *Nature*, 443:973–976.

Yoshino, T., Nishi, M., Matsuzaki, T., Yamazaki, D., and Katsura, T. (2008). Electrical conductivity of majorite garnet and its implications for electrical structure in the mantle transition zone. *Physics of the Earth and Planetary Interiors*, 170(3-4):193–200.

Yoshino, T. and Noritake, F. (2011). Unstable graphite films on grain boundaries in crustal rocks. *Earth and Planetary Science Letters*, 306(3-4):186 – 192.

Zhu, M., Xie, H., Guo, J., Bai, W., and Xu, Z. (2001). Impedance spectroscopy analysis on electrical properties of serpentine at high pressure and high temperature. *Science in China Series D: Earth Sciences*, 44(4):336–345.